Wireless Networks

Abbas Jamalipour
Md Arafat Hossain

Smartphone Instrumentations for Public Health Safety

Springer

Wireless Networks

Series editor

Xuemin Sherman Shen
University of Waterloo, Waterloo, ON, Canada

More information about this series at http://www.springer.com/series/14180

Abbas Jamalipour • Md Arafat Hossain

Smartphone Instrumentations for Public Health Safety

Springer

Abbas Jamalipour
The University of Sydney
Sydney, NSW, Australia

Md Arafat Hossain
The University of Sydney
Sydney, NSW, Australia

ISSN 2366-1186 ISSN 2366-1445 (electronic)
Wireless Networks
ISBN 978-3-030-02094-1 ISBN 978-3-030-02095-8 (eBook)
https://doi.org/10.1007/978-3-030-02095-8

Library of Congress Control Number: 2019958913

This Springer imprint is published by the registered company Springer Nature Switzerland AG
The registered company address is: Gewerbestrasse 11, 6330 Cham, Switzerland

Preface

Field-portable instruments for ubiquitous detection and analysis of biological, environmental, and agricultural items are becoming extremely important over the traditional methods as a means to ensure public health safety in many fields. One significantly convenient approach that has emerged in recent years is the harnessing of smartphone features to create field-deployable scientific instruments, allowing measurements to be made on-site and in real time. This book will cover a number of self-contained smartphone instruments with the particular focus on spectroscopic-based measurements.

The first work presented in this book is a smartphone-based intensity fluorimeter that has been developed by using the inbuilt white flash LED as an optical source and the CMOS camera as a detector. A color filter attached over the LED selects an excitation band centered around $\lambda \sim 450$ nm with a 3dB bandwidth, $\Delta\lambda \sim 21$ nm, which aligns well within the absorption band of a pH-responsive chemosensor dye. The green fluorescence is readily detected within a 3D-printed smartphone attachment and a simple red–green–blue Android app. To demonstrate the application of such an instrument, pH measurements were taken of potable tap, lake, and seawater at various locations in fields, and their real-time pH-maps were generated in a central computer using GPS service. In advance to this steady-state measurement, time-resolved fluorescence intensity measurements at various temperatures are demonstrated. A Peltier is integrated to allow measurements of the intensity over $T = 10$–40 °C with a maximum temperature resolution of $\delta T \sim 0.1$ °C.

For spectroscopic measurements, a low-cost dispersive element fabricated by nano-imprinted technology has been added into the system within a 3D-printed enclosure to smartphone camera. Performances of all these instruments have been analyzed by a range of applications in public health safety. By adding an optical fiber bundle, the functionality of the device was extended further to make possible spectral acquisitions from solid surfaces in hard-to-reach places. In order to demonstrate the potential application of such a device in the food industry, spectral analysis of apples and olive oils was performed for quality assurance.

With the IoT compatibility, all the smartphone instruments presented in this book can be integrated into a large network of devices as well as other sensors. As such, data can be monitored, shared, and processed to build real-time regional and global maps for a range of phenomena.

Sydney, NSW, Australia
August 2018

Abbas Jamalipour
Md Arafat Hossain

Acknowledgment

All the materials presented in this book were resulted from research and development carried out at the University of Sydney. The authors acknowledge Professor John Canning at the *i*nterdisciplinary Photonics Laboratories (*i*PL) of the University of Sydney. Financial and in-kind support of the University of Sydney, School of Electrical and Information Engineering, and School of Chemistry are highly appreciated.

Contents

Nomenclature

α	Current amplification factor
$\delta\lambda$	Spectral resolution, nm
δt	Time resolution, s
$\Delta\lambda$	Spectral bandwidth, nm
$\Delta\varphi$	Solid angle, °
θ	Angle, °
θ_0	Initial angle, °
θ_{diff}	Diffraction angle, °
λ	Wavelength, nm
λ_{abs}	Absorption wavelength, nm
λ_{em}	Emission wavelength, nm
λ_{ex}	Excitation wavelength, nm
Λ	Periodicity of diffraction grating lines, nm
$\varnothing_f$	Diameter of the polymer light guide, cm
φ	Angle between incident and diffracted light, °
ω_{slit}	Slit width, mm
a	Surface area, cm^2
A	Absorbance
d	Spacing between lines in diffraction grating, nm
f	Focal length, cm
G	Line density of diffraction grating, /mm
h	Height, m
H	Humidity, %
I	Intensity/fluorescence intensity, a. u.
I_0	Initial intensity, a. u.
I_{452}, I_{670}	Intensity at 452 and 670 nm, respectively
I_{r}	Relative intensity, a. u.
k_{R}, k_{B}, k_{G}	Calibration coefficient at red, green, and blue channels, respectively
L_1	Length of the polymer light guide, cm
L_2	Length of the endoscope fiber bundle, cm
L_{D}	Detector size, mm

pH	Acidity/alkalinity
pKa	Acid dissociation constant
R	Resistance, Ω
t	Time, s
T	Temperature, °C
T_{ir}	Response of IR temperature sensor, °C
T_r	Transmittance
T_{th}	Response of thermocouple, °C
V	"Value" in HSV color model

Acronyms

2D	Two dimensional
3D	Three dimensional
3G	Third generation
4G	Fourth generation
5G	Fifth generation
µUSB	Micro Universal Serial Bus
ABS	Acrylonitrile butadiene styrene
AMOLED	Active matrix organic light-emitting diode
AuNP	Gold nanoparticle
CCD	Charge-coupled device
CMOS	Complementary metal–oxide–semiconductor
CT	Charge transfer
DMSO	Dimethyl sulfoxide
ECL	Electrochemiluminescence
EVO	Extra virgin olive
FOV	Field-of-view
FWHM	Full width at half maximum
GPS	Global positioning systems
HEPES	4-(2-hydroxyethyl)-1-piperazineethanesulfonic acid
HSV	Hue, saturation, and value
IoT	Internet-of-Things
IR	Infra-red
LD	Laser diode
LED	Light-emitting diode
MP	Megapixels
NFS	Near-field sensor
NIR	Near Infra-red
NHMRC	National Health and Medical Research Council
NSW	New South Wales
N-MOSFET	N-type metal–oxide–semiconductor field-effect transistor
OLED	Organic light-emitting diode

OTG	On-the-Go
PET	Photo-induced electron transfer
QD	Quantum dot
RGB	Red, green, and blue
RhB	Rhodamine B
Rh6G	Rhodamine 6G
RO	Refined olive
SPDT	Single-pole-double-throw
SPR	Surface plasmon resonance
TPP	5,10,15,20-tetraphenylporphyrin
USB	Universal Serial Bus
UV	Ultra-violet
WHO	World Health Organization
Wi-Fi	Wireless fidelity

Chapter 1
Introduction

1.1 Smartphone Devices and Sensors

The smartphones and smartphone-driven technologies have advanced at a relentless pace to a point where they now become an integral part of our everyday lives—a must-have tool that many simply cannot do without. The technology has progressed so far that the average smartphone people take for granted now holds more computing power than so-called supercomputers of the 1980s [1], men were even put on the moon with less computing power than we hold in our pockets today.

The key factor that has made this smartphone boom is not only the rapid market growth of information and telecommunication sectors in the recent decades, but also a number of attractive embedded features, including a vast range of in-built sensors, increased battery capacity, communications and computational resources, and multitude of available and easy-to-use apps. The plethora of easily-obtainable apps has combined with phone's hardware features to extend the utility of smartphones far-beyond mere communication devices. Cameras, gyroscopes, GPS, Wi-Fi and high resolutions active matrix organic light-emitting diode (AMOLED) touchscreens are just some of the technological breakthroughs that now make possible a diverse range of application domains such as social networking, "augmented reality" interactive maps, healthcare and environmental monitoring [2–4]. The ever-increasing spectrum of a smartphone's capabilities means that there is now fierce competition between manufacturers to come-up with extra features, shrink internal components, improve cameras and screen resolutions, device power consumption and so on. Some of the features found on even the low-end smartphones of today are surprisingly hi-tech enough to perform the equivalent tasks of the key components in many scientific analytical devices. In recent years, this has led to growing research interest in the development of various scientific instruments based on smartphone platforms. The emerging research areas include point-of-care medical diagnosis [5–9], environmental monitoring [10–12], agricultural [13–15] and industrial [16, 17] analysis. The use of smartphone greatly advantages the low-cost and portability

A. Jamalipour, M. A. Hossain, *Smartphone Instrumentations for Public Health Safety*, Wireless Networks, https://doi.org/10.1007/978-3-030-02095-8_1

benefits of such an instrument. Further advantages include the prospect of wider accessibility via wireless networking that interconnects multiple smartphone instruments in the field—the cornerstone of the next generation smart sensing network. The key features of smartphone that will continue advancing this emerging research area and open-up many opportunities are briefly reviewed as below:

Availability and low-cost: Today's smartphones are arguably one of the most produced and publicly available devices carrying with people across the world, reaching a market figure of ~2.5 billion by the end of 2019 [18]. This relentless demand has sparked in driving down costs, making the technology more affordable. The increasing affordability means that smartphones are now ubiquitous in every corner of the globe, with usage growing everywhere steadily even in the third world and developing countries where access to technology assuring public health safety are critically available.

Light-weight and compact: One of the key attributes of current generation smartphones is perhaps their light-weight and compact size, letting most users to have it in their pocket for most of the time without any fuss. Whilst features like screen sizes vary depending on model, thicknesses tend to be less than typically 1 cm with compact Li-ion battery, meaning phones can be carried effortlessly in one's pocket or bag. Furthermore, high-end technologies like large pixel array of CMOS camera, infra-red (IR) emitter and detector, power efficient flash LED are all fitted nicely with today's smartphones.

Connectivity: Today's smartphone offers a great deal of networking options having connectivity and interfacing capability with other devices. The most significant one that has enabled smartphone instruments to operate across the globe is the wireless connectivity such as 3G/4G/5G, Wi-Fi, Bluetooth, GPS and near-field sensors (NFS) which cannot be deployed easily in bulky benchtop instruments. Other features such as waterproof operation, accelerometers and digital compasses greatly assist smartphone instrument operating in harsh environments and rugged areas in particular.

Internet-of-Things compatibility: The wireless connectivity of smartphone instrumentation has enabled them to become compatible to Internet-of-Things (IoT) network through which multiple devices can be interconnected. With such capability, many tasks can be performed by trans-receiving data through a cloud using high-speed connectivity options in smartphone. This has created the opportunity to establish smartphone enabled smartgrid sensor networks that underpinning the next generation IoT.

Self-contained: One of the most promising features of current generation smartphones is their large number of in-built sensors and devices that can be utilized for many health safety applications without the requirements of any add-on parts.

This has made the smartphone as a self-contained device for scientific instrumentation. In particular, bright illumination of the flash LED and imaging with the CMOS chip of smartphone are as good as, or even superior to, equivalent function of many benchtop imaging and spectroscopic devices. In contrast, however, the cost is considerably lower, driven by the massive consumer communications and social media market.

Processing capability and programmability: Today's smartphones are capable of running much advance programs and doing many computationally intensive tasks such as image processing, voice recognition, map generation etc. A big step-forward on smartphone processors over the last few years has enabled them to perform tasks on the same device which required desktop computer in the past. Other attractive side is the open source nature of their operating systems (both Android and iOS). Programmable smartphones are becoming mainstream platforms for instrument designers to collect information-rich data through their internal and external sensors. Advanced smartphone apps have been developed for a vast array of applications.

In combination of all above attributes, smartphones were found as an attractive platform for the development of portable instrument aiming at public health safety in recent years. These instruments largely cover colourimetric and microscopic based analysis but more advance optical detection technique such as spectroscopy has begun to receive much attention. The following section will present a brief history of smartphone usages in public health safety applications in the form of different types of scientific instrumentation.

1.2 Smartphone Instrumentation in Public Health Safety: A Brief Review

It is less than a decade ago when smartphone-based instrumentation took off to perform scientific analysis and is now becoming a burgeoning research topic aiming to serve many public health safety applications. The largest part of these applications deals with measurement of direct biological samples which were initially led by simple colorimetric and microscopic based demonstrations. With the advancement of mobile CMOS camera, processing capability and availability of integrated optics, more advanced measurements such as spectroscopic analysis are now performed by smartphones. This section will outline a brief history of smartphone-based instrumentation mainly in some major categories—colorimetry, microscopy, intensity-based fluorimetry, spectroscopy, and surface plasmon based sensing—focusing the range of achievements in public health safety.

1.2.1 Smartphone Colorimetry

Smartphone colorimetric instrumentation is based on direct imaging color information of samples onto the smartphone's CMOS image sensor which is relevant to the presence of a substance or analytes in the sample. From the beginning of smartphone instrumentations, this approach has been utilized in most of demonstrations due to simplicity of the method and the excellent detection capability of color information by a smartphone camera and their reproduction by adjusting the red, green and blue LED emission on the screen. In addition, this has proved to be a versatile tool capable of rapid on-site field detection of health critical information from biological samples. Further enhancement in smartphone colorimetric detection has been achieved with the integration of microfluidic paper based devices into smartphone platform which reduce the complexity associated with sample processing and made the instrument user friendly in field applications [19].

The earliest work in smartphone colorimetric detection was performed by digitizing the color information from a microfluidic paper device having different assay zones, where each zone is designed to react with either protein or glucose from urine samples [20]. The presence of these parameters changes colors of the paper strip which are then captured using the phone's camera. Although the feature phone used in this work was not capable enough to process the color information, its communication capability was utilized by sending the captured images as a multimedia file from testing location to a laboratory computer to be analyzed using dedicated software run by a healthcare professional. The test results were sent back to the patient's phone for immediate awareness about their health condition. This pioneering work not only confirmed a simple smartphone colorimetric demonstration but also proved the capability of smartphone camera to be useful for much more advance optical instrumentation.

This concept was immediately followed by many research including colorimetric and microscopic measurements that took advantage of improvements in smartphone's processing power, making possible computationally intensive analysis on the actual smartphone device itself [21–23]. In addition to this, advanced detection algorithms have been applied sometimes to improve detection accuracy, optimize computing speed or even to extend the battery life-cycle. By combining these attributes on a smartphone colorimetric platform, detection and quantifications have been performed for various disease biomarkers such as the ovarian cancer biomarker [24], HIV virus [25], HE4 [26], blood sugar and acidity level [27, 28] and so on.

Smartphone instrument in public and field-portable applications require consistent and reliable operations. However, the most challenging issue found in direct colorimetric imaging in such applications using smartphone cameras is the variation of ambient illumination which introduces significant errors in measurements. To address this challenge, a subsequent work introduced color calibration algorithm using the chromatic value of a 3D color model that uses a combination of three color values close to the RGB instead of the direct RGB color model [28, 29]. In another work, adaptive color models and correction algorithms, suitable to a target

application, have also been applied to make possible the detection of multiple analytes (pH, protein, glucose etc. in urine sample) from a single test strip [30]. This urine test strip has multiple active zones each dedicated for single parameter detection. Colorimetric techniques utilizing the cameras of smartphones have also been applied to the detection of a whole host of other health critical information both from direct biological samples and other sources. For example, it is now possible to detect cholesterol level in human blood [31], Kaposi's sarcoma associated herpesvirus from raw biopsy samples [32], cholinesterasemia [33], hemoglobin concentration and HIV antibodies [25], vitamin D in blood [34] etc. Numerous examples have been noticed on the detection of *E. coli* bacteria and *Salmonella*—two major factors cause the largest percentage of food-borne diseases—from environmental sources like drinking water, milk, meat or other foods. The detection of environmental sources that directly impact the public health life includes pH in water [35–37], bromide ion in wastewater [38], chlorine concentration in fisheries water [39], metal ions in ground water [40] etc. Furthermore, the colorimetric detection is also found useful in food industries where it can now be deployed for a range of uses such as the pH measurement in sweat and saliva [27], determining banana ripeness [13], grape variety and oxidation status of red wine [41] etc.

In addition to color correction and image processing, a great deal of hardware design has been applied to take the smartphone colorimetric instrumentation to its current stage. In particular, 3D-printable custom designed chambers have been reported in many later works that have been taken to address the issue of background noise interfering with measurements. The use of such a "dark box" blocks ambient light reaching the camera sensor and unexpectedly biasing results. 3D printing is such a technology that offers the possibility that anyone, anywhere in the world can produce any object they need on demand. This tool has been used by researchers in many applications such as the detection of salivary cortisol [42], H_2O_2 with bis(2,2,6-tri-chlorophenyl)oxalate [43], pesticide thiram [44], bile acids and cholesterol from serum and oral fluids [45], blood cells [46] etc. Further advancements on smartphone colorimetric instrumentation have been made by adding a reference into the measurements to greatly reduce the error introduced by background light fluctuations. In this approach, a section of the sample image can be used [14, 47] or the image of the reference solution can be taken directly to normalize the data obtained from the sample [48]. There has also been a significant research focus on improving detection sensitivity, with significant enhancements achieved from proper sample preparation techniques [49, 50]. For example, plasmonic-based gold nano-particles (AuNP) have been added with an aptamer-based colorimetric assay to enhance the emission [51, 52]. The AuNP has also been added into paper microfluidic strips to enhance the emission [53].

From the very first demonstration to date, colorimetric-based smartphone instrumentations are found as the most versatile and popular technique for point-of-care detection and still continuing its implementation in numerous application for public health safety. Some of them have already reached to a matured stage to be useable publicly. A range of colorimetric analyzer using smartphone camera as a detection and procession platform is under way to reach in the market [54].

1.2.2 Smartphone Microscopy

In addition to simple colorimetric imaging, other scientific instrumentations have drawn significant attention utilizing the in-built capabilities of smartphone. The second approach that has been most widely used in public health safety applications is the smartphone microscopy. Microscopy is one area which has drawn significant attention for the diagnosis of many diseases, especially for infectious diseases such as malaria and tuberculosis [55–60]. As like in direct colorimetric imaging, there are many examples on smartphone microscopy that use ambient light to illuminate samples [61]. However, most commonly reported smartphone microscopy demonstrations use external light sources at proper orientation [55]. The 3D printing technology has been leveraged again in multiple demonstrations for low-cost fabrication and avoiding the effect of ambient illumiation during imaging. The image collection on the CMOS camera sensor is achieved by adjusting the focus of an external lens in an optical axis with the cameras in-built lens - all fitted within a 3D-printed enclosure [56–60]. Both bright-fields as well as fluorescent microscopy have been demonstrated over time using smartphone's CMOS camera [62]. Significant improvements on both spatial resolution and field-of-view (FOV) have been recorded over the time. The application of these instruments are particularly focused on biological analyses such as blood cells [56, 62], tuberculosis-infected sputum samples, water-born parasites [62], single DNA molecules [63], *E. coli* concentration [49], freshwater micro-organisms and Salmonella [64].

1.2.3 Smartphone Fluorimetry: Intensity Fluorimeter

One of the major challenges in smartphone-based optical sensor platform is the availability of stable light sources required to illuminate samples uniformly. Although the use of ambient illumination has been reported in both colorimetric and microscopic demonstrations [30, 61], for consistent and bright illumination, additional sources such as LEDs or laser diodes (LDs), are required in most applications [48, 49, 65–67]. The use of additional light sources offers the possibility of selecting specific spectral lines and power levels, therefore, opens up other applications such as fluorescence excitation.

Measurement of fluorescence intensity on a smartphone platform is of the particular interest given the range of biomedical sensing applications. This was first demonstrated by utilizing the phone AMOLED display screen as an excitation source which has emission at distinct red, green and blue spectral bands that can be selected and controlled by adjusting their driving currents from a smartphone app [68]. For example, the green LEDs can be selected to excite the fluorescence of a Rhodamine dye [68, 69]. In this work, the fluorescence intensity was imaged onto a second smartphone camera. Smartphone screens have also been used as optical source in a range of other applications [69–71]. For example, the screen LEDs has

been utilized to measure angle resolved surface plasmon resonance (SPR) as reported in [71]. In subsequent works, fluorescence measurements were demonstrated in a number of smartphone instrumentations of different types. Smartphone microscopic instrumentation has been greatly advanced after taking the advantage of labeling samples with different fluorescent markers as a signal tag. This has proven to be an effective approach for improving the resolution of microscopic images obtained using smartphone cameras [69–73]. To this end, smartphone-based fluorescent microscopes can actually offer higher resolution than that of a bright-field microscope [74]. Using fluorescence markers, it has been possible to achieve unprecedented resolution to detect DNA, viruses, and nanoparticles [72, 73] using a smartphone camera. However, adjusting the focus of an external lens in conjunction with the in-built camera lens has always been a challenge. As a result, it has become more convenient to measure simple fluorescence intensity, as opposed to capturing a full image. A stand-alone device has been designed with an external photodiode and LED, (instead of using the phone's camera and source) with a microcontroller to perform fluorescence intensity detection [75]. In this device, the phone was used only to control and display the measurement via Wi-Fi connection. Many other groups have also demonstrated smartphone-based fluorimetry using the phone camera instead of an external photo-detector or second phone camera for a wide range of public health diagnoses [49, 76–79]. Paper microfluidic devices with fluorescent biomarkers have also been used with smartphones for identification of viruses and bacteria [80]. For example, by utilizing the intensity of green fluorescence, the sensor platform can detect the nucleic acids of Salmonella below its infectious doses. Smartphone cameras have also been used to quantify fluorescent quenching signals of quantum dots (QDs) in the RGB channels of the smartphone camera [79].

1.2.4 Smartphone Spectroscopy

The method of direct colorimetric or fluorescent imaging of samples using a smartphone camera does, however, have its limitations. One major drawback is that the spectral resolution is limited to three specific color bands defined by the red, green and blue filters of the camera's CMOS image sensor. However, by exploiting the high resolution pixel array used in a smartphone's CMOS camera, it is possible to utilise multiple pixels for simultaneous detection of individual wavelengths emission within the whole visible spectrum. This can be achieved by adding a dispersive element such as prism or diffraction grating into the system to disperse light of a broadband source across the CMOS sensor area. For example, white light emission would be dispersed into a continuous spectral spread across the sensor, each pixel detecting the intensity of a narrow spectral band [81]. Integrating across the width of the sensor, the values from each pixel can be processed to plot an intensity spectrum of the emission. The principle has been utilized to demonstrate smartphone spectroscopic instrument which opens up the possibility of performing much

advance measurements for a range of potential applications in public health safety. To this end, a smartphone spectrometer was demonstrated by placing a visible transmission grating over the window of a phone camera to serve as a dispersive element [82]. In that demonstration, the light from an external broadband source was collimated using a PVC collimating tube before reaching the grating surface. The diffraction of white light from the grating was imaged onto the CMOS camera sensor. The image processing, required to generate a spectral plot of wavelength (λ) vs transmittance (S), was achieved with software program run by a desktop computer. Calibration of the wavelength scale along the diffraction direction was performed against the emission spectrum of fluorescent lamp, which has multiple sharp emission peaks at different wavelengths. A spectral resolution ($\delta\lambda$) of this initial set-up was obtained as 10 nm, which can be improved by a factor of 2 using an optical slit. Furthermore, this work demonstrated applications of such a device to determine blood oxygenation levels, achieved by recording differences in visible light absorption by the human finger at two wavelengths characteristic of oxy- and deoxy-hemoglobin.

There has been a continuous research drive to progress the functionality of smartphone spectroscopy beyond simple colorimetry and imaging. This has been reflected in the past 5 years by a growing number of smartphone instruments capable of either absorption or fluorescence spectral measurements [83–97]. The application areas range from biological [79, 84, 93] and environmental analysis [85] to food quality monitoring [94, 98] and educational purposes [90]—all focusing to serve the public health safety assurance. 3D printing is continuing to be harnessed by researchers in the field for housing the components of smartphone instruments. For example, in the work of [83], a 3D-printed cradle holder was used to hold and align all optical components including the diffraction grating, collimating lens and sample. In this work, the fluorescence of a molecular beacon probe has been collected and analyzed to detect micro-RNA sequences, which exhibits comparable performance to that of a laboratory spectrofluorimeter. Here, the fluorescence spectrum measurement was performed across a broad wavelength span, $\lambda \sim 500$ to 700 nm, rather than three RGB point detections. A similar design is also used by transmitting light through the sample and measuring the absorption of an enzyme-linked immunosorbent assay [84]. In another demonstration, the internally-reflected light inside a glass prism generates an evanescent wave on the prism surface on which various absorbing dyes are placed. The output light of the prism is then diffracted onto the smartphone camera using a transmission diffraction grating [86]. Similar instrument has been also applied for dye assisted pH measurement of colourless aqueous media [87]. A more recent example of compact miniature smartphone spectrometer is the GoSpectro, which has been developed and already commercialized by ALPhANOV [99]. Similar to other arrangements, an external attachment to the smartphone camera unit is designed to hold the transmission grating and other optics for measuring emission, absorption, reflection and transmission of light sources, optical filters and various colored objects. Optical resolution is reported as 10 nm with a spectral accuracy of 1 nm.

One of the common issues in designing high performance miniature spectrometers is that important figures of merit such as resolution and sensitivity often suffer as a result of making the system compact and portable. One approach to address this issue is to replace multiple components with a single part that can perform multiple functions as well as save space. For example, a G-Fresnel device, which is capable of performing multiple functions such as optical dispersion and collimation, has been used in a smartphone spectrometer reported in [96]. The G-Fresnel device can be fabricated in a similar way to that of a negative mold of diffraction grating [102]. By using this device, the spectrum of a Bradford assay was analyzed, as a proof-of-principle, to determine the concentration of proteins in solutions.

The common approach noted in almost all of the smartphone spectroscopic devices reported to date is that they are designed for single-channel detection. This means that only one sample can be monitored or measured in each measurement. However, for on-site diagnostics in the field, there is often the need for simultaneous analysis of multiple samples. In smartphone spectroscopy, the work of [95] is the only published work so far that has aimed to address this issue. Here, the spectrometer uses a micro-prism array that increases the FOV by tilting incident light at different angle each makes a single channel and detecting signal simultaneously from one column of a 96-well microplate. The demonstration validated the performance of this multichannel smartphone spectrometer with a large FOV via measuring the concentrations of protein and immunoassaying a type of human cancer biomarker.

1.2.5 Other Smartphone Instrumentations

In addition to the above demonstrations, some other types of smartphone instrumentations involve SPR based sensing [71, 100–103], electrochemical sensing [104–107] etc. In SPR sensing, optical illumination (from the smartphone's screen, LEDs etc.) was adjusted to excite the plasmon on a metal coated surface. The reflected light carries the angle resolved SPR signal intensity, the image of which is captured on the smartphone camera [71, 100]. The light from source to detector can also be guided through an optical fiber demonstrating a SPR optical fiber sensor on a smartphone [102, 103]. SPR-based smartphone devices have been shown to be capable of detecting cancer biomarkers [71] or other antibody binding to a functionalized sensing element on the surface of the fiber [103].

In the case of smartphone electrochemical instrumentation, this requires electrical potential to initiate a chemical reaction and generate a detectable signal emission. In smartphone instrumentation, most of the electrochemical detection to date has been performed by detecting luminescent emission, called electrochemiluminescence (ECL), from the sample generated by a potential supplied by the smartphone [105–107]. For example, orange luminescence emission generated from tris(2,2′-bipyridyl)ruthenium(II) ($Ru(bpy)32^{+}$) in a Zensor paper microfluidic device is monitored on a smartphone camera, working as a photodetector [104].

Although an external supply was used to deliver the step potential of about 1.5 V needed to generate luminescent signal, ideally this could be supplied from the phone's battery. In later work, the ECL reaction was controlled by supplying potential through an audio jack of the smartphone and playing an appropriate audio file [105]. Potential via audio jack is also used for the ECL measurement of nitride concentration in water [107]. However, variation in the audio signal output across different brands and models of smartphone is a limitation for the generation of ECL excitation [106]. This has been addressed later by using a simple tone-detection integrated circuit to switch power source from the phone's universal serial bus (USB) 'On-the-Go' (OTG) port, using audible tone pulse played over the phone's audio jack [106].

1.3 Research Opportunities on the Track

The capability of smart sensing in the field using cheap, hand-held portable instruments is a highly attractive prospect with enormous potential in areas such as healthcare, bio-science and the food industry. Traditional assessments equipped with non-portable bench top instruments, based on collection of samples, transportation to a laboratory, and subsequent measurement in a controlled setting, is cumbersome not to mention expensive. Whilst some may be internet enabled, they are generally not accessible being without global connectivity and largely unable to perform cloud-driven analytics—a much needed feature for adapting with the next generation IoT-based health diagnosis systems. A system that would enable self-contained low-cost measurements in the field while providing wireless connectivity, data analysis and rapid detection would be of huge benefit to many areas particularly in public health safety. Portable smartphone instrumentations are continuing to be receiving strong research focus given their capability of addressing these issues mentioned above. There has been rapid growth in the research of smartphone instrumentation over the last decade and many groups have begun to commercialize a range of analyzers [5, 108], most of which are based on simple colorimetry and imaging. Although a lot of efforts have been made by many research groups on improving throughput, resolution, and detection sensitivity, there is still tremendous scope for improvement of current instruments and the development of other devices as smartphone technology continues to evolve at a tremendous pace. This book presents the demonstrations of a number of smartphone instruments that focus on addressing the issues as discussed below.

- **Self-capability**: The majority of smartphone-based optical sensor instruments reported to date generally use the in-built CMOS camera as a detector but also rely on the availability of optical sources and other expensive components such as diffraction gratings, fibres, lenses and so on [48, 49, 82–103, 109–111]. In addition to increasing the functionality, availability of these components and their longer functional life-time in many resource limited settings are essentially

important. Furthermore, the optical sources used in most of the current generation smartphone devices are external lamps, LEDs, LDs etc., which are powered by an external non-rechargeable battery [82–87, 109–111]. This limits the device's credential where it is needed in a resource limited setting particular example would be a rural area or agriculture field where power supply is not easily obtainable. There have been a number of smartphone-based sensing demonstrations which have tried to address this issue by utilizing the smartphone display illumination as an optical source [68–71]. Although the broad spectral illumination from a smartphone display has been utilized for some specific applications by selecting the individual RGB emission, the overall irradiance is too low for most applications. There is also a higher degree of mechanical engineering involved in their practical implementation because the camera and display source are often not collocated or on opposite sides of the smartphone [68, 69]. Furthermore, the dispersive elements used in most of the instruments (transmission grating [82–84], prism [86], G-Fresnel device [93] etc.) are expensive and not easily replaceable by users in the field.

- **Multi-functionality**: It should be noted that considerably less works have been reported on smartphone spectroscopy compared with direct colorimetry or imaging based techniques. However, spectroscopy, particularly absorption and fluorescence spectroscopy are extensively used in a wide range of analytical applications in chemical and biological science. Although there has been some recent works that took the opportunity to demonstrate these measurements on a smartphone platform, the functionality of devices is limited to a predefined function either for absorption or fluorescence measurements. However, many applications in resource-limited environments often require instruments to offer multiple functionality using the same hardware. In this case, the capability of performing both absorption and fluorescence measurements on a single platform will reduce a lot of resources and complexity. Recently, this has been addressed to some extent by increasing FOV and adding multiple dispersive elements to cover the measurements of multiple samples simultaneously [95], however, they are also limited to specific functions.
- **Spectral calibration**: The function in many of the smartphone-based spectrometer is limited to capturing images of the diffracted light whereas processing and quantification of results are done by a customised program on a computer [86, 87, 90]. More importantly, the spectral calibration does not consider the color correction factors added by smartphone camera imaging [82–84]. In order to get the accurate data of color measurement, it is needed to read the RGB values which is detected at the CMOS camera input rather than the processed image on the screen. However, the smartphone camera imaging does not work on that way rather adding correction factor on its three color channels according the sensitivity of human eye at different wavelengths. To get the accurate data, one needs to read the camera RGB values or apply a dynamic color calibration algorithm that can recalibrate the whole spectrum against a standard instrument.
- **Application diversity**: Another drawback of commonly available instruments is that they are only capable to work with sample in a specified form. For example,

majority of them are based on direct imaging or recording emission from a sample, typically liquid, in a specified cuvette cell [82–84, 86, 87]. However, reflection spectroscopy of solids or even arbitrary samples is often more important in industrial and agricultural sectors or within a human body. There are a growing number of micro-spectrometer suppliers who aim to cover those sectors using optical fiber-coupled portable spectrometers with separate light, power, and computer components [112, 113]. There have only been a few smartphone-based devices with a fiber coupled system but their functionality is still limited to imaging only [114]. The integration of multimode optical fibres into smartphone spectrometers to improve light collection will open enormous opportunities in food and agricultural health analysis or even biomedical endoscopic applications.

- **Time-resolved and thermal analysis**: Another common limitation of all smartphone based fluorescence measurements reported to date has been the capability of performing steady-state measurements only. Further advanced measurements such as time-resolved fluorescence are often important to explore and understand the evolution of fundamental information from different molecular process in chemical and biological science. Many of these processes are often influenced by different physical parameters, usually involving temperature. Therefore, in addition to time-resolved measurements, temperature based analyses are also significantly important to investigate various properties. However, these analytical capabilities tend only to be offered by heavy benchtop set-ups connected with a separate temperature controlling unit—there is certainly scope for smartphone instruments to offer more practical and deployable alternatives.

1.4 Lab-in-a-Phone: The Technology Outlined in this Book

The material presented in this book contributes to emerging areas of smart sensing, identifying some key challenges and proposing solutions through the development of the "lab-in-a-phone" technology [115–133]. In contrast to some stand-alone smartphone based measurement tools that may already enable immediate measurements on-site, the proposed instrumentation makes full use of the array of self-contained phone features. These features include internal battery power, optical source, connectivity, and general ubiquity of smartphone systems - a convenient approach that places priority on cost-effectiveness, portability, and ease-of-use. By combining these attributes, a number of smartphone-based devices have been developed which include a smartphone intensity fluorimeter, temperature-tunable intensity fluorimeter, multi-functional spectrometer and optical fiber spectrometer.

- **Smartphone intensity fluorimeter:** The first work to be presented in this book is a smartphone intensity fluorimeter. It has been developed by combining the attributes of a smartphone's in-built flash LED as an optical source and the CMOS camera as detector [115, 117]. By using the white LED, the instrument

not only avoids the requirements of an external source and necessary power supply but also overcomes the issues associated with low irradiance and large mechanical hardware in using other in-built sources such as AMOLED display [68–71]. Furthermore, the broad spectrum of the white LED can be filtered selectively in order to select any suitable excitation band for different application specific fluorescence sensors. For instance, the blue filtered emission (λ ~ 450 nm) has been utilized to excite a pH-responsive 4-aminonaphthalimide fluorophore [123], which fluoresces in the green region in the visible spectrum. The pH-responsive green fluorescence at λ ~ 530 nm is readily detected using the smartphone camera and a customised RGB app. In order to improve accuracy, reference measurements are included into the system and the emission is calibrated to enable smartphone for quantifying pH of different types of water samples (environmental and drinking) at various locations around the city of Sydney [118, 119].

- Beyond monitoring the water quality at any specific location, the smartphone intensity fluorimeter also demonstrates the capability of generating a real-time pH map by collecting data from multiple points with the GPS coordinates of the corresponding locations [119]. By performing such networked analysis, the smartphone fluorimeter also demonstrates a new security concept- network environmental forensics utilizing the potential of novel smartgrid analysis with wireless sensors for the detection of potential disruption to a public water quality. The demonstration is also applicable for other types of applications reported in this book as well as in the literature.
- ***T*-controlled smartphone fluorimeter:** In addition to steady-state measurements, time-resolved fluorescence measurements is significantly important especially for those applications where fluorescence is dependent on physical parameter such as temperature (T). A smartphone intensity fluorimeter capable of measuring time-resolved intensity at various temperatures have been demonstrated for the first time [125, 126]. The temperature of the sample has been controlled by using a Peltier device powered by smartphone through an Arduino microcontroller connected with a temperature sensor, cooling fan and the excitation source. Data sending and receiving are performed from the smartphone app via the Bluetooth communication with the microcontroller. The temperature dependence of four emitters are characterised as a proof-of-principle. The instrument will allow the understanding of different molecular processes, for example, it was used for time-resolved and temperature dependent fluorescence studies of chemosensor dyes - a novel way to distinguish multiple metal ions from a sample [127–129]. The study can also be useful to design and understand molecular optical devices and molecular machines [130, 131].
- **Smartphone spectrometers with "dual" functionality:** The next smart instrument to be demonstrated here is a smartphone spectrometer with "dual" functionality. To enable measurements over a specific spectral range rather than a specific wavelength, a dispersive element is added into the system to demonstrate a smartphone spectrometer [85, 120]. The spectrometer utilizes a high

resolution home-made dispersive element fabricated inexpensively using a low-cost polymer and nano-imprinting technology, greatly reducing the need for expensive optical components. Other equally efficient, but cheap, dispersive elements such as a DVD surface can also be utilized to demonstrate the further low-cost instrumentation instead of the expensive and bulk optics used in conventional methods. By integrating a blue or UV excitation source into the white LED circuitry and powering by smartphone battery the entire system remained self-contained, whereas multiple functionality such as combined "dual" absorption and fluorescence measurements are demonstrated for the first time [85]. Functionality of the smartphone spectrometer has been demonstrated by measuring both absorption and fluorescence spectra of pH- and metal ions responsive chemosensor dyes [121, 122].

- **Optical fiber smartphone spectrometers:** Considering the importance of measuring reflection from solids and surfaces, an optical fiber bundle is added into the system that demonstrates an endoscopic smartphone spectrometer [98, 123, 124]. The endoscope allows transmission of the smartphone camera LED light to a sample, and collection from sample to the detector therefore removing complications from varying background illumination whereas providing access to some places that are difficult to access. This device is suitable for a number of applications in agricultural and food industries providing access to measure spectra and assess the quality of foods in the field [94, 98]. The proof of principle operation has been demonstrated by measuring the visible absorption spectra of apples for analyzing essential pigment contents [98]. Beyond absorption measurements, UV LEDs are added into the system to generate fluorescence and are powered by smartphone's battery to retain the self-capability of the instrument [94]. Fluorescence spectroscopy using the smartphone spectrometer allows characterization of vegetable oils [94]. Thermal- and photo-degradation of olive oils have been understood using the instrument [134].

In order to implement the lab-in-a-phone technology, the actual prototype devices for all of the above instrumentation have been developed by using a low-cost fabrication technique. The 3D designs of the instruments have been done on an Inventor software platform AutoCAD. Their designs are optimized to collect maximum signal intensity on the detector while reducing background scatterings and to hold all optical components properly aligned with the optical source and detector.

Chapter 2
Smartphone Intensity Fluorimeter

2.1 Introduction

Fluorescence is the photophysical property of a material whereby molecule of the material emits light at a specific wavelength when irradiated by light of a shorter wavelength [135]. The measurement of fluorescence intensity (I) allows the determination of the presence of fluorophores (polyatomic fluorescent molecules) and their concentration. They have a wide range of applications particularly in sensing across a range of chemical and biological areas. A basic understanding of fluorescence principles, fluorophores properties, measuring instruments and techniques is a prerequisite to the study of a number of biological systems.

Although fluorescence emission is regarded as highly sensitive and specific to target molecules, their measurements in filed particular in remote areas are prone to the effects of different external parameters. As a result, field-portable fluorescence measurements have a great significance to a number of biological and environmental applications directly and indirectly linked to our health safety. In order to enable such measurements, miniaturized fluorimeter devices have recently been receiving more and more research attention, many of them harnessing advantages offered by a smartphone platform [68–79]. With their highly sensitive CMOS cameras, smartphones have so far been used as a fluorescence detecting devices, relying on externally-powered light sources such as xenon arc lamps, LEDs, laser diodes etc. to provide excitation sources in most of the smartphone fluorimeter systems [48, 49, 65–67]. However, the need for in-built optical sources is of critical importance for the development of an entirely field-portable and self-contained fluorimeter. In some cases, this has been addressed partially by utilizing the in-built optical sources such as the AMOLED screen of smartphone [68, 69].

This chapter demonstrates the design, fabrication and application of a self-contained smartphone fluorimeter—a first demonstration of the lab-in-a-phone technology having entirely field-functioning capability [114–118]. The fluorimeter design maximizes the utilization of most of the smartphone's in-built components

A. Jamalipour, M. A. Hossain, *Smartphone Instrumentations for Public Health Safety*, Wireless Networks, https://doi.org/10.1007/978-3-030-02095-8_2

including the optical source to make the device fully field portable and independent of other components or instruments. In this chapter, the step-by-step fabrication process will be discussed. After calibrating the fluorimeter, the performance of the device will be analyzed by demonstrating pH measurements of water from different sources, particularly environmental and drinking tap water, in the fields. Traditional approaches for accurate pH measurements of water is generally performed using a sophisticated glass electrode connected to an electronic meter (microprocessor based) that needs to be repeatedly calibrated with standard buffer solutions [136]. This compromises their ease of use especially in resource-limited settings, for example when someone need to check their drinking tap water condition at home or an environmental scientist is in a rural area and perhaps working in adverse weather conditions. A smartphone fluorimeter, in contrast, is capable running the measurements without any repeated calibration and less user interpretation. The capability of the smartphone fluorimeter system for networked monitoring of water quality within a public water supply system is presented and demonstrates the Internet-of-Things (IoT) capability of the system. This application also demonstrates a security concept for public water supply systems where rapid identification of any hazardous disruption could be achieved and early warnings issued. Furthermore, with the IoT capability, water supply disruption can be easily mapped across multiple locations, greatly assisting the location of the disruption caused.

2.2 Basics of Fluorimeter and Components Available in a Smartphone

Fluorimeter is a device used to measure parameters of fluorescence: its intensity and wavelength distribution of emission spectrum after excitation by a certain spectrum of light (typically at higher wavelength) [135]. By means of an intensity fluorimeter, the instrument is capable of measuring the fluorescence intensity at a particular wavelength (λ). The main components used in a typical fluorimeter system are the optical source with integrated optical components (such as lens, mirror, filter, fibre, coupler etc.), a sample chamber (typically cuvette), and highly sensitive detectors (such as CMOS, CCD arrays, photodetector) [135]. Among them, the optical source is a key component which is used to generate a broad band of electromagnetic radiation needed to excite fluorescence. Ideally the source should yield a constant intensity over all wavelengths with low noise and long-term stability. The most common types of light sources used for fluorimeters are lamp sources, such as xenon arc lamps, which give a relatively uniform intensity over a broad spectral range from the ultraviolet to the near infrared. A band pass filter (referred to as an excitation filter) is used in front of the light source (Fig. 2.1) to attenuate the unwanted emission and transmit only the spectral range required to excite the fluorescence. The fluorescence emission is directed onto a detector through a second band pass filter (called an emission filter) that removes any background reflection from the sample.

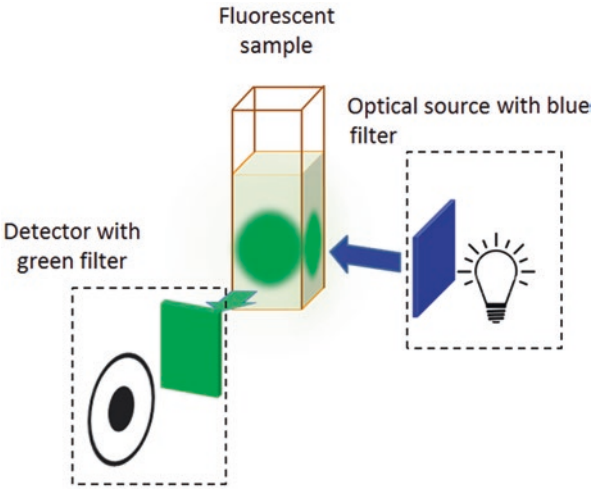

Fig. 2.1 Schematic of basic fluorimeter configuration

For accurate fluorescence detection, high sensitivity photodetectors such as photomultipliers or charge-coupled device (CCD) cameras are commonly used. Other optical components include lenses, mirrors or other collimating optics those are used to improve light collection either from source to sample or from sample to detector as discussed in the following chapter.

In addition to other internal components, the lab-in-a-phone technology demonstrated in this book has placed a particular emphasis on the utilisation of the smartphone's in-built optical source. In traditional benchtop fluorimeters, xenon, deuterium arcs and tungsten-halogen lamps are widely used as optical sources [135]. However, compact low-cost sources are mostly preferred for portable fluorimeter devices. Therefore, switching between optical source such as LEDs and LDs with external power supplies is the approach taken by published works in the area to date [48, 49, 65–67]. LEDs are compact, can be placed close to sample, even stacked together for multiple functionalities and in certain set-ups can allow the central emission wavelength to be tuned varying supply voltage. Furthermore, unlike a xenon lamp, LEDs do not generate significant infra-red, thus negating the requirement for an additional heat filter [135]. In order to obtain multiple excitations, an array of LEDs with different wavelengths can be used. Other option for optical sources could be LDs which emit monochromatic radiation, in contrast to broadband emission, and generally offer much higher powers than LEDs.

The use of LDs is convenient because the output is collimated and can therefore be easily directed with mirrors or readily focused with lenses. Further advantages of this semiconductor device, in contrast to conventional arc lamps or incandescent lamps, are the pulsation or modulation capabilities. In terms of power requirements, LEDs and LDs in most of the smartphone based sensing devices are driven by external power supply such as non-rechargeable batteries [48, 49, 65], as opposed to being driven by the smartphone battery itself, which isn't always desirable especially when taking measurements in the field.

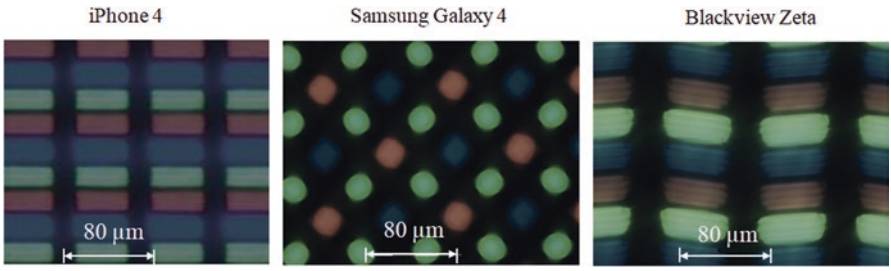

Fig. 2.2 Microscopic image of the AMOLED display of smartphones of different brands

This issue has been partly addressed in early generation smartphone fluorimeter by using the in-built AMOLED display as an optical source [68, 69]. Like other LED display devices, smartphone screens have a matrix array of red, green and blue (RGB) LEDs arranged in a regular pattern making up each pixel on the display screen. Figure 2.2 shows the microscopic images of the AMOLED patterns of some smartphone models from different brands. Using a smartphone app, the emission of the LEDs can be controlled by adjusting the driving current to each of these LEDs, thus enabling the generation of any arbitrary color. It has been shown that this screen emission can be selected from a smartphone application (app) and used as a fluorescence excitation source [68].

2.3 A Smartphone Intensity Fluorimeter: Materials and Methods

This section mainly demonstrates the development of a smartphone intensity fluorimeter through the optical design and prototype fabrication. The operation of the instrument has been demonstrated using a customized smartphone application (app). In addition, the proof-of-principle application and performance have been demonstrated by fluorescence intensity measurements.

2.3.1 Optical Design and Operation

The smartphone intensity fluorimeter was designed by utilising the self-contained excitation source, power supply and detector offered by the smartphone. The optical layout of the smartphone fluorimeter system is shown in Fig. 2.3. The smartphone fluorimeter was designed considering the configuration of an Android-driven Kogan Agora HD smartphone (OS: Android 4.2; Processor: 1.2 GHz quad-core; Camera: 8MP, Display: 5.0″ IPS capacitive touch screen). Although the smartphone has similar spectrally pure display emissions as those reported in [68, 69], the arrangement

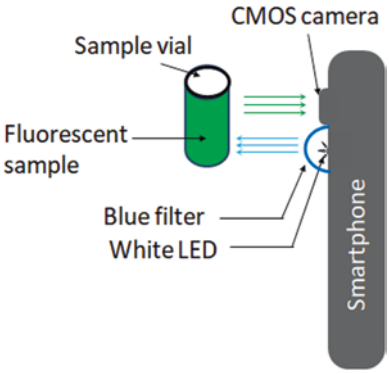

Fig. 2.3 Schematic of the smartphone intensity fluorimeter configuration (side view)

is somewhat simpler in terms of the optical source and detector locations. In this smartphone, the flash LED is located next to the camera of the phone, thus offering greater irradiance to the sample under test.

Furthermore, this approach avoids the need to use external sources as used in some demonstration of early generation smartphone fluorimeter [48, 49, 65–67] as well as mirrors or other beam deflection hardware in [68, 69]. This in-built source, integrated with a suitable driver circuit internally connected to the smartphone's battery, has a more consistent irradiance and is also collocated with the camera, allowing optimal illumination during imaging. Therefore, the primary optical source in the smartphone fluorimeter is the in-built white flash LED. The white LED of the smartphone offers a wide span of emission, $\lambda_{em} \sim 400$ to 700 nm that can be utilized, after filtering, to excite many fluorophores having significant absorption in the visible spectrum. In this case, a blue thin film filter ($\lambda_{peak} \sim 437$ nm) is placed over the white LED so that only blue light is transmitted in order to excite the sample placed in front of the LED. The sample is typically a liquid solution dissolved with an application specific fluoro-ionophore (details in Sect. 2.5) contained in a glass vial (2 ml).

The sample vial is also located in front of the smartphone camera and centred between the source (LED) and the detector (camera) to optimize the excitation as well as the fluorescence collection to the camera. The filtered emission from the source is centered at ~ 437 nm with a 3 dB bandwidth of $\Delta\lambda \sim 21$ nm, making it suitable as a fluorescent excitation for the specific chemosensor dye. The emission intensity of the chemosensor dye is sensitive to its concentration or responsive to some other parameters in the solution. For example, this blue filtered emission suitably fits within the absorption band of a pH responsive chemosensor dye as shown in the Fig. 2.4. Detail of the pH sensing mechanism has been illustrated in somewhere else (Sect. 2.5). The absorption spectrum of this dye spans over a bandwidth of ~ 55 nm with the peak absorption at $\lambda_{absm} \sim 440$ nm. The same LED can also be used to excite many other application specific molecular probes within the visible spectrum by using a tunable band pass filter. This can extend the fluorimeters' capability further, making it suitable for measuring multiple analytes on the same platform.

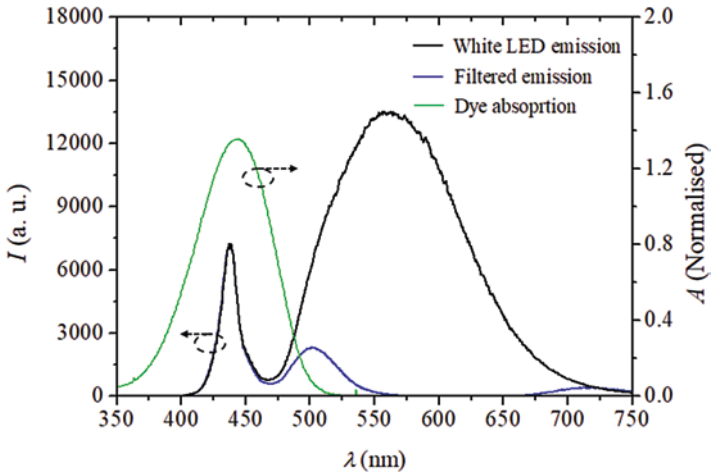

Fig. 2.4 A comparison of absorption spectrum of a PET type 4-aminonaphthalimide pH probe (**1**), 2-butyl-6-((2(dimethyl-amino)ethyl)-mino)-1*H*-benzo[*de*]isoquinoline1,3(2*H*-) dione with mobile source emission with and without a blue filter

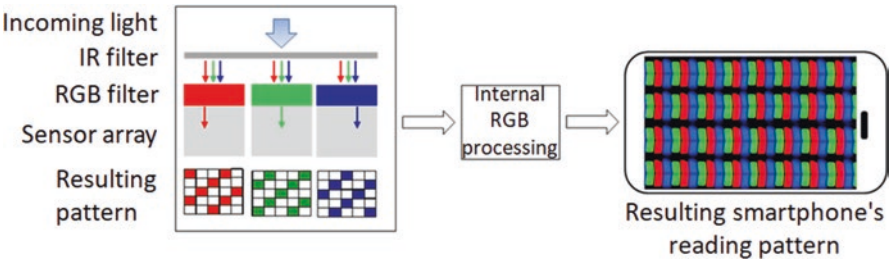

Fig. 2.5 Schematic showing colour image detection and reconstruction technique by smartphone CMOS image sensor

2.3.2 Smartphone Data Acquisition Technique

In the smartphone fluorimeter, the camera unit of the smartphone is used as the fluorescence detector, which reads and display results on the screen. The detection of fluorescence intensity by the smartphone's camera follows the same procedure as the reading of red, green and blue (RGB) intensity from a color image on the screen. This data acquisition technique on the screen can be demonstrated by the schematic presented in Fig. 2.5. The CMOS image sensors in the current generation smartphone is a Bayer sensor [29], which is a pixel array with red, green and blue filters arranged in a Bayer pattern as shown in Fig. 2.5 (left). Each pixel in the camera is filtered to record only one of the three colors; therefore, the data from each pixel cannot fully specify each of the red, green, and blue values on its own. To obtain a

full color image, various demosaicing algorithms can be used to interpolate a set of complete RGB values for each pixel. These algorithms make use of the surrounding pixels of the corresponding colors to estimate the values for a particular pixel. In the smartphone system, this value is recorded as an 8-bit number within 0 to 255 and manipulated to reconstruct the corresponding color image on a screen, which is also a matrix of red, green and blue LEDs arranged in a 2D regular pattern (also shown in the microscope images in Fig. 2.2). Therefore, the value of the fluorescence intensity on a smartphone camera is finally read as a RGB value on the smartphone screen which varies within 0–255. These RGB values can be read using customized app software. Detailed function of such a smartphone app demonstrating pH-responsive fluorescence intensity detection is presented in the Sect. 2.6.

2.4 Fluorimeter Design and Fabrication

A low-cost and easy fabrication of the smartphone intensity fluorimeter was possible with the help of 3D printing technology. This fabrication technology offers the possibility that anyone, anywhere in the world can build any object they need on demand. Recently, the technology has grown enormous interests in additive manufacturing industry and has great advantages in rapid fabrication and prototyping. The overall process of 3D printing involves three main steps. At first, a 3D model of the smartphone fluorimeter is designed using Inventor software (AutoCAD Inventor Fusion). The design is shown in Fig. 2.6. The smartphone fluorimeter mainly consists of a smartphone attachment which is denoted here as fluorimeter box and is designed to fit over the top of the camera unit. Within the fluorimeter box, a sample cell holds the sample vial at a distance of 3 cm far from the CMOS camera lens. The smartphone can be inserted from the left or right side of the attachment to place it such that the camera can be fitted suitably to the window dedicated to it. A suitable

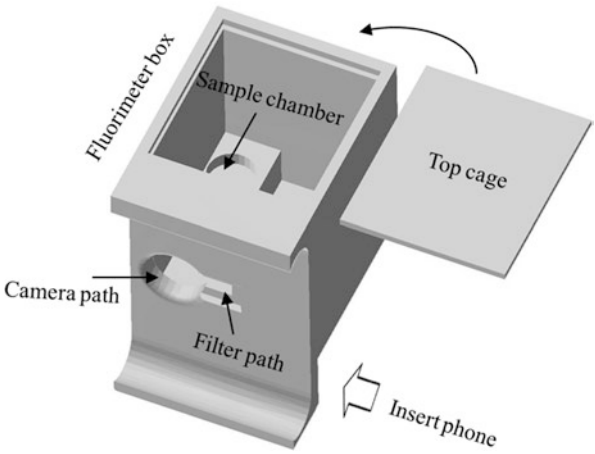

Fig. 2.6 3D AutoCAD design of the fluorimeter box

slot for the colour filter is positioned just next to the camera window so that it covers the flash LED illumination perfectly. To exclude the ambient light reaching the camera, the cell insertion side is closed using a suitable cover once the sample is in place.

In the second step of the fabrication process, the AutoCAD design is sliced using Simplify3D software which slices each coordinate of the 3D structure to generate a corresponding machine readable code (.gcode) to the 3D printer. The printing parameters such as printing resolution, temperatures, speed, all can be set for printing a specific material. Finally, the "gcode" file is uploaded to a 3D printer to fabricate the model by melting and deposition of polymer material in a layer by layer fashion. In fabricating the smartphone fluorimeter, low-cost acrylonitrile butadiene styrene (ABS) polymer material (filament diameter: 1.75 mm) of back color was used. The black color was chosen to avoid any unwanted reflection or stray light reaching to the camera while performing the measurements.

This simple design of the smartphone fluorimeter was capable of measuring fluorescence intensity by direct imaging of the sample on the camera. However, a reference is needed somewhere when the measurements of any particular sample can be affected by external parameters such as time, temperature etc. A reference measurement is also important to provide self-calibration of the intensity fluctuation. Therefore, the smartphone intensity fluorimeter, as described above, is upgraded by introducing an additional cell chamber to house the reference solution (Fig. 2.7). In order to further improve signal-to-noise ratio over the previous design, a green filter is also added on the fluorescence imaging path that helps to remove background scattering of blue light, a potential source of error. A schematic demonstrating the operation of a smartphone fluorimeter containing a reference is shown in Fig. 2.7a and the 3D AutoCAD design is depicted in Fig. 2.7b. The design contains a sample and a reference cell chamber in front of the camera and suitable slots for the color filters. The design is optimized for a Samsung Galaxy Express smartphone (OS: Android 4.1.2; Processor: 1.2 GHz dual-core; Camera: 5MP, Display: 4.5″ super

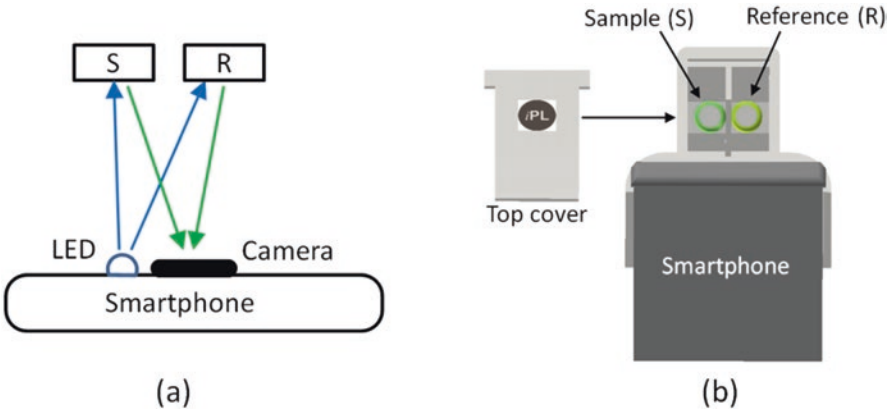

Fig. 2.7 Layout of the smartphone intensity fluorimeter with reference: (**a**) the optical configuration; (**b**) the 3D AutoCAD design

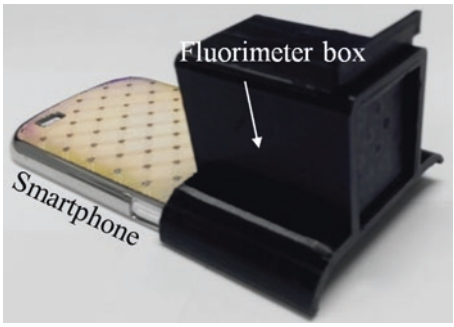

Fig. 2.8 The 3D printed smartphone intensity fluorimeter installed on a Samsung Galaxy Express smartphone. (**a**) Front-angle view and (**b**) back side view [118]

AMOLED capacitive touch screen), however, it can be also used for any other smartphones including the previously used Kogan Agora phone as well as on Tablets and iPads through simple modifications to the 3D-printed enclosure. In this design, a blue filter (λ_{peak} ~ 437 nm) is attached over the white flash LED to excite uniformly both the sample and reference cell located in front of the LED. A separating wall between them in the 3D design stops any stray fluorescence interaction between the sample and the reference. The top side of the fluorimeter box is similarly designed to be closed using a 3D-printed suitable cover once the sample and reference are in place.

The 3D-printed smartphone fluorimeter attachment installed on the smartphone is shown in Fig. 2.8. The fluorimeter attachment with all optical assembly fixes firmly to the rare facing camera unit of the smartphone. The unit is robust for transport, which keeps the sample well shielded from the outside, and excludes light from external.

2.5 Chemosensor Material: Properties and Applications

The smartphone fluorimeter is able to detect a wide range of biological and environmental chemicals properties such as acidity or alkalinity, presence of bacteria, metal ions concentrations and so on using the application specific chemosensor dye. In this demonstration, the fluorimeter relies on a pH-responsive probe (**1**), 2-butyl-6-((2(dimethyl-amino)ethyl)-mino)-1*H*-benzo[*de*]isoquinoline1,3(2*H*-) dione, which has absorption and excitation wavelength peak $\lambda_{abs/ex}$~ 440 nm with a 3dB bandwidth of ~ 55 nm overlapping well with the smartphone's excitation source (blue) as shown in Fig. 2.4. The demonstration of a pH probe has the benefits of rapid and reversible signal changes since protonation and deprotonation reactions occur faster than other chemical reaction such as complex formation with metal ions. Also, there is a large Stokes shift (emission in the green, at λ_{em}~ 500 nm and higher) noticed in their emission. The probes based on the 4-aminonaphthalimide fluorophore have some other advantages including relatively high quantum yields and high thermal- and photostability, reproducibly producing large signal changes and bright emission. Probes of this type have been applied extensively in sensing applications due to their bright and

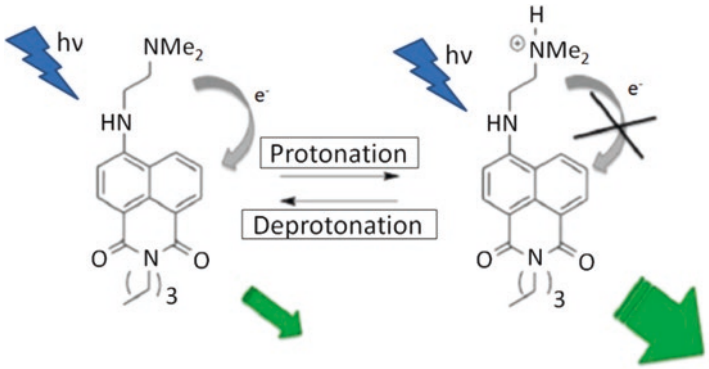

Fig. 2.9 Fluorescence switching mechanism of the pH-responsive probe 2-butyl-6-((2(dimethyl-amino)ethyl)-mino)-1*H*-benzo[*de*]isoquinoline1,3(2*H*-) dione [122]

robust spectral properties [137] and the ease of synthesis, enabling for the detection of a wide variety of analytes [138–142]. The synthesis process of this photo-induced electron transfer (PET) type dye can be found in [137]. The high quantum yield of the fluorophore is caused by a charge transfer (CT) from the 4-amino group to the naphthalimide, the electron acceptor as shown in Fig. 2.9 [143].

The green fluorescence intensity of the probe is low in the deprotonated form at higher pH as a result of PET from the dimethylamino-group (proton-acceptor) to the 4-aminonaphthalimide fluorophore (Fig. 2.9). As the pH of the solution decreases, protonation of the dye leads to an enhanced emission as a function of pH down to pH ~ 4 [143]. Ideally a dye can be found to work the whole range of pH (0–14) or dyes of this type can be engineered to work across all pH regions as required.

Another attractive feature of this probe is the thermal stability under typical environmental conditions—for example in Australia, environmental temperatures may vary from subzero to 50 °C. This is critically important for application in the field particularly in harsh environmental condition. Thermal robustness of the probe was confirmed experimentally at different pH values between pH ~ 4 and 11 where the variation in fluorescence response, measured on the spectrofluorimeter, was within experimental error over a temperature range of 22–40 °C shown in Fig. 2.10.

2.6 Smartphone Fluorimeter App

A RGB-based color detecting smartphone app is used initially to measure fluorescence intensity on the smartphone camera, although most of the instruments demonstrated here run with custom design smartphone app. A number of smartphone apps capable to analyse intensity using indifferent color models are available in the Google's play store. The "Color Grab" is such an app [144] which displays the RGB

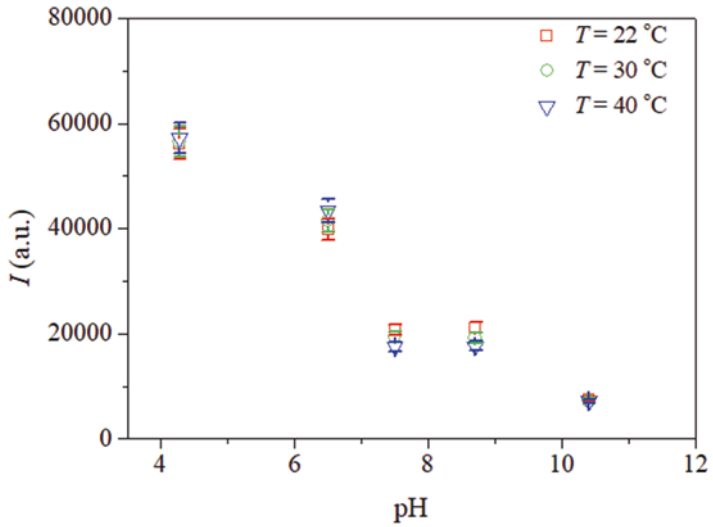

Fig. 2.10 Fluorescence intensity of the chemosensor with varying pH at three distinct temperatures. Within experimental error there is no significant change [115]

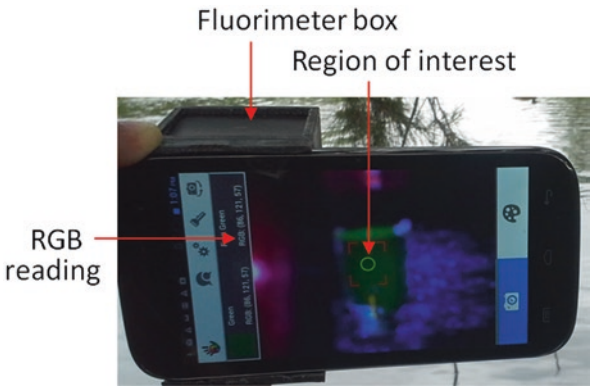

Fig. 2.11 Photograph of the smartphone based fluorimeter in action; a fluorescent green image is displayed on screen and the green intensity within a circular region of interest is directly displayed on top both corners of vertical screen

content of a live image in video mode in one corner of the screen image as pictured in Fig. 2.11. Among them the green pixel value, G has been used to quantify the pH-responsive fluorescence intensity of the naphthalimide dye. Other intermediate color values can also be obtained by interpolation of the RGB values or other color models based on the RGB values (e.g. HSV) can also be applied. Once the sample water containing the dye molecule is excited, the value for green fluorescence intensity is readily detected within a circular region of interest (see Fig. 2.11). Data recorded on the smartphone fluorimeter can be readily stored on phone memory or transmitted wirelessly to a computer for further analysis.

Although the app displays the fluorescence intensity directly, determination of the pH of a sample requires additional manipulation of the data using a calibration equation. A user-friendly Android application was developed to allow pH measurement from direct imaging of the sample on to the smartphone camera and enable further analysis such as archiving and real-time mapping. The app has been designed to determine the relative fluorescence intensity of a sample with respect to a reference solution, displaying the pH value directly and finally share results with others. The screenshots of the app illustrating the fluorescence measurement are shown in Fig. 2.12. After attaching the hardware to the camera unit of the smartphone, the user needs to hold the phone vertically and then run the measurements with this smart app. The user can select various functions from the main menu of the application (Fig. 2.12a). These include start of a new test, generating a device-specific calibration curve, checking a previously run tests, and reading the operation guidelines. Once capturing the fluorescent image, the user can first preview the image on the screen (Fig. 2.12b) before proceeding to analyze it. This enables a user to reject a measurement taken by inappropriate orientation. The algorithm was designed to compare the fluorescent green intensity in a fixed region of 20 × 20 pixels at the

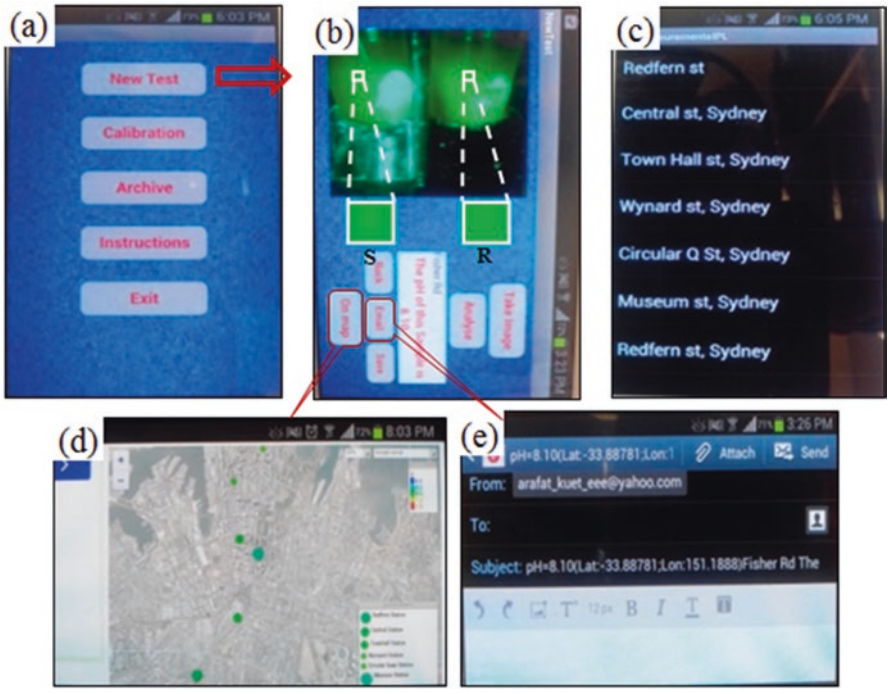

Fig. 2.12 Screenshots of the pH measurement app running on an Android phone: (**a**) The main menu; (**b**) The testing screen displaying results with location after analysis. Upon the selection, the results can be (**c**) stored on the phone's memory; (**d**) mapping with GPS coordinates on the same mobile platform (clear images are shown in Fig. 2.19); and (**e**) sending for quick, centralized mapping of results from many sources/instruments

centre of the sample image with respect to that from a fixed reference solution. In advance to the other RGB-based color analyzing apps, this custom designed app enable the users to process the results differently. For example, pH values from various sites can be stored on the phone's available memory (Fig. 2.12c) for mapping on the same platform (Fig. 2.12d) or transmitted back automatically with location names and GPS coordinates (Fig. 2.12e) to a central server for regional pH mapping, using, for example, a Google Maps-based interface. The GPS coordinates of a particular site is recorded automatically, sent together with the results via an email option in the phone (see subject line Fig. 2.12e).

2.7 Fluorimeter Calibration

In order to enable the smartphone intensity fluorimeter to measure an unknown pH, the Android app and hardware attachment must first be calibrated against reference samples. A total of 14 standard buffer solutions ranging from pH 4.28 to 10.40 were prepared using HCl and NaOH at an average temperature of 23 °C. The pH of each of the buffer solutions were confirmed using a standard benchtop pH meter. The chemosensor solution was prepared in dimethyl sulfoxide (DMSO) with a concentration of 2 mM. The sample solution at each pH value was prepared by adding 8.0 μL of the 2 mM dye-solution to 1.59 mL of buffer (giving a final solution of 1.6 mL at ~ 10 μM dye) in glass vial of 1.2 cm diameter. Finally, the green fluorescence intensity of each sample was measured both with a standard benchtop spectrofluorimeter and the smartphone intensity fluorimeter. The smartphone app was used to analyze each image taken and process the data. The sample cell ensures a fixed distance of 3 cm from the flash LED during each measurement—this was kept constant throughout the measurements of all samples. Figure 2.13a compares the

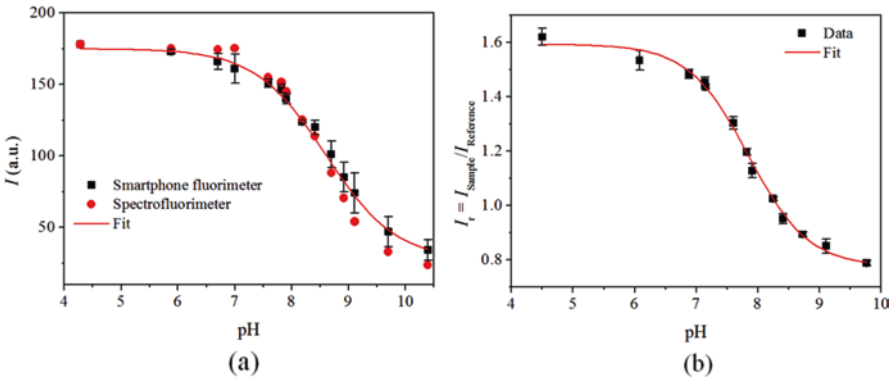

Fig. 2.13 Calibration of the mobile fluorimeter against the commercial spectrofluorimeter—(**a**) variation of fluorescence intensity, I with pH and; (**b**) variation of relative fluorescence intensity, I_r (normalized by I of pH ~ 8.19 solution) with pH

fluorescence intensity measured using the smartphone with that made using the spectrofluorimeter across the measured range of pH. The relative intensity (normalized by a reference solution) measured on the second version of the smartphone fluorimeter is shown in Fig. 2.13b. The smartphone results are found in good agreement with the spectrofluorimeter and standard deviations found are within experimental error. From the both set of measurements, it can be noted that the fluorescence intensity decreases with a linear trend from pH ~ 7.0 to 9.7. Therefore, a simple linear fit equation within this range can be used to measure pH directly; however, a sigmoidal fit covering the whole data range can make the smartphone fluorimeter workable for a wider range. From the nonlinear fit of these data, the empirical equation relating pH to intensity is

$$pH = 8.59455 + 0.61666 \times \log\left[\frac{174.9 - I}{I - 27.9}\right] \tag{2.1}$$

When the data are fitted to the Henderson-Hasselbalch equation, the calculated acid dissociation constant, pKa ~ 8.6 [first term of Eq. (2.1)] is found very close to the reported values for this type of probe [143]; the small variation observed is presumably due to the different solvent system used. The calibration equation was then uploaded to the app to enable pH measurements of field samples.

2.8 pH Measurements of Water

The smartphone fluorimeter was applied to measure the pH of different sources of water sample in the field. Water pH is considered as one of the important chemical properties which directly indicate the water quality. As a result, different organizations release a general guideline for acceptable pH range of drinking and environmental water. Aligned with the World Health Organization (WHO), the Australian government's National Health and Medical Research Council (NHMRC), for example, provides a generally acceptable alkaline range of pH ~ 6.5 to 8.5, which avoids skin corrosion at the lower end (acidic) and irritation of skin, eye and mucous membranes at the higher end (basic) [145]. The NHMRC authorizes for pH monitoring at defined frequencies both at the supplier and consumer ends and average data of which are archived at a publicly accessible website [146]. The smartphone fluorimeter will definitely improve such monitoring by more frequent measurement and more monitoring points logging. The sample water measured in the following sections includes environmental as well as drinking tap water sources. In addition, the smartphone fluorimeter has also been demonstrated for a security concept in water supply system for rapid detection of any hazardous activities in the system.

2.8.1 *Environmental Water*

The smartphone intensity fluorimeter was applied for pH measurement in two different types of environmental water samples: sea and lake water. A total of 11 samples, which includes 7 sea and 4 lake water samples, were collected from different locations around Sydney (Fig. 2.14a). Measurements with the smartphone intensity fluorimeter were performed real-time at the site where samples are collected. In order to check the accuracy of the measurements, the same samples were also measured back in the laboratory with a commercial non-portable, benchtop, high accuracy pH meter (METER TOLEDO, accuracy: ±0.01). To preserve the integrity of the collected samples in transit, they were stored in 250 mL borosilicate bottles filled to the top these and transported to the lab within 2–3 h under ice in a container, which also cuts out background light. Before performing the laboratory measurements, the samples were brought to the same temperature as the ones recorded during the 'live' field measurements with the smartphone fluorimeter. To evaluate any potential effects of salts and other solutes on the fluorescence intensity of the dye that may exist in samples, the chemosensor was first tested against salt solutions in the laboratory using samples containing NaCl (0.2 M) and $MgCl_2.6H_2O$ (0.2 M) (the most abundant dissolved species present in seawater [147]), at pH 8.41. In addition to these, a tap water sample in the laboratory with unknown chemical composition was also tested. All these measurements were performed with identical dye concentration and instrumental set up. All sets of data obtained are presented in Figs. 2.15 and 2.16.

Firstly, the dye was found to be sufficiently stable to work under various salts and chemical compounds commonly available in seawater. The results of such measurement are shown in Fig. 2.15. Comparing with standard pH meter measurements, it is clear that the dye used in the smartphone fluorimeter platform is robust under various environmental conditions.

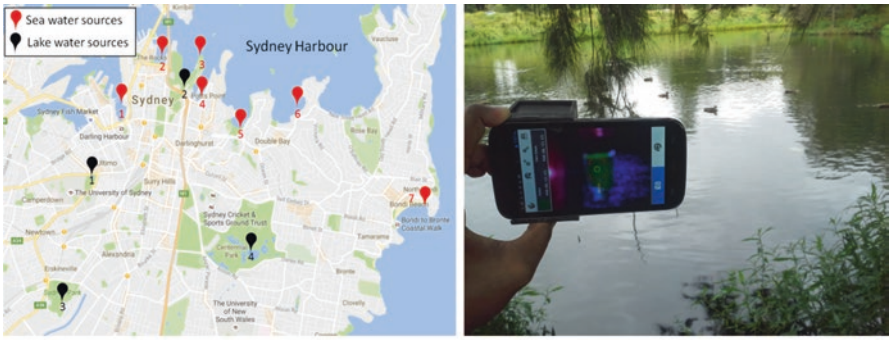

Fig. 2.14 pH measurement of environmental water at the field. (**a**) Sample measurements were taken across Sydney as shown above and (**b**) the instrument measuring pH at the Centennial Park Lake, Sydney

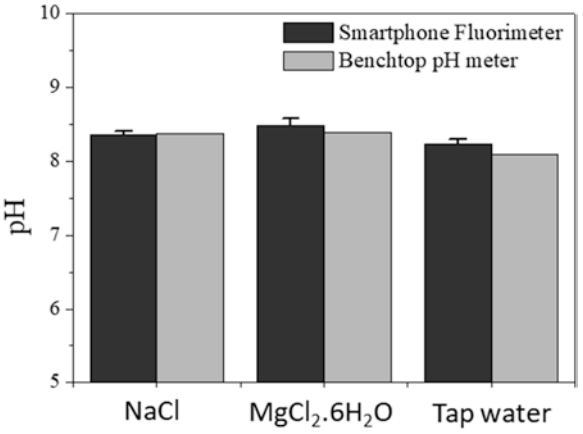

Fig. 2.15 Results of pH measurements for lab water with different chemicals [122]

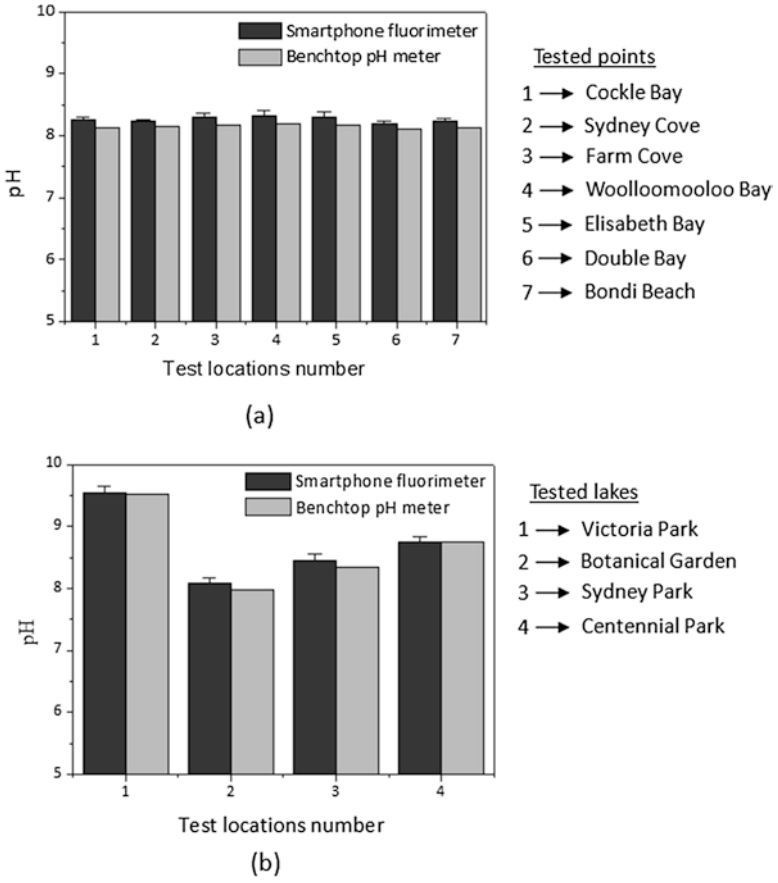

Fig. 2.16 Results of pH measurement for—(**a**) seawater and; (**b**) lake water. Measurements in both systems were performed at identical temperature for each sample [122]

The results of seawater pH measurements taken on site at different points along the coast of the Sydney Harbour with the smartphone fluorimeter and the results are presented in Fig. 2.16a. They are compared to standard electrode based measurements (made after transporting samples back to the lab). Using the mobile fluorimeter the pH of the seawater samples were measured, giving results that are comparable with the electrode based system and in good agreement within a small experimental error. The water within these locations is found to be slightly basic, with pH ranging over (8.07–8.19) ± 0.12. This compares favourably to data reported using field portable electrode based pH meters [148].

In case of lake water, the samples were filtered with a common syringe filter to remove extraneous particulate materials such as algae, a potential source of background fluorescence. Figure 2.16b shows the results of lake water pH measurements. The pH measured in the lake waters are found to vary widely, from (7.95 to 9.52) ± 0.15, presumably a reflection of the diverse local ecologies. The measurement of pH can be extended to other areas including biological and agricultural environments by expanding the measurable range through the design of customized dyes for each application.

2.8.2 Drinking Tap Water

In addition to the environmental water analysis, the smartphone fluorimeter is applied to measure pH of different public tap water sources, the most common source of drinking water in Sydney, Australia region. Measurements were performed at different buildings within The University of Sydney and at different train stations around Sydney City. Results of these measurements were compared against the data obtained from a commercial, portable pH meter (PHMETER, PH-035). The pH meter was calibrated with a standard buffer solution before each measurement. Unlike the smartphone, this conventional system does not allow networking with other devices and also requires a distinct power supply that may not be available at many sites globally. On the other hand, the mobile fluorimeter uses the same calibration procedure each time ensuring the instrument is ready for multiple samples and truly field-portable whilst providing results good agreement within a small experimental error. Figure 2.17 shows the results of pH measurements with smartphone fluorimeter and the comparison with the standard pH meter. The water within these locations is found to be slightly alkaline, with pH ~ (7.89–8.27) ± 0.10 and an average $pH_{av} = 8.08 \pm 0.04$. Finally, all collected data were sent wirelessly via email for archiving on a central computer, demonstrating the potential of the instrument for wireless data transmission and off-site analysis. Furthermore, these collected data can also be analyzed by real-time mapping and sending a response back to the consumer. This is something ideal for sensor smartgrids collecting and emerging for analysis similar data from many portable instruments, something that is a cornerstone of the next generation

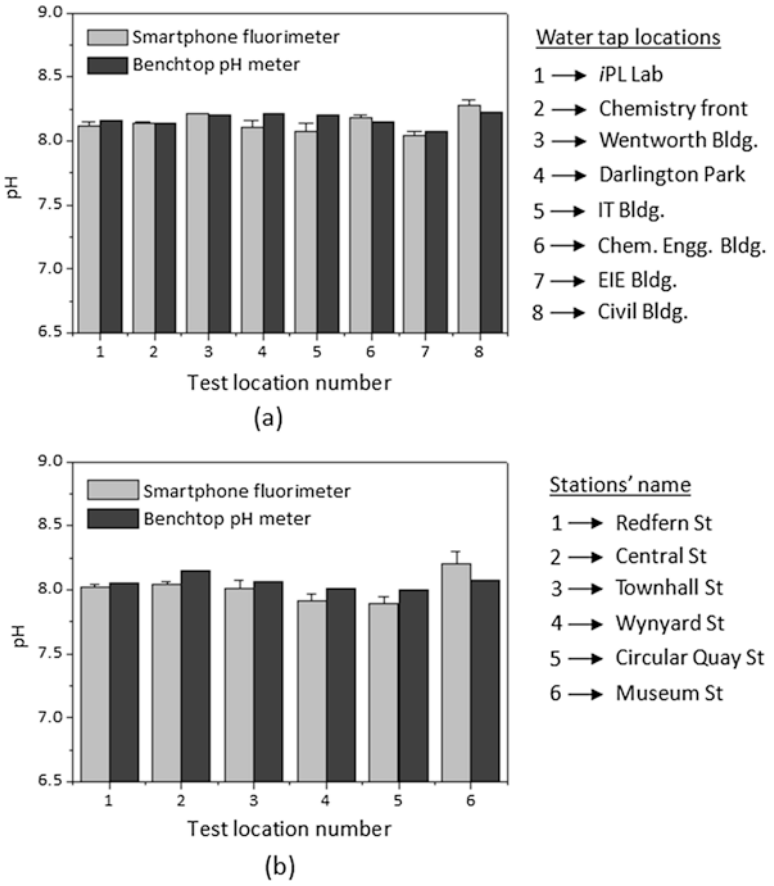

Fig. 2.17 Results of tap water pH measurement within—(**a**) The University of Sydney and; (**b**) Sydney City Circle train stations. Measurements in both systems were performed at identical temperature for each sample [118]

IoT. The concept can be illustrated through demonstration of a real-time water quality monitoring system presented in the following section.

2.9 Water Quality Monitoring and Mapping

As mentioned earlier, the smartphone fluorimeter holds massive networking capability which can be utilised for more frequent monitoring of water quality from more points across a public supply system. Existing technologies monitor daily water quality at the supplier end [149], but less frequently at the consumer ends. It

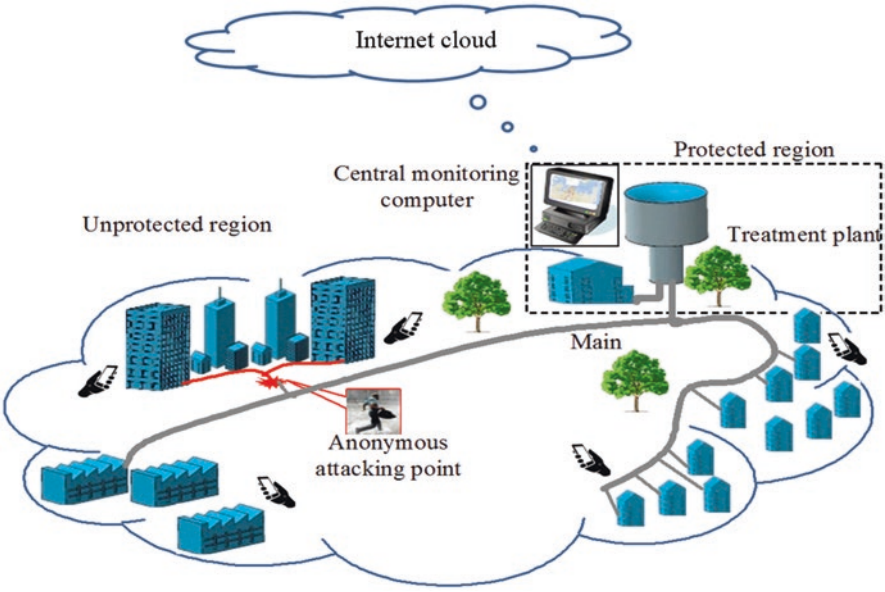

Fig. 2.18 Schematic demonstrating the scenario of detecting any disruption happening in the drinking water supply system with a wirelessly inter-connected smartphone system [125]

is practically impossible at present to assess all access points using the current methods. It seems likely the growing local and global risk of water disruption [150] will demand a more frequent and faster way of measurements than is currently undertaken. The smartphone sensing will aid the process tremendously via integration into the growing wireless sensor networks [151], which would allow rapid collation, detection and monitoring of propagation, and site identification and response, ideally coordinated through an automated data receiving center capable of handling and processing big data. The proposed smartphone fluorimeter system meets all these aspects by performing the pH measurements of water and sharing results with other devices. This section demonstrates a smartphone fluorimeter enabled water security system by measuring water pH at all public access point and centralizing data and mapping real-time to identify any disruption in water quality. Any other variations of the measurements are clearly possible.

The general picture of an urban water supply system can be illustrated as shown in Fig. 2.18. As expected, a number of smartphone intensity fluorimeter devices are distributed across consumer access points for quickly measuring and subsequently sending the results to a central computer located at the treatment plant or elsewhere. The authority monitoring the system can map water quality to quickly find out if any disruption is occurring in the system. In contrast to the smart

sensing approach, traditional approaches use in-line chemical sensors and non-portable analyzers [149, 151, 152]. Additional limitation is their high installation cost which restricts the application of the existing approach across the whole system. In contrast, the smartphone sensing approach described here utilizes mostly the in-built components of the smartphone, requiring less external components. This makes it low-cost and truly field-portable whilst retaining smartgrid friendliness in the field.

In addition to simply pH measurements, the smart app can be utilized to generate real-time maps within the same platform, and share results with others for centralised mapping. To do this, GPS coordinates of each measurement location were recorded and saved within the phone's memory. These can be used to generate a pH map within the phone app or send with the pH data wirelessly to a local server. In this case, the results were sent to a central computer at the *i*nterdisciplinary Photonics Laboratories (*i*PL) in The University of Sydney for quick mapping and monitoring. This offers further advantages over the conventional electrode based meter, enabling direct integration into smartgrid sensor network for direct access to central laboratory analysis. Figure 2.19 represents two pH maps generated from smartphone fluorimeter data sent from the measurement locations. The pH values are depicted by a color bar as well as dot size. The maps generated for these regions indicate no rapid changes in results, reflecting the fact that there was no disruption of pH detected in public drinking water at The University of Sydney or City Circle train stations during the period that these measurements were made. The recorded pH data are also within the upper limit of the New South Wales (NSW) government's tolerable alkalinity (pH = 8.50) and are also consistent with the values most recently recorded for this region (pH_{av} = 8.10) [146].

This result particularly demonstrated the concept of using a smartphone-based ubiquitous capable device for rapid identification of any hazardous disruption in drinking water supply system. The concept can be applied for analyzing other chemical properties of environmental and drinking water including metal ions. In a fully implemented wireless sensor network, monitoring of those parameters would be done on a regular basis and diagnostics and analysis automated at the data mapping centre. There is significant room to improve the device capability and scalability of the system. For example, the monitoring range can be extended to a national and even a global scale by collecting similar data from many portable instruments (where resources permit, supplemented by permanent analytical systems), connected to the wireless infrastructure. This approach has great potential for monitoring many other areas including environmental analytes, and for remote biological analysis on national and global scales.

Fig. 2.19 Results of tap water pH mapping at (**a**) Sydney City Circle train stations, (**b**) the University of Sydney and (**c**) the colour gradient from red to blue and dot size indicate the pH value [118]

2.10 Summary

In summary, this work demonstrates the first functioning field-fluorimeter using a smartphone platform. Other than the 3D-printed fluorimeter box, the optical source, power supply, interrogation and imaging unit are contained within the smartphone itself—no external sources are required. Through wireless communications, the mobile instrument can be networked into global smartgrids allowing instant access to additional analysis at a different location. The particular instrument was based on application specific chemosensor dye that needs to be excited by the blue spectral emission of typical smartphone's white LED which generally used for image illumination with the camera.

The smartphone intensity fluorimeter successfully performed the measurement of water pH from different sites in Sydney in good agreement with a conventional electrode-based measurement. The test results can either be stored in the smartphone memory or transmitted to a central computer for real-time data processing via mapping. Needless to say that, the technology has a great potential to be extended further enabling detection of many species, including metal ions and other species of public health concern. Furthermore, it has clear biological and biomedical potential and can apply greater focus on specific innovations by significantly improving the signal-to-noise ratio. There is considerable room to improve the instrument allowing it for increasing the capabilities and accuracy. For example, fluorescence collection can be improved significantly by using collection lens, fibres etc. Multiple analytes can be measured simultaneously by allowing detection over other wavelength points rather than just red, green and blue channels.

Chapter 3
Temperature-tunable Smartphone Fluorimeter

3.1 Introduction

Fluorescence measurement is considered as an effective means of sensing and understanding various molecular processes in chemical and biological science. The time scale of those processes can range from femtoseconds to milliseconds and longer [153]. Longer processes are characterised by changes in physical parameters, often involving temperature (T). Therefore, in addition to time-resolve measurements, T-dependent fluorescence is also important in a variety of applications. More generally, T-dependent fluorescence measurements are extremely useful for investigating many other diagnostic processes in detail. For example, the in-channel fluid temperature in various microfluidic systems has been monitored by using temperature-dependent fluorescent dyes [154, 155]. Temperature-dependent fluorescence has also been utilised to investigate stress or cell damage that may induced by temperature [156]. Low temperature fluorescence with gas chromatography has been demonstrated as an effective method for detecting mercury ion at extremely low concentration [157]. Temperature-dependant fluorescence was also used to characterise molecular probes with regards to their intrinsic fluorescence switching mechanisms and the thermal stability of different fluorescent sensor materials [156].

However, many of these examples have been developed inside a stable laboratory environment because field-deployable instrumentation capable of time-resolved, temperature measurements of fluorescence are not yet readily available. Existing systems are designed to run an external heating and cooling unit and are assigned for benchtop operation only within a properly controlled laboratory. A significantly large amount of energy required to drive the thermal unit is typically delivered from an external source. The key challenge for achieving field-portable T-dependent measurements is the availability of a suitable, low powered easy-to-control thermal unit. To address the challenge of developing a thermal unit compatible with a smartphone device, in this chapter, the use of a Peltier heating and cooling element is explored. This approach yielded excellent temperature regulation, leading to the

A. Jamalipour, M. A. Hossain, *Smartphone Instrumentations for Public Health Safety*, Wireless Networks, https://doi.org/10.1007/978-3-030-02095-8_3

demonstration of the world's first self-contained *T*-tunable smartphone fluorimeter capable of both time-resolved and steady state measurements.

In this chapter, the *T*-tunable smartphone intensity fluorimeter has been developed and applied to perform similar measurements [124, 125]. Fluorescence enhancement and quenching mechanism of the particular metal ion chemosensor dye has been understood in detail which can be useful to design molecular optical diodes and molecular machines.

3.2 Temperature-tunable Smartphone Intensity Fluorimeter

Similar to the intensity fluorimeter, the *T*-tunable smartphone fluorimeter also utilizes smartphone's CMOS camera to detect the intensity on its RGB color channels. However, fluorescence excitation is provided here using an external UV LED which can be powered internally through the smartphone battery. A Peltier unit is housed within a 3D-printed package designed to improve insulation and help mitigate power consumption for heat up or cool down the sample. An Arduino board plugged into the smartphone and controlled by an Android smartphone app allows the collection and wireless transmission of all data. This *T*-tunable instrument is used to measure the fluorescence responses of four systems: two laser dyes, a porphyrin emitter, and a metal ion chemosensor—all have a range of applications in sensing. To enable such measurements on a hand-held smartphone platform, this section demonstrates the development of a *T*-tunable smartphone intensity fluorimeter. The instrument has been applied to perform *T* dependent fluorescence measurements of different chemosensor systems.

3.2.1 The Fluorimeter Components and Operation

The complete system diagram of the smartphone intensity fluorimeter with a *T* controlling unit is shown in Fig. 3.1. The fluorimeter operates with an external microcontroller-based hardware system interfaced with a smartphone, which controls all active and passive elements including the fluorescence excitation source, sample heating element and temperature sensing circuit. These components were operated via an Arduino Uno microcontroller module (ATmega328P–assembled), which is an open-source hardware and software prototyping platform, for building digital devices and interactive objects capable to sense and control physical devices [158]. This module can be programmed to communicate either through wired connections or wirelessly, and are able to drive multiple input-output devices simultaneously through its 14 digital output and 6 analog input ports. For example, one of the digital output ports connects the fluorescence excitation source to the system. By tuning the voltage from the digital output port, ON-OFF switching as well as intensity of the excitation source can be controlled. A greater flexibility on output

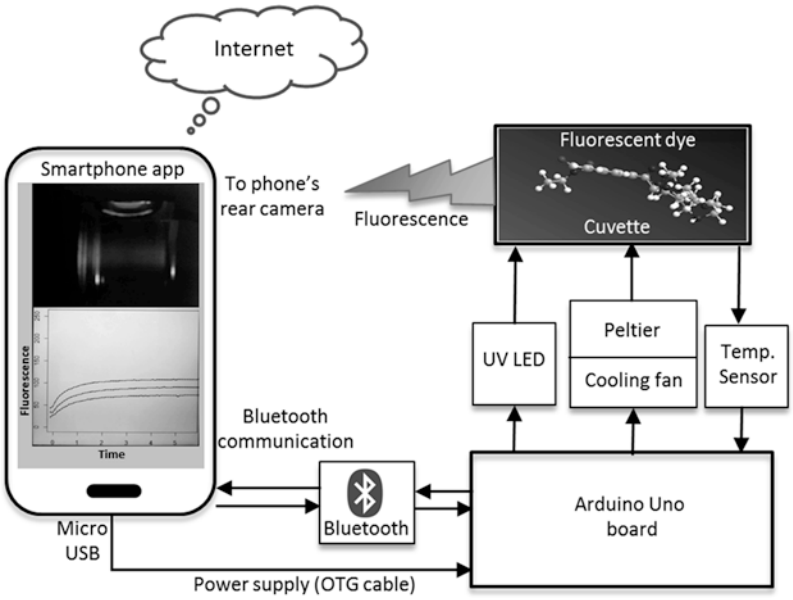

Fig. 3.1 Layout of an Arduino microcontroller-driven smartphone fluorimeter system [131]

voltage accuracy can be achieved by tuning the inputs from a 256 step values (0–255 binary numbers). Since the absorbance of most fluorescent sensor dyes lie in the UV region of the spectrum, a UV LED (3.0 V, 20 mA, 370 nm) was used as the fluorescence excitation source in this study. However, the fluorimeter also supports the integration of excitation source at any other wavelength or even multiple sources of different wavelengths, extending the fluorimeter's capability further. In order to limit current and voltage, a series resistor, $R = 120\ \Omega$ is used with the UV LED circuit.

To raise or lower T of the sample, a Peltier unit is used in the smartphone fluorimeter. Peltier devices are popular thermoelectric energy conversion modules used for heating or cooling any object/sample. The module provides a T change by applying potential across the junction of two different materials transferring energy from one side to the other (typically many junctions of P-type and N-type semiconductors). Practically, these junctions are electrically connected in series but thermally in parallel to produce a significant heating or cooling effect on a total surface area. When one side of the Peltier block heats up, the other side cools down and vice versa. One of the major advantages that makes Peltier module suitable for both cooling and heating applications is their reversible polarity. The heating or cooling effect can be altered by reversing the polarity of the supplied voltage, therefore, avoids the need for separate unit for heating and cooling or altering the Peltier sides manually. This can be achieved automatically by using a polarity reversing switch. The other challenging issue that needs to be addressed here is the thermal isolation between the surfaces of the Peltier module. A properly designed thermal isolation

system can help to maintain the *T* difference between hot and cold surfaces. This has been managed by using an aluminum heat sink (8.0 × 6.0 × 6.0 cm) with a mounted cooling fan (3 ~ 5 V). The ON-OFF switching as well as speed of the fan can be tuned to control the rate of cooling via one of the digital output port of the Arduino. Furthermore, a properly designed feedback loop has been created into the Peltier circuit that ensures *T* stability of the overall system. The feedback loop is created by measuring the sample's *T*, feeding the data to the Peltier circuit and adjusting the current to deliver and maintain the desired *T* and stability over time. The large surface area of the Peltier (2 × 2 cm) utilized in this work is sufficient to cover the entire surface of one side of the sample cuvette, enabling rapid heat transfer between Peltier and sample. To circumvent maximum currents from any output port (20 mA) of the Arduino which is needed to drive the Peltier, a current amplier circuit has been used. In the Peltier circuit, an *N*-type metal-oxide semiconductor field-effect transistor (*N*-MOSFET, $\alpha = 20$) current amplifier circuit is used to amplify current. Actual temperatures at the cuvette were measured using an infra-red (IR) temperature sensor (−33 to +220 °C with ±0.6 °C). The Arduino board is connected and powered by the smartphone through the micro-USB port and an On-the-Go (OTG) cable. Data transfer to and from the Arduino board and app is performed through an attached HC-06 Bluetooth module (4 pins, 3 ~ 6 V).

3.2.2 3D Design, Fabrication and Packaging

A 3D model of the entire fluorimeter was designed in AutoCAD that encloses all components in position and holds the phone firmly align with the optical path of fluorescence emission. The design is shown in Fig. 3.2. The entire 3D design of the smartphone fluorimeter consists of four different parts: the electronics panel, the fluorimeter box (Fig. 3.2a), the sample chamber (Fig. 3.2b) and the thermal unit (Fig. 3.2c). The fluorimeter box is a support frame to hold and align the smartphone at 30° inclined to the horizontal axis. This inclination helps user to read the smartphone screen easily and optimizes contact between the sample cuvette and the Peltier surface. The electronics panel assembles all input-output circuits of the Arduino onto a 6 × 6 cm copper printed circuit board (PCB), which is then placed securely in a dedicated chamber inside the fluorimeter box and enclosed by a 3D-printed cover. There are also dedicated slots in the fluorimeter box to hold the sample chamber and the thermal unit. The sample chamber is located at the top side of the fluorimeter box and just below the smartphone's rare facing camera position of the frame. On the top of the box where a frame holds the smartphone, a suitable port allows connection of the OTG cable from the smartphones micro-USB port to the power supply port of the Arduino—this can be packaged internally. Ventilation allows heat dissipation from all active components.

Figure 3.2b shows the interior design of the sample chamber. The main components in this chamber are slots for a sample cell, the excitation source and the

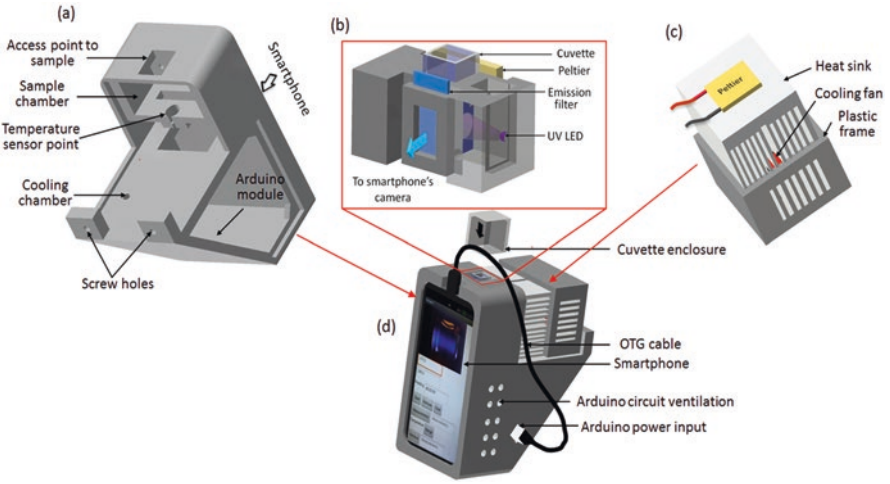

Fig. 3.2 The complete 3D AutoCAD design of the fluorimeter. (**a**) The smartphone fluorimeter chamber; (**b**) the interior design of the sample chamber; and (**c**) the heat sink element with a cooling fan. The complete design installed on a smartphone is shown in (**d**) [125]

emission filter. The sample slot is designed considering a quartz cuvette cell of path length, l = 1 cm. The excitation source is 3 mm single UV LED mounted onto a 2 × 2 cm mini PCB attached to the side-wall of the sample chamber. The excitation filter slot is designed to fit a thin film filter of maximum dimension, 5 cm × 2.5 cm × 1 mm. The cuvette cell is designed in such a way that one side of the cell is enclosed by the surface of a Peltier, making efficient contact between the sample cell and Peltier's hot/cold surface. This allows efficient heat transfer between the Peltier and sample. In order to reduce the levels of UV radiation reaching the CMOS camera directly and maximize the fluorescence readout, the UV LED is positioned orthogonal to the fluorescence emission path from the sample contained in a (1 × 1 × 4.5) cm quartz cuvette. An emission filter at λ_{em} ~ 450 nm is used to further reduce background scattering and allowed blue fluorescence to pass which can be replaced or complemented by other bandpass filters where required. The main fluorimeter box contains a window at the top of the sample cuvette chamber so that the user can easily access the sample in the chamber; this can be closed by a 3D-printed cover once the sample is in place. Temperature of the sample was detected using an IR T-sensor. A round slot in the fluorimeter box, just underneath of the sample cuvette unit, holds the T-sensor. The complete smartphone fluorimeter design after placing all components in position is shown in Fig. 3.2d. Once the design is completed, the individual part of the fluorimeter is fabricated with a 3D printer using ABS material of black color and assembled to build the complete smartphone intensity fluorimeter as shown in Fig. 3.3.

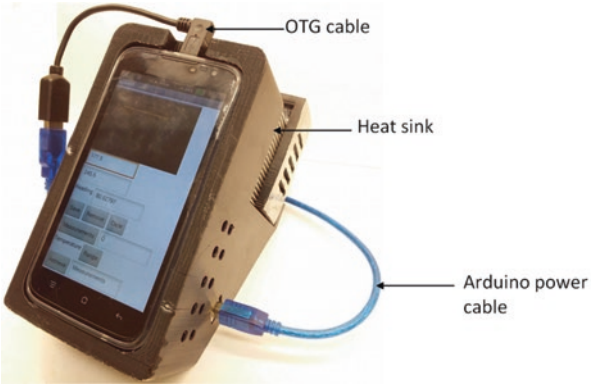

Fig. 3.3 3D-printed Arduino-based temperature tunable smartphone fluorimeter installed on a Blackview ZETA smartphone [125]

3.3 Time-resolved Fluorescence Measuring Smartphone App

A customized smartphone app is developed that enables the fluorescence measurements and controls all input/output devices connected to the Arduino board through Bluetooth communication. The app allows time-resolved as well as steady-state fluorescence measurements on the smartphone camera. Before performing any measurements, the user is required to pair the smartphone's Bluetooth with the Arduino device using the app. In the app, the steady-state fluorescence measurements are performed using the same algorithm as used in the intensity fluorimeter of Chap. 2. In order to achieve time-resolved fluorescence measurements, the smartphone app automatically captures images of the fluorescent sample at a specified time interval (δt), which is determined by the total recording time (t) and total number of images to be taken (n) as set by the user's input. To avoid the effects of other apps running simultaneously, therefore impact processor speed and time, δt is calibrated against a stop-watch. After taking the images, they are automatically stored on the phone's memory. Another command from the app determines the fluorescence intensity (I), normalized against the initial fluorescence (I_0), if necessary, from the stored images and plots time-resolved fluorescence as I vs t. Other functions such as tuning T, fan speed, ON-OFF LED all can be controlled from the app. The smartphone fluorimeter can send the results of these measurements to other devices through the cloud and in principle relay this information anywhere. The data can be accompanied by location identification through GPS positioning coordinates taken automatically by the phone.

3.4 Calibration

A step-by-step calibration of all individual components were carried out before performing the measurements with the T-tunable fluorimeter. This includes the optical stability of the excitation source at different T, and response of the Peltier device and T-sensors. Figure 3.4 summarizes the data of the calibration. Figure 3.4a shows that

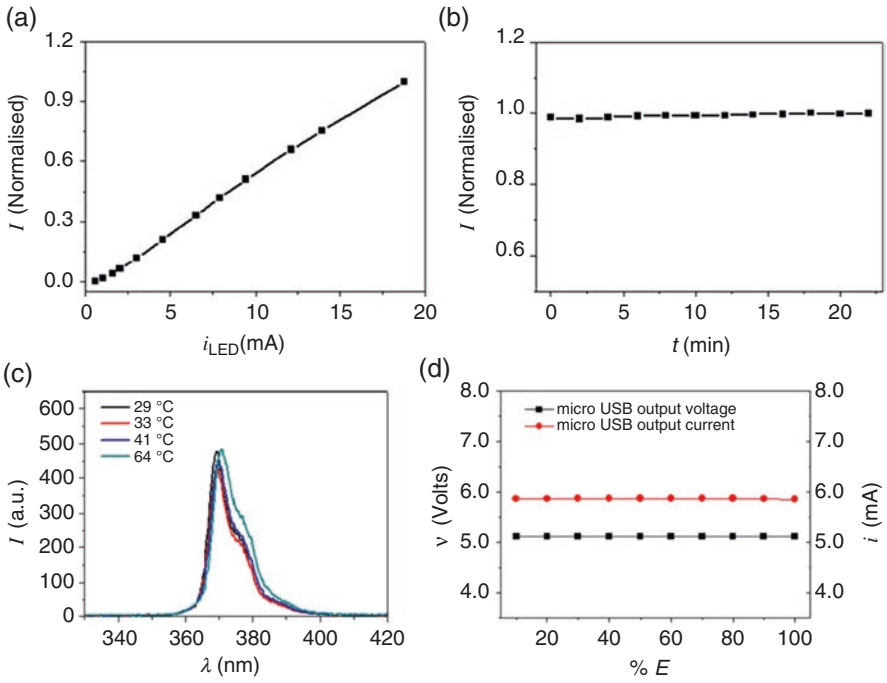

Fig. 3.4 Characterization of the excitation source and power supply of the smartphone fluorimeter. (**a**) Linearity of optical emission (I) at different levels of diode current (i_{LED}); (**b**) stability of optical emission over the time (t); (**c**) thermal stability of the excitation source; and (**d**) stability of the supplied voltage (v) and current over the full discharging cycle (100%) of the smartphone battery energy (E) [132]

the output emission of the excitation source varies linearly with input current. This allows the user to control the optical power of the excitation source using a potentiometer, instead of adjusting slit-width as used in many commercial spectrometers which sacrifices the spectral resolution. The UV LED also shows good stability over time and T as shown in Fig. 3.4b,c. The stability of the smartphone's battery power supply has been verified by monitoring the output voltage and current from the micro USB port at different levels of load current. Both current and voltage are found to be stable at 5.87 mA and 5.11 V respectively across a load $R \sim 300\ \Omega$ over the full range of battery electricity (Fig. 3.4d).

3.4.1 Temperature Calibration

A standard *K*-type thermocouple (Fluke 50-Series II Model 52) was used to calibrate the response of the temperature sensor used in the smartphone fluorimeter. To do this, the temperature of the sample cuvette, filled with de-ionized water, was monitored simultaneously on the smartphone fluorimeter and the thermocouple.

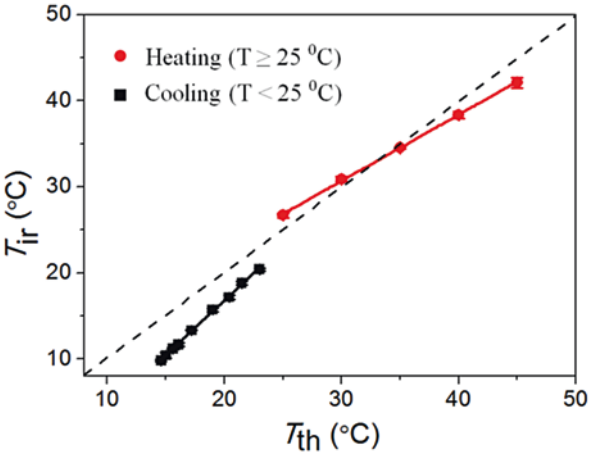

Fig. 3.5 Calibration of the smartphone fluorimeter IR temperature sensor with respect to a separate thermocouple. Raw data are taken from IR temperature sensor. Dashed line is the thermocouple read-out [124]

The thermocouple reading was taken after immersing its lead directly into the water. The bottom surface of the cuvette is coated with a non-transparent black paint so that the temperature sensor receives reflection only from the cuvette surface and blocks emission from the top or side-wall of cuvette. A comparison of *T*-response recorded in both systems is shown in Fig. 3.5. From the linear fit of the plotted data, different correlations between the two systems are obtained for heating and cooling conditions. The difference observed here is presumably due to unequal current distribution among the Peltier and other electronics during heating and cooling. However, two empirical equations were obtained and uploaded to the smartphone app to correct the *T* response during measurements:

For heating ($T \geq 25$ °C)

$$T_{ir} = 0.77T_{th} + 7.6 \tag{3.1}$$

For cooling ($T < 25$ °C)

$$T_{ir} = 1.26T_{th} - 8.5 \tag{3.2}$$

3.4.2 Battery Lifecycle

Another determining parameter after *T* calibration is the working life-cycle of the smartphone fluorimeter while driving all components which is determined by the battery capacity of the smartphone. The total working times were recorded under different loading conditions to the battery. With minimum components connected, *i.e.* when only the excitation source, temperature sensor and Bluetooth module are ON, the smartphone fluorimeter can operate continuously for $t \sim 5$ h. However, the battery was significantly drained after turning the Pettier (4 x 4 cm) ON. With the

Peltier connected to the system, the total lifetime of the device was reduced to $t \sim$ 1 h; these conditions were referred as "medium load". The t reduced further to $t \sim$ 40 min when turning the cooling fan "ON" ("maximum load"). Since the power supplied by the battery is fixed, the addition of the extra load into the system causes voltage regulation and significantly affects the other components connected. For example, the power drawn by the Peltier is slightly reduced to ~ 0.66 W, and most importantly, voltage across the UV LED dropped below its threshold value, and as a result the excitation source failed to switch ON. To avoid such voltage regulation across the excitation source, the Peltier and fan circuit can be switched OFF momentarily during measurements; the LED circuit can be separated from the heavy load components. However, the working time can be improved by using a Peltier of lower power rating. By replacing the Peltier with one of reduced size (2 × 2) cm, power consumption by the Peltier can be reduced by ~ 58%. This results in an overall improvement of working time by ~ 33%. Adding a second battery can extend the device lifetime substantially; however, this time was sufficient for the measurements reported here and sufficient to have a fully functioning, field-portable fluorimeter that can perform as well as many benchtop instruments.

3.5 Temperature-dependent Fluorescence Measurements

After complete installation of all components and calibration, the Arduino-controlled smartphone intensity fluorimeter was applied to measure temperature dependent fluorescence. At first, the temperature based measurements were demonstrated by steady-state fluorescence measurement of three systems as a proof-of-principle demonstration. Finally the time-resolved fluorescence of a Zn^{2+}-responsive probe (6-(1,4,8,11-cyclam-1-yl)ethyl-1,2,3-triazol-4-yl)2-ethyl naphthalimide, chemosensor **2**) has been performed on the smartphone fluorimeter to demonstrate the concept and capability of detecting multiple metal ions from environmental samples.

3.5.1 Steady-state Fluorescence Measurements

Performance and capability of the Arduino-controlled smartphone fluorimeter was analyzed by tuning T to the sample and measuring fluorescence intensity at different T. The temperature response of steady-state fluorescence intensity (I) from two commonly available laser dyes, (Rhodamine B (RhB, **3**) and Rhodamine 6G (Rh6G, **4**)) and a porphyrin emitter (**5**) were measured as a proof-of-principle.

The laser dyes RhB and Rh6G and their derivatives have a wide range of applications in chemical and biological research whilst having opposite response with changing temperature. RhB, for example, is often applied in non-invasive sensing of T-changes produced by radiofrequency radiation, specifically in small biological

samples [159]. The opposite temperature effect of two Rhodamine dyes was used to characterize the millimeter wave propagation inside a rectangular waveguide [160]. This characteristic makes these dyes excellent test subjects for the fluorimeter. Figure 3.6a shows the measured decrease of fluorescence emission in response to increasing T for the RhB in de-ionized water ([RhB] = 0.1 mM). Similar to this, an increase in T generally results in a reduction in the fluorescence quantum yield. This happens due to an increase in molecular collisions in solution and a rise in the amplitude of internal molecular vibrations with T rise, which leads to higher non-radiative relaxation of the excited state and therefore greater fluorescence quenching. In contrast, some organic molecules in aqueous solution form associated complexes (dimers, trimers, and so on), the concentration of which increase with temperature. These complexes are better shielded and have higher yields that produce an increase of fluorescence of Rh6G with T increase. Consistent with that, Fig. 3.6b shows the measured increase of Rh6G (0.2 mM) fluorescence with increasing T. The rate of fluorescence change can be obtained from the slopes of the plotted data in Fig. 3.6 and expressed in percentage as:

$$\eta = \pm\left(\frac{\left(I - I_0\right)/I_0}{\Delta T}\right)\times 100 \tag{3.3}$$

From the linear fits in Fig. 3.6a,b, the rates of fluorescence change in RhB (λ_{em} = 600 nm) and Rh6G (λ_{em} = 550 nm) are calculated as $\eta_{RhB} = -1.58\%/°C$ and $\eta_{Rh6G} = 0.51\%/°C$ respectively. These recorded rates reasonably found within the values reported in other works [159, 161]. The significantly higher value of η_{RhB} makes Rhodamine B very useful for different T-responsive sensing applications.

Unlike the laser dyes, porphyrins are robust, thermally stable conjugated ring systems. They are considered as an important cofactors found in many bio-molecules including chlorophyll and haem. Using the smartphone fluorimeter, the fluorescence (λ_{em} = 650 nm) of 50 μM 5, 10, 15, 20-tetraphenylporphirin (TPP, **5**) in acetone was recorded over the T range 10–40 °C. The result shows a very slow decrease of fluorescence for TPP with increased T (Fig. 3.6c). The rate of fluorescence decay is recorded as $\eta_{TPP} = -0.45\%/°C$. The robustness along with rigidity compared to the dyes makes the porphyrin much thermally stable. Relatively high thermal stability of porphyrin dyes is also reported by others where no decomposition was found until 200 °C [162].

3.5.2 Time-resolved Fluorescence Measurements

The temperature-controlled smartphone fluorimeter was also applied to measure time-resolved fluorescence of the chemosensor **2**. As reported in [126], temperature effects can reverse the metal ion selectivity of this chemosensor dye between Cu^{2+} and Zn^{2+}, making it possible to use fluorescence to monitor multiple metal ions in one sample [126]. For instance, it has been shown that, in the presence of electron

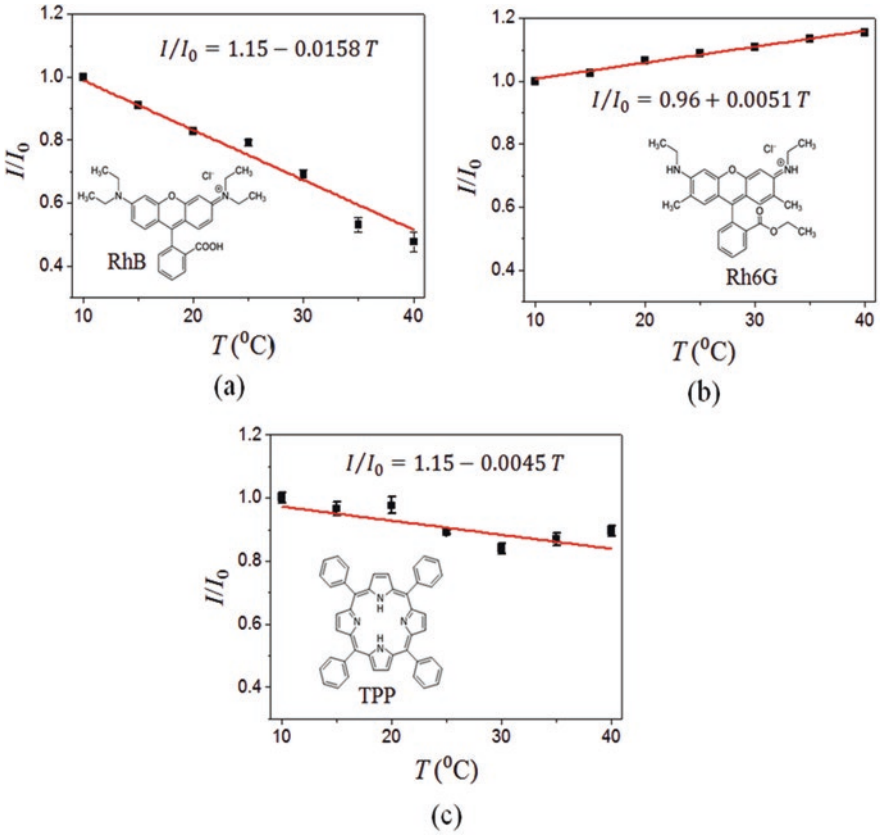

Fig. 3.6 Temperature dependent fluorescence measurements of two laser dyes (**a**) rhodamine B; and (**b**) rhodamine 6G, and (**c**) a porphyrin emitter 5,10,15,20-tetraphenylporphirin on the Arduino driven smartphone fluorimeter [124, 125]

donor Cu^{2+}, PET in the ligand **2** increases whereas net fluorescence (ΔI) decreases as a function of T, which is exactly the opposite of the case with Zn^{2+}. However, the rate at which the ligand/complex bends can be slowed by reducing the temperature of the solvent system, which means that at sufficiently low T ($\leq$10 °C), the effect of Zn^{2+} on the overall fluorescence emission is greatly diminished and is effectively zero. Therefore, only Cu^{2+} can react with the ligand.

To demonstrate the potential in a practical scenario when both Zn^{2+} and Cu^{2+} are present with the ligand **2** in a concentration ratio 1:1:1, a net decrease in fluorescence with decreasing temperature is observed as shown in Fig. 3.7. This net fluorescence decreases at T = 10 °C to the same value in the sample containing Cu^{2+} alone [126], indicating that the Zn^{2+}-bound species is not triggering a change in fluorescence output at this temperature—Cu^{2+} preferentially binds with the ligand ahead of Zn^{2+}. Thus by decreasing T to sufficiently low, the presence of the Cu^{2+} can be identified.

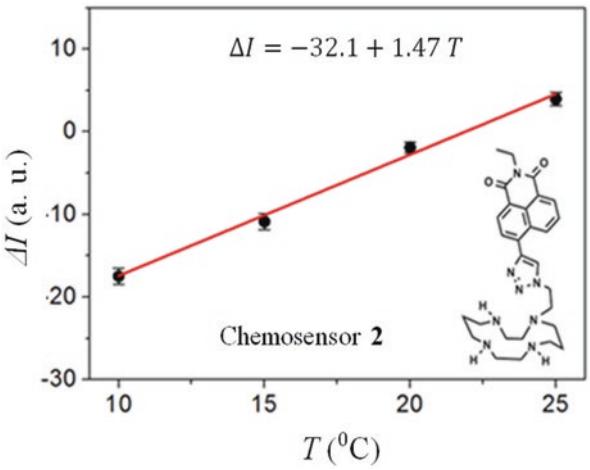

Fig. 3.7 The change of net fluorescence, ΔI (I-I_0) at different T of a chemosensor dye **2** with dye:Zn^{2+}:Cu^{2+} = 1:1:1 concentration ratio. Data were obtained using the Arduino driven smartphone fluorimeter [125]

A theoretical study of molecular structure of the chemosensor **2** reveals that, in the presence of Zn^{2+} only, the ligand is bent, and the fluorescence emission through intra-molecular charge transfer is characterized by an intensity growth of up to 1 min [126]. This is a remarkably long timescale caused by a physical movement of the electronic distribution around the molecule. As the bend is directly linked to the intra-molecular charge transfer and so the presence of metal ion (Zn^{2+} in this case) in the solution, the bend can be directly estimated from the change of fluorescence emission. Here, the smartphone fluorimeter has been used for the time-resolve evolution of fluorescence measurements to determine this twisting and bending rate, identified through a bending rate constant. In this case, the smartphone app operates in time-resolved mode where it captures a total of $n = 75$ images of the fluorescent sample at a regular interval, $\delta t = 4$ s. The normalized fluorescence intensities were plotted locally on the smartphone screen as (I/I_0) vs t and also sent to a computer for detail analysis as well as archiving.

In order to investigate the factors that can tune this mechanical bending, both the optical and thermal excitation using the smartphone fluorimeter were varied and the rate of "bending and twisting" measured. Figure 3.4a shows linear relationship between optical output and diode current which enables varying optical excitation directly by adjusting the current through the UV LED. On the other hand, thermal excitation was varied by adjusting the temperature of the sample from different Peltier current. The emission intensity is constant to the peak wavelength of the fluorescent emission ($\lambda \sim 450$ nm) which, as expected, grows at a constant rate with time for all given excitations. The normalized fluorescence intensity plotted in Fig. 3.8 (as (I/I_0) vs t for different 370 nm diode currents) shows little variation within experimental error. A little, reproducible increase in intensity with increasing diode current is preassembly due to local heating of the components which is not able to be dissipated quickly enough.

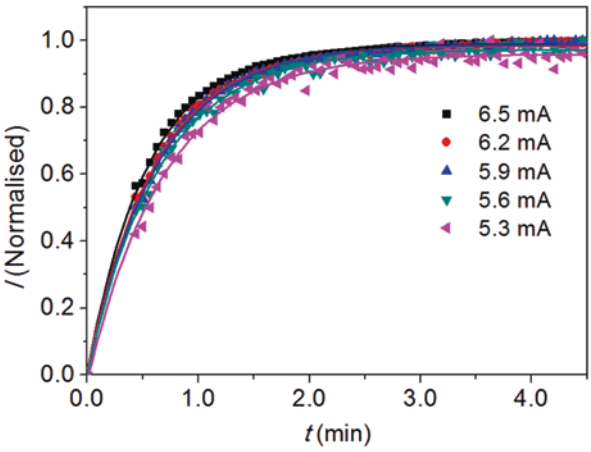

Fig. 3.8 Emission intensity, *I* of **2** (normalized to the final intensity) with Zn^{2+} (1:1) at room temperature (22 °C) for different excitation current as a function of time, *t*. Data collected on to the smartphone fluorimeter [124]

A reasonable conclusion is that there is no observed control of the rate of bending and twisting arises from optical excitation—this is obvious given that electronic transition is relatively fast whereas mechanical relaxation is slow. So fine tuning this optical "nanobot" using light is not possible [163].

To impact the rate of bending, the structure requires direct alternation of the mechanical process—the most obvious way to achieve this is by varying temperature which was hinted in the data of Fig. 3.8. So the fluorescence evolution was observed on the smartphone fluorimeter by varying *T* of the sample. Figure 3.9 shows the normalized intensity as a function of time for experiments at a range of different *T*. As anticipated, the rate of fluorescence change increases with increasing *T*. From the emission data, it is plausible to quantify the rate of molecular bending as a function of bend angle, assuming that bending is the dominant process involved here. The single exponential growth of emission data can be expressed directly to express the rate of bending as a function of *T*:

$$\theta = \theta_0 (T) e^{-kt} \tag{3.4}$$

where θ_0 is the initial angle, *k* is the rate constant, *T* is the temperature and *t* is the time of exposure. At a given T, the bending angle can be quantified by knowing the initial angle θ_0. From the exponential fits of the normalized data (solid lines), it is possible to extract the rate constant in min^{-1} at each temperature used in Fig. 3.9 as well as for each excitation current used in Fig. 3.8. These are summarized in Table 3.1. These values were also compared with those obtained from a benchtop fluorimeter measurement and found reasonably matched each other [126].

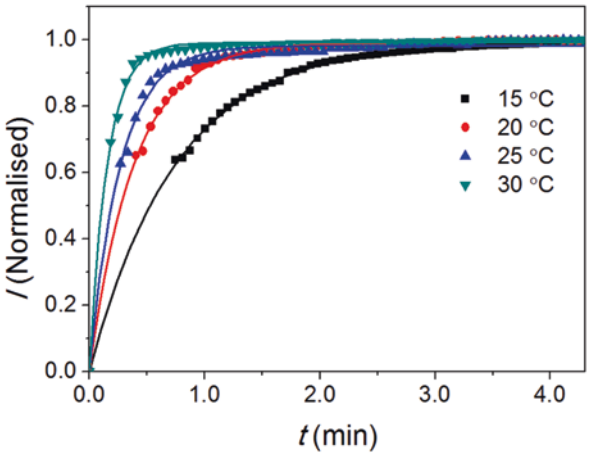

Fig. 3.9 Emission intensity, *I* of **2** with Zn^{2+} (1:1) at four temperatures (15, 20, 25 and 30 °C) for fixed excitation at 370 nm as a function of time, *t*. Data collected on to the smartphone fluorimeter and normalized to the final intensity [124]

Table 3.1 Bending rate constant (*k*) at different excitation energy and temperature

T (°C)	*i*(mA)	*k* (min^{-1})
22	5.3	1.45
22	5.6	1.55
22	5.9	1.61
22	6.2	1.64
22	6.5	1.81
15	5.9	1.94
20	5.9	2.57
25	5.9	2.84
30	5.9	3.64

3.6 Summary

In summary, the time-resolved and temperature responsive fluorescence measurements have been understood through the lab-in-a-phone technology. Temperature and time-resolve fluorescence response of a naphthalimide dye was studied. Chemosensor dyes of this type are significantly important for environmental and biological sensing and therefore widely studied in literature. The process proposed and explored here provides a novel strategy for selective identification and separation of two environmentally and medically important metal ions, Cu^{2+} and Zn^{2+}, along with concentration estimates through titration and careful fluorescence measurements. The instrument has a great potential in performing similar measurements for other types of chemosensors having T-responsive emission property.

Chapter 4
Smartphone "Dual" Spectrometer

4.1 Introduction

Traditionally, most smartphone-based colorimetric devices including the intensity fluorimeters demonstrated in the previous chapters are designed to detect intensity through three specific color bands (red, green and blue) set by the color filters used in the smartphone's CMOS camera pixels [19–34]. More advanced instrumentations, such as spectrometers, are receiving ever more research attention due to their capability of extracting more information by looking at range of wavelengths [82–84, 86–93]. This chapter will discuss the developments of a number of smartphone spectrometers, covering optical design, fabrication, app development, calibration and finally some proof-of-principle applications.

For spectroscopic measurements, a light dispersion element of some sort is required with other optical components. For example, a collimating tube has been utilized in an early version smartphone spectrometer with a transmission grating to measure sample spectra on the CMOS chip of a smartphone. The work claimed a spectral resolution of ~ 10 nm, which can be improved by a factor of 2 after image processing [90]. In other work, a thin-film transmission grating was attached in front of the smartphone CMOS chip to capture absorption spectrum of an enzyme-linked immunosorbent assay [84] and also allowed the detection of narrow band reflection from a photonic crystal biosensor [164]. These applications invariably involved external emission sources such as broadband white light sources which required their own power supply [82–84, 86–93]. Another example exploits a simple prism to probe samples with the transmitted evanescent wave component of reflected light [86]. The necessity of an external power source, however, serves as a hindrance in terms of the portability of the device and ease of deployment in the field. This somewhat limits the potential of these systems as true lab-in-a-phone spectrometers for environmental and bio-diagnostic field applications.

A key challenge, therefore, is to build spectrometers that are completely self-contained where the smartphone battery, which can be recharged anywhere, powers

A. Jamalipour, M. A. Hossain, *Smartphone Instrumentations for Public Health Safety*, Wireless Networks, https://doi.org/10.1007/978-3-030-02095-8_4

the entire system [68]. Low-cost and ease of use are also important. Furthermore, system efficiency and overall diagnostic capability can be greatly improved if the system supports multiple spectroscopic capabilities. To this end, this chapter demonstrates a combined “dual” absorption and fluorescence spectrometer, using a low-cost nano-imprinted dispersive element. Absorption measurements are made using a white light LED which has sufficient irradiance and spectral breadth to suit a vast range of applications. For fluorescence measurements, it demonstrates the simple integration of low-cost visible (VIS) and ultra-violet (UV) LEDs into the smartphone, allowing dual (or tri-fold) measurements to be undertaken with only one instrument. Absorption and fluorescence spectroscopies are selected to demonstrate multiple spectroscopy since they are the dominant methodologies used to investigate a wide range of molecular properties in chemical and biological science for sensing and diagnostics. The general concept of multiple spectroscopy by the lab-in-a-phone technology can be applied to any other smart interrogation methods, not only in a phone but also within smart watches, tablets, glasses [69] and many wearables.

4.2 Basics of an Absorption and Fluorescence Spectrometer

Spectroscopy is a process in which light is collected, broken-up into its various spectral components, recorded on a sensor (typically a CCD array) and then digitized into light intensity as a function of wavelength, the resultant plot is displayed on a screen on the instrument or connected computer [165]. The first step in this process is to direct light into the spectrometer through the entrance slit. The light is then collimated by a convex lens or mirror and directed onto the surface of a dispersive element the spectral components of the light at slightly varying angles, which are then focused by a second convex lens and imaged onto the detector array. The output diffraction is scanned through an exit slit and detected on a charged couple device (CCD) or a photodetector array such as CMOS camera. Once imaged, the photons are converted into electrons that are digitized and read out on a processing device (e.g. desktop computer). Software interpolates the signal based on the number of pixels in the detector and the linear dispersion of the diffraction grating to create a calibration that enables the data to be plotted as a function of wavelength over the given spectral range.

There are a number of spectroscopic techniques available with a variety of instrumental set ups. Among them, absorption and fluorescence spectroscopies are two widely used techniques and also commonly reported, to date, on smartphone platforms [82–84, 86–93]. Figure 4.1a shows a basic spectrometer system showing absorption measurements from sample solutions contained in a cuvette. In an absorption spectrometer set-up, absorbance (A) is defined by the absorption coefficient of the sample at that particular wavelength and path length of the light through the sample. The absorbance may be expressed by the Beer-Lambert law as below.

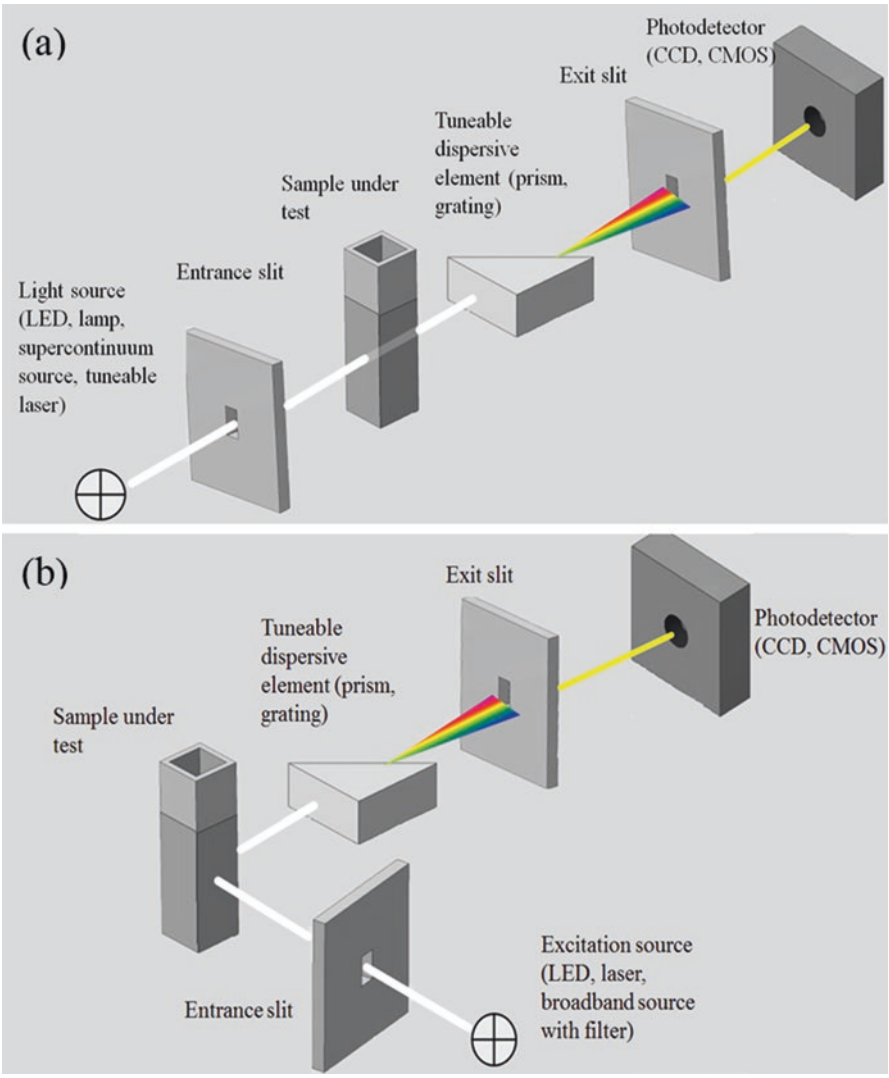

Fig. 4.1 Basic configurations of—(**a**) absorption spectrometer; and (**b**) fluorescence spectrometer systems

$$A = -\log_{10}\left[\frac{I_0}{I}\right] \tag{4.1}$$

where I_0 is the intensity of light entering the sample, and I is the intensity leaving the sample. In order to record I_0, a reference measurement is performed without any sample in place. I_0 can also be recorded in a double-beam instrumental set up where the optical signal is split and passes through both the sample and a reference.

However, the single-beam spectrometer is preferable for compact miniaturized instrumentation such as that of a smartphone platform. Although the sample cuvette is placed *before* dispersion of the light beam, there are also spectrometers which are designed for opposite scenario *i.e.* the sample is placed *after* the light dispersion [165]. For a portable system, spectrometers are typically designed in order to have the minimum number of required optics, placing the sample *before* the monochromator is therefore desirable and also allows for the maximum light intensity to interact with the sample.

In contrast to absorption spectroscopy, fluorescence spectroscopy measures electronic transitions from the excited state to ground state of a molecule which is typically achieved by exciting the molecule with light of higher photonic energy than the electronic transition [136]. In fluorescence spectroscopy, the instrumental set up enables the emission intensity across all wavelengths to be displayed. In order to maximize the photon detection and reduce the background scattering from the excitation source, the excitation source is positioned at an orthogonal angle to the emission path as depicted in Fig. 4.1b.

4.2.1 Dispersive Elements for Smartphone Spectrometer

A monochromator is the key component of a spectrometer system as its function is to disperse polychromatic or white light into their individual wavelength components and select a narrow band of this spectrum using a slit. Traditionally this dispersion was accomplished by using prisms but modern spectrometer systems now tend to use highly efficient diffraction gratings instead. Physically, a diffraction grating is a periodic structure of evenly spaced ridges or grating lines. These grooves or opaque lines diffract the incident light depending on its periodicity, d and wavelength of the light, λ. Optically they can either operate in transmission or reflection, which determines the spectrometer design configuration [166]. In the case of white light passing through a prism, a rainbow-colored pattern is clearly discernible on a projection surface. Low-cost, compact size dispersive elements are typically preferred for portable spectrometers. Diffraction gratings are typically expensive components as they often involve complex holographic manufacturing techniques or other sophisticated methods such as diamond scribing. For portable instrumentation that needs to be cost-effective for field application, custom designed optics such as 3D-printable micro-prisms, G-Fresnel lens, 3D-printable micro-fibres etc. have been produced using low-cost techniques. In lie with this purpose, a diffraction grating used in the work is fabricated in-house using a simple nano-imprinting method. Here, a silica transmission phase mask is used as a template upon which a liquid monomer is deposited, the monomer polymerizes with high spatial resolution, similar to that used to make transmission phase gratings [167].

The process of fabricating nano-imprinted polymer diffraction grating is described through the step-by-step layout shown in Fig. 4.2. In step 1, the transparent polymer solution is slowly spread on the surface of a silica phase mask using a

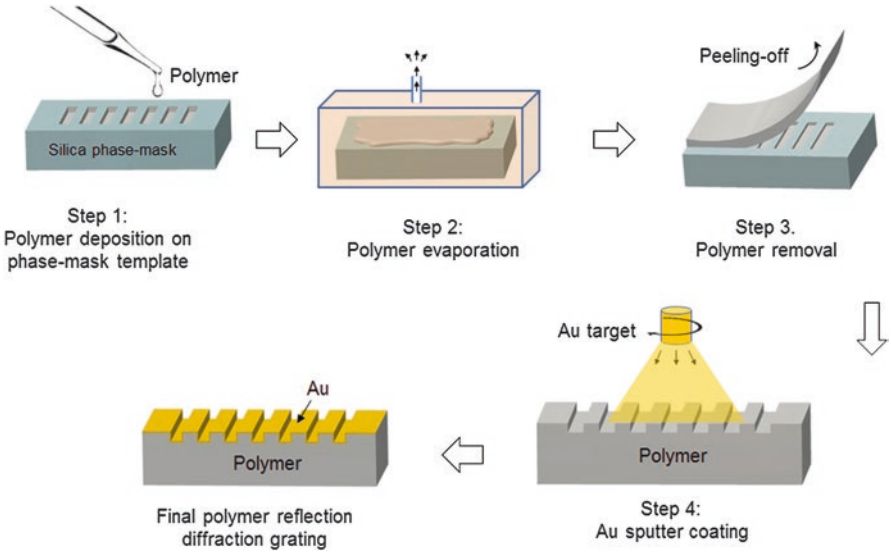

Fig. 4.2 Fabrication process layout of the polymer diffraction grating using a phase mask template

pipette drop so that the polymer uniformly covers the whole surface area of the phase mask. The phase mask is then kept in a closed chamber for approximately ~ 24 h (step 2). The chamber has a very narrow ventilation window to allow slow evaporation of the polymer. The end result is a very thin layer of dried polymer formed on the surface of the phase mask. The next step involves removing the dry polymer layer from the phase mask which can be peeled-off with relative ease using tweezers (step 3). Removing the polymer from the phase mask template produces a periodically pitched grating d ~ 1064 nm on its surface (a "carbon copy" of the master template) which performs excellently as a transmission grating. To obtain a reflection grating and improve diffraction efficiency, a layer of gold can be sputtered over the polymer surface using a sputter coater (step 4). An image of the diffraction pattern of white light from the final version of the grating is shown in Fig. 4.3.

The performance of the monochromator is typically defined by the dispersion efficiency and level of stray light. Therefore, dispersive elements are also chosen for high efficiency to maximize the ability to detect low light levels. Resolution is also important factor, with high resolution required to observe narrow spectral features. The line density, G, is another important figure of merit and has a significant impact on the dispersion efficiency and spectral resolution. The high G value of the polymer diffraction grating is comparable with many commercial gratings. Monochromators based on concave gratings can have fewer reflecting surfaces, lower stray light, and can be more efficient. A concave grating can serve as both the diffraction and focusing element. In order to serve as a low-cost dispersive element, the surface of a standard blank DVD disc can be utilized. The alternating grooves and highly reflecting surfaces of DVD serve well as a reflecting diffraction grating. Details of

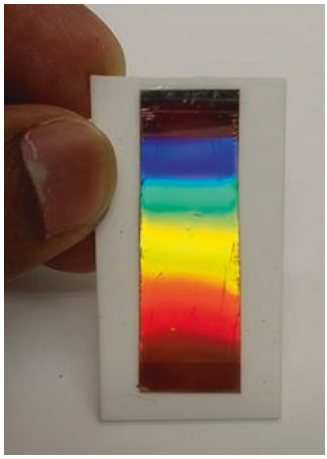

Fig. 4.3 Polymer diffraction grating showing white light diffraction [85]

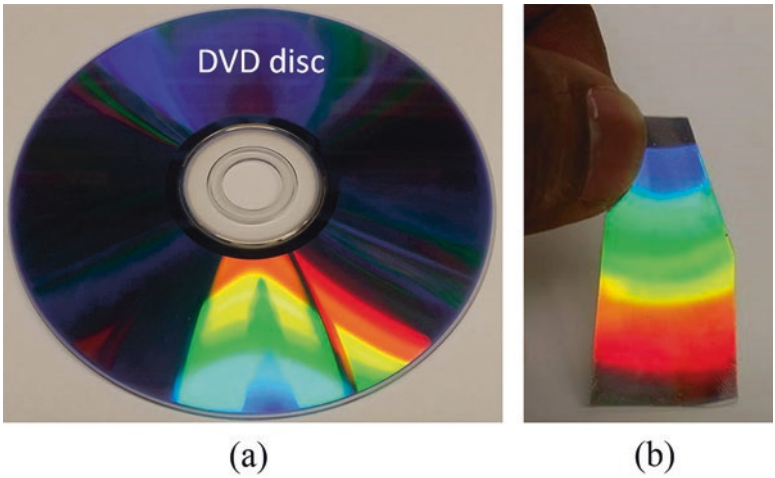

Fig. 4.4 DVD functioning as a diffraction grating. (**a**) A blank DVD disc and (**b**) the dispersion of white light from a rectangular piece of the DVD used in the smartphone spectrometer

their grove patterns reported in many reports [165]. Figure 4.4 shows an image of the typical white light diffraction from a DVD surface. This low-cost available dispersive element also has been utilized in one of the smartphone spectrometers discussed in Chap. 5. An estimation on its groove density, $G = 1/d$ is also made by measuring the diffraction angle, θ of a monochromatic light and Bragg's equation.

$$dsin\theta = m\lambda \tag{4.2}$$

4.3 Smartphone "Dual" Spectrometers

Similar to the intensity fluorimeter, the spectrometer also utilizes the smartphone driven in-built detector and optical sources. Additionally, by integrating multiple optical sources into the smartphone's flash LED circuit, the spectrometer offers multiple functionality—both absorption and fluorescence spectroscopy on a single device [89]. This can be illustrated by combining both the configurations of Fig. 4.1a, b into a single platform as shown in Fig. 4.5a. The instrument demonstrates the world's first smartphone battery powered spectroscopic device while providing the additional benefit of multiple functionalities. The proof-of-principle application

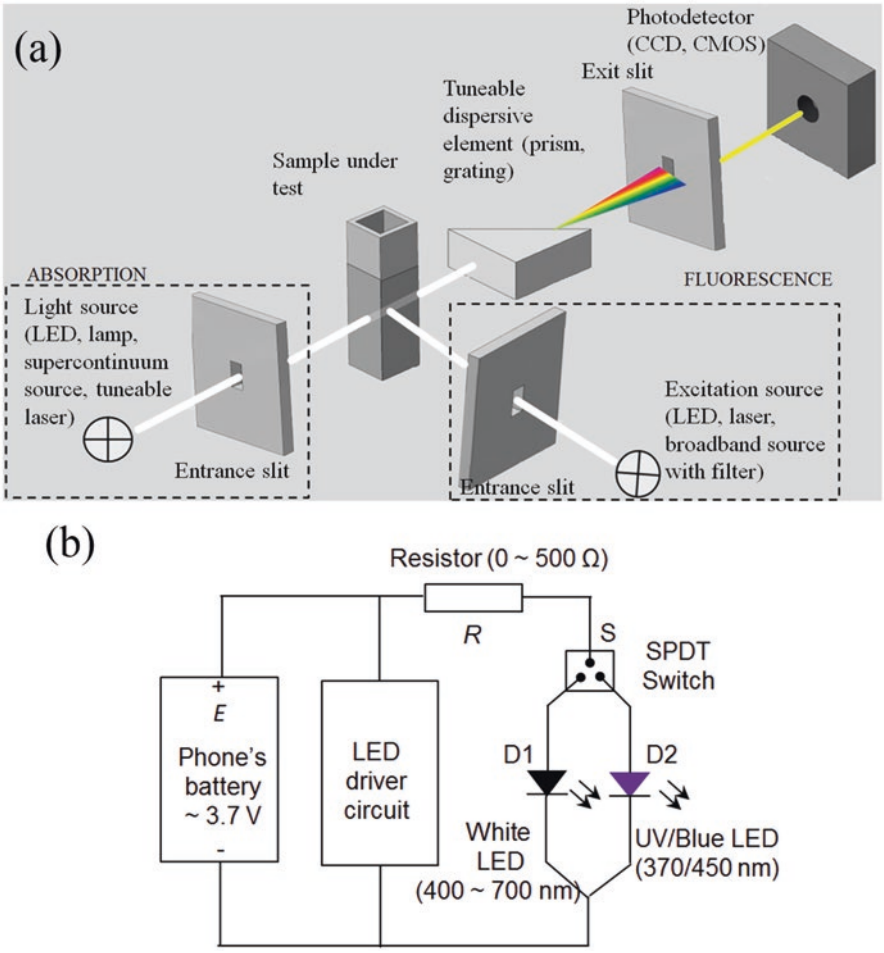

Fig. 4.5 Illustration of the combined "dual" absorption and fluorescence smartphone spectrometer: (**a**) schematic of the optical layout; and (**b**) electrical connections of optical sources [85]

has been demonstrated by measuring absorption and fluorescence spectra of various chemosensor dyes used in public health safety.

4.3.1 Optical Layout

The general optical layout of the smartphone "dual" spectrometer is shown in Fig. 4.5a. The excitation source for generating fluorescence is integrated into the phone by connecting a VIS (blue, λ_{ex} = 450 nm) or UV LED (λ_{ex} = 370 nm) in parallel with the existing white LED. The design considered these wavelengths because absorbance of most of the sensor dyes lie in this region of the spectrum, however, any other wavelength can also be added to extend the fluorimeter's capability further. An electrical connection diagram of the sources is shown in Fig. 4.5b. To ensure appropriate current for all systems, a resistor, R = 500 Ω is used in series with the LEDs. Selection between the LEDs was performed using a single pole double throw (SPDT) switch (S). The white LED is physically positioned in the optical axis to send the light directly through the sample contained in a cuvette whereas the UV LED is placed at an orthogonal angle to the cuvette as used in the intensity fluorimeters (Chaps. 2 and 3). This positioning of the UV LED reduces the unwanted UV scattering reaching the dispersive element and finally to the detector. The fluorescence emission is collected from the front facing surface of sample and diffracted using the polymer diffraction grating fabricated using the nano-imprinting technique. Therefore, the position of the grating in the smartphone spectrometer is designed to receive reflection to the smartphone camera as shown in the 3D design of the spectrometer in Fig. 4.6. The grating disperses the incoming light over

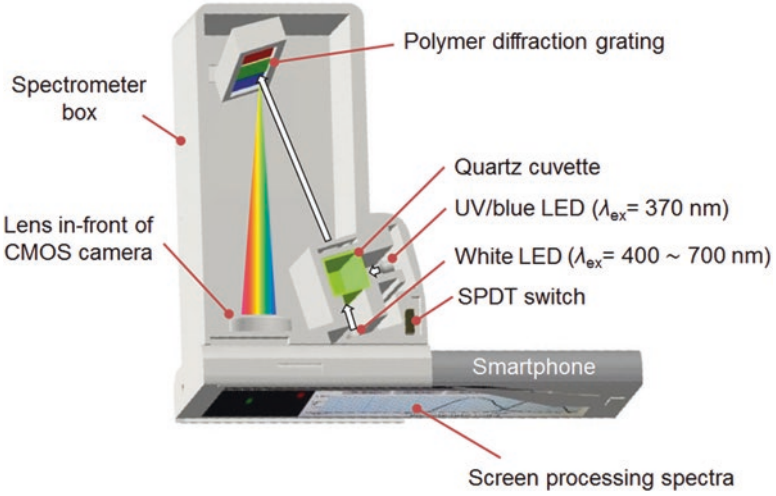

Fig. 4.6 3D AutoCAD design of the combined "dual" absorption and fluorescence smartphone spectrometer

a solid angle θ, calculated using the following diffraction equation derived from the Bragg's equation for an uncrossed Czerny-Turner type spectrometer, where λ_c denotes the centre wavelength and φ denotes the angle between incident and diffracted light [168].

$$\theta = \varphi - \left[\sin^{-1}\left(\frac{\lambda_c G}{2\cos(\varphi/2)} \right) - \frac{\varphi}{2} \right] \tag{4.3}$$

From Eq. (4.3), diffraction within the visible wavelength range ($\lambda \sim 400$–700 nm) requires $\theta = 28°$, which varies over a solid angle of $\Delta\varphi \sim 9°$ from blue to red end (when $\varphi = 45°$). The solid angle spread by the first order dispersion ($m = 1$) of the grating over the CMOS chip is sufficient to cover the visible band of the electromagnetic spectrum ($\Delta\lambda \sim 300$ nm). Considering the physical dimension of the smartphone's CMOS chip and its focusing lens, an external focusing lens is used to collect and cover the whole range of dispersion on the CMOS chip.

4.3.2 3D Design and Fabrication

At first, positions of all optical components including the diffraction grating and CMOS camera were calculated by testing the components on an optical bench. Once the parameters are fixed, the 3D structure of the smartphone "dual" spectrometer is designed in AutoCAD as shown in Fig. 4.6. The actual device is then fabricated in ABS polymer using a Redback 2X 3D printer. The 3D design contains a suitable chamber to place the sample cuvette from the top-side window. Optical sources (white and UV/Blue LEDs) are placed in two different slots in front of two different faces to the sample cuvette. The grating holder is a separately-printed element that is designed to hold the polymer reflection grating on a 5 × 2.5 cm substrate. The holder keeps the diffraction grating aligned 25° from horizontal axis and 34° from the vertical axis and located 8.0 cm from the CMOS chip.

This position of the grating and camera produces the required diffraction angle calculated in Eq. (4.3). The spectrometer was then attached to an Android driven Kogan Agora HD smartphone. However, the spectrometer box can be adapted to accommodate other smartphones as well as Tablets with only slight modifications in the AutoCAD design required. The 3D printed case holds all the components for light illumination, dispersion and collection and a suitable chamber for a sample cuvette. The upper part of the spectrometer box is closed with a cover once the sample is in place (Fig. 4.7). The whole assembly fixes firmly to the camera unit of the smartphone, is sufficiently robust for transport, and excludes light from external sources.

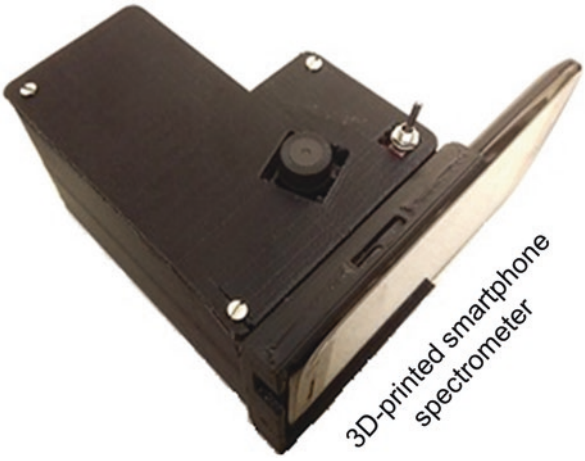

Fig. 4.7 The 3D-printed version of the combined "dual" absorption and fluorescence smartphone spectrometer

4.3.3 Smartphone Spectrometer App

A customized Android app is developed to digitally process the images produced by the diffracted light on the CMOS detector and then generate a plot of intensity, I vs. wavelength, λ. The functionality of the app consists of mainly two process-steps: the first step is to collect the image of the diffracted light and save to a blank canvas as a background image. In the second process, the image information is processed to generate a spectrum of I vs. λ as well and display the results on the smartphone screen. The front lens of the CMOS was adjusted to produce a diffraction image of 2D matrix of pixels (240×30) as a multi-color band of the diffracted light from the grating as illustrated by the schematic in Fig. 4.8. In the smartphone image processing system, this image is also a representation of a 2D color matrix or RGB pixels whose values are a real numbers ranging between 0 and 255 (as discussed in Chap. 2). Although the primary RGB elements of the 2D image matrix are directly used in many smartphone-based measurements [82–84], from an analytical perspective absolute intensity values formulated only from RGB are not accurate because the composition of these color bands does not change monotonically with spectral wavelength and intensity [109].

The transformation to an alternate color model, HSV (Hue-Saturation-Value) colour map, for example, from primary RGB color is one way to improve this consistency [83]. HSV is a cylindrical coordinate representation of points in an RGB color space, where the V axis represents brightness or intensity, I of a corresponding colour determined by

$$V = I = \max\left[R,,G,,B\right] \tag{4.4}$$

Therefore, the RGB values in the work detailed here are converted into HSV by following Eq. (4.4) and assumed to be sufficiently accurate in terms of absolute

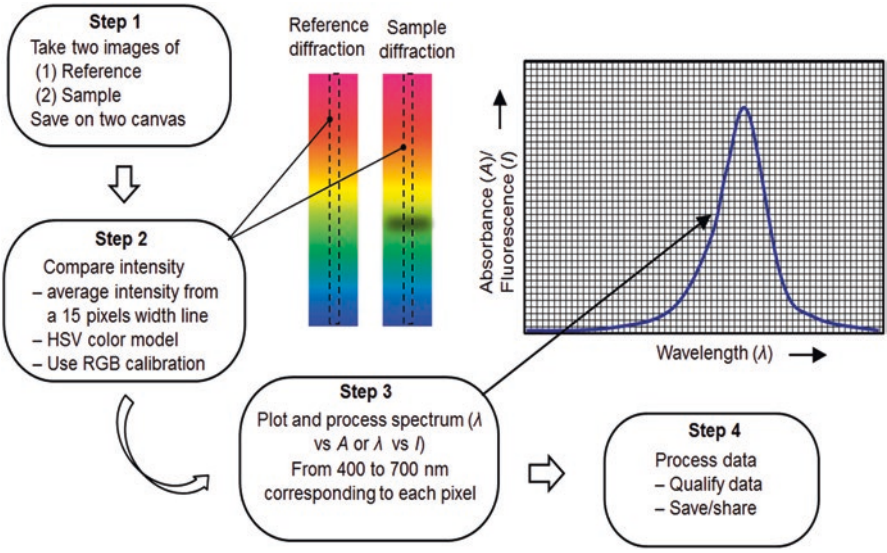

Fig. 4.8 General workflow of the smartphone spectrometer app

intensity. For illustrating absorption measurements, two images (one with the sample and the other one with a reference), saved on two adjacent canvases on the app screen are shown in Fig. 4.8 (Step 1). In contrast to absorption measurement, for fluorescence, only the image of the sample is taken whilst the reference image is a dark background. In step 2, the pixel intensity difference between the colour bands of the two images were extracted (averaged from a 15 pixel wide shown within the dotted line box) and plotted on a previously saved blank graphical screen as A (or I) vs. λ in step 3. The 8MP CMOS chip of the Kogan Agora phone gives a single pixel wavelength increment of $\sim$ 0.13 nm/pixel; however, the final resolution of the spectrometer is determined by the phone's display. The maximum number of screen pixels (720 = 240 × 3, including red, green, blue sub-pixels), leads to a spectral resolution of $\delta\lambda$ = 0.42 nm/pixel. Absorbance, A is calculated by considering the Beer-Lambert's law (Eq. (4.1)). The A or I at any specific λ can be monitored by selecting that λ position. In the final step, the app allows to share the results with other devices as well as save within the phone's memory.

4.3.4 Calibration

The wavelength axis of the spectrometer app was calibrated against a standard commercial fiber-coupled spectrometer (Ocean Optics HR4000) and a bicolor LED (λ_{green} ~ 562 nm and λ_{red} ~ 637 nm). To do this, the bicolor LED was placed at the same position as the original LED and its spectrum at different wavelength was

recorded on the smartphone camera. Figure 4.9 is the screenshot of the smartphone spectrometer app showing the spectra of both bands of the bicolor LED. The known wavelength of the LED lines and their separation was used to set the wavelength span corresponding to the pixel scale along the illumination direction. The second correction factor can be applied from the scaled difference between intensities measured on the reference spectrometer and the smartphone spectrometer. A complete calibration of smartphone spectrum considering both wavelength and intensity scale is presented in Chap. 5. The spectra presented by the "dual" spectrometer and presented in this following section are screen images taken directly from the smartphone.

4.3.5 Spectrum Measurements

The proof-of-principle of the smartphone dual spectrometer has been demonstrated by measuring both absorption and fluorescence spectrum of two readily synthesised organic chemosensor dyes and compared them with standard benchtop instrument measurements. Chemosensor dyes of these types are widely used in environmental sensing applications. The pH-sensitive probe used herein is the same as that used in Chap. 2 (probe **1**) and the Zn^{2+}-responsive is same as that used in Chap. 3 (probe **2**) [141, 143]. The emission bands of both probes fall within the smartphone spectral range when excited by $\lambda_{abs} = 450$ (pH-chemosensor) and 370 nm (Zn^{2+}-chemosensor), and have been used in previous studies for pH measurements and Zn^{2+} ion detection in aqueous solutions. The ability to quantify a pH value and Zn^{2+} ion concentration in different environmental, biological and medicinal samples is important for both environmental and human health applications. Accurate monitoring of pH as well as metal ions such as Zn^{2+} ensures that the quality of water supplies is maintained.

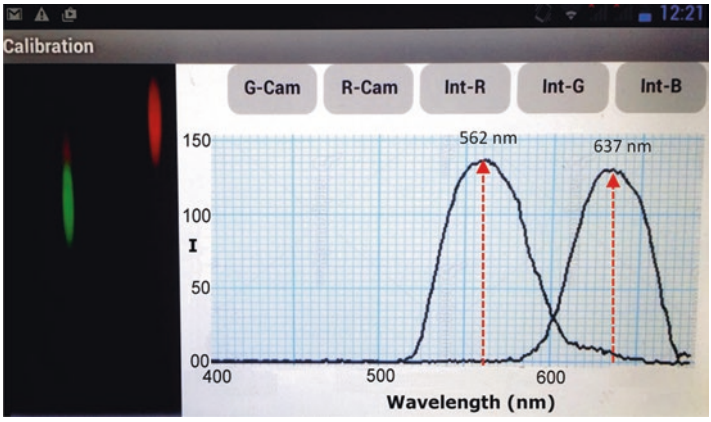

Fig. 4.9 Spectrum of green (λ_{green} = 562 nm) and red (λ_{green} = 637 nm) LEDs measured on the smartphone spectrometer screen to calibrate the wavelength scale [85]

4.3.5.1 Absorption Spectroscopy

To measure the absorption spectra, concentrated ligand solutions were prepared using dimethyl sulfoxide (DMSO) as a carrier in case of the fluorescent pH-probe ([**1**] = 1 mM). On the other hand, the Zn^{2+}-responsive fluoro-ionophore was dissolved in de-ionized water ([**2**] = 100 μM). In order to measure pH, the DMSO solution of the concentrated pH-probe was diluted using the HEPES buffer of different pH. The Zn^{2+}-detective measurements were performed by mixing the probe into solutions containing varying concentrations of the metal ion.

In order to measure absorption spectra, the switch S was set to turn-ON the white flash LED and turn-OFF the source for fluorescence excitation (UV or Blue LED). Images of the diffracted light taken for both sample and reference solution for the pH probe are shown in Fig. 4.10a. Figure 4.10b shows the measured absorption spectrum plotted on the smartphone app screen. The absorption spectrum of the same solution was also measured on a commercial benchtop spectrophotometer. Figure 4.10c shows the spectrum of the sample obtained by the spectrophotometer.

The absorption spectrum obtained from the smartphone spectrometer showed a peak at λ_{abs} ~ 450 nm with a 3dB bandwidth of FWHM ~ 70 nm. This characteristic for the Zn^{2+} probe was not measured since it absorbs below 400 nm (λ_{abs} ~ 358 nm)—the short wavelength limit of the smartphone camera.

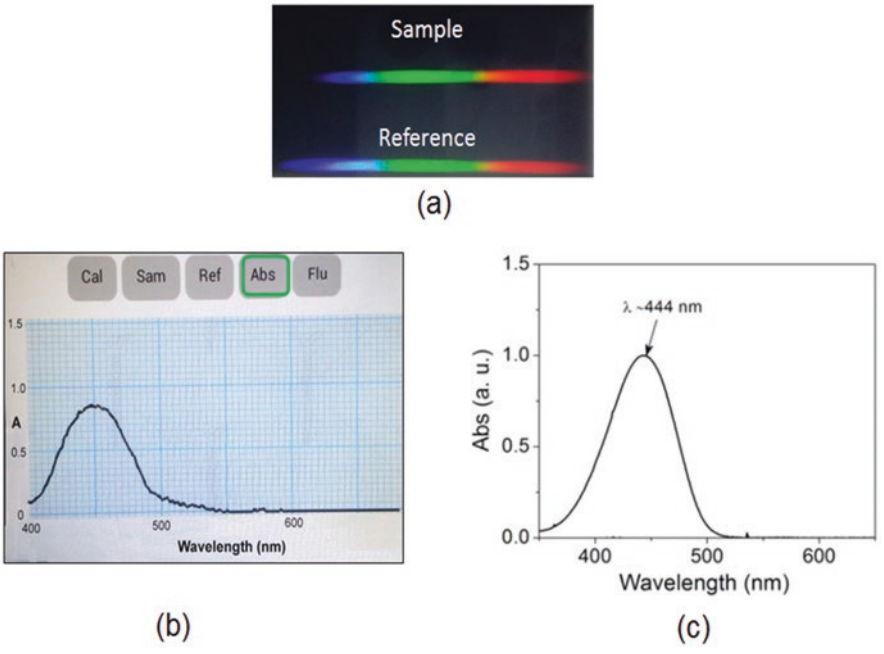

Fig. 4.10 Spectra measured on the smartphone and benchtop spectrometer. (**a**) Images captured on the mobile camera showing the optical dispersion from the diffraction grating of light transmitted through the sample solution and water as reference. Absorption spectra of the pH probe acquired with: (**b**) smartphone; and (**c**) benchtop spectrophotometer (SHIMADZU UV-2401PC) [85]

4.3.5.2 Fluorescence Spectroscopy

The fluorescence measurements on the smartphone spectrometer have been demonstrated with both the chemosensors dyes since their emission spectra fall within the detection range of the smartphone camera. For generating fluorescence, a blue LED (λ_{ex} ~ 450 nm) was used to excite the pH probe whereas a UV LED (λ_{ex} ~ 370 nm) was used for the Zn^{2+} probe. The spectra obtained from individual measurements on the smartphone spectrometer are overlaid in Fig. 4.11a. The spectra show the emission peaks for the Zn^{2+}- and pH-responsive probes at λ_{em} ~ 450 nm and λ_{em} ~ 525 nm, respectively.

The changes of fluorescence intensity for the probe in solution of three different pH value (pH ~ 6.09, 7.20 and 8.25) are consistent with the spectrum obtained from the benchtop measurements (Fig. 4.11b) as well as with previous work [122]. The pH probe shows a weak emission signal in the deprotonated form and increased fluorescence intensity with protonation. The small deviation in shape of the smartphone spectra compared to the benchtop instruments are preassembly arise due to the color intensity correction which could be partly avoided by the use of a reference for relative measurements.

4.3.5.3 [Zn^{2+}] Detection in Water

To evaluate the performance of the smartphone spectrometer, the instrument was used for the quantification of Zn^{2+} concentration via fluorescence spectroscopy. The fluorescence enhancement of the probe **2** with Zn^{2+}-coordination is shown in Fig. 4.12a. Detail of the coordination mechanism is discussed in [126]. The spectral changes were monitored on the smartphone camera by making a series of titrations increasing the absolute Zn^{2+} concentration from [Zn^{2+}] ~ 0 to 50 μM with each step

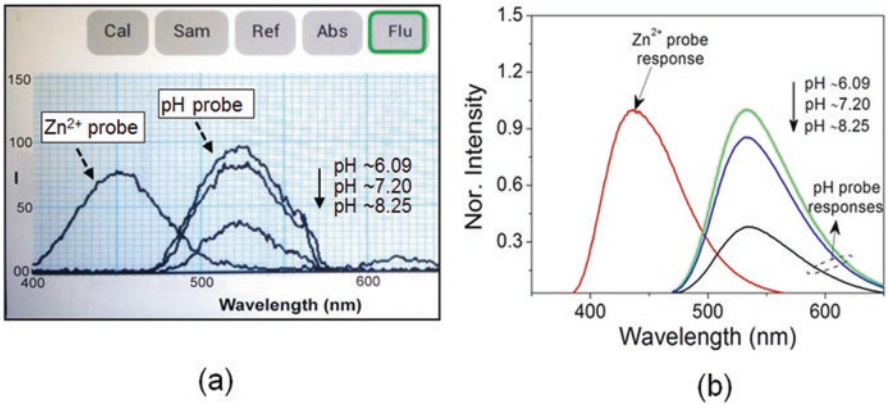

Fig. 4.11 Fluorescence spectra of the Zn^{2+}-responsive and pH-responsive dye acquired with—(**a**) the smartphone "dual" spectrometer; and (**b**) a benchtop fluorimeter (VARIAN) [85]

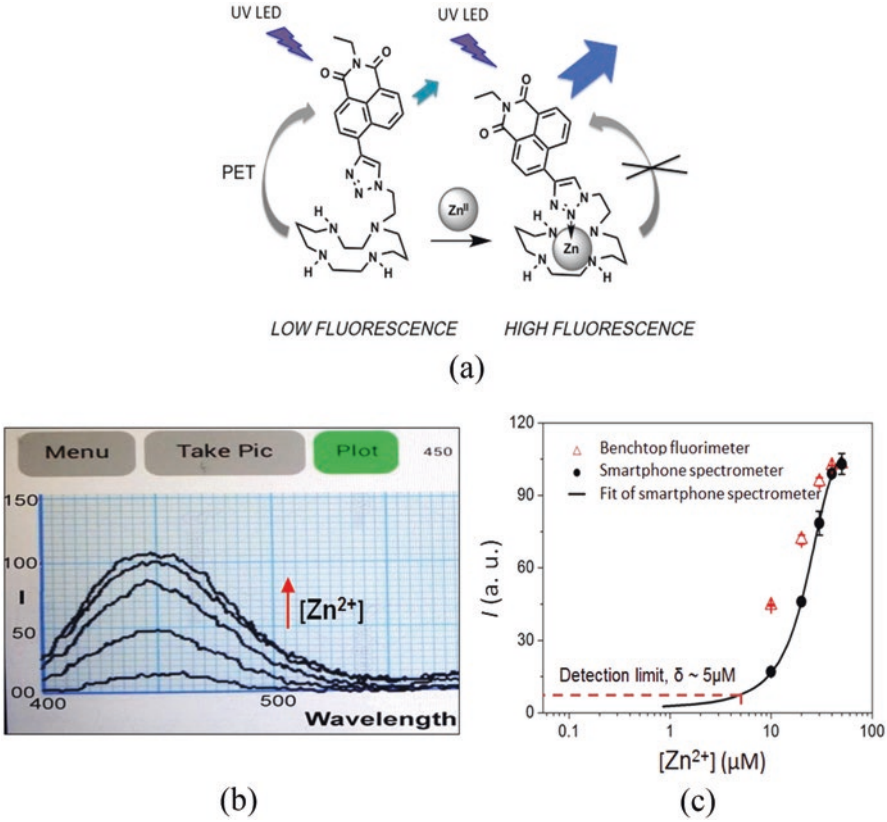

Fig. 4.12 Fluorescence measurement of $[Zn^{2+}]$. (**a**) Molecular structure of the probe **2** ((6-(1,4,8,11-cyclam-1-yl)ethyl-1,2,3-triazol-4-yl)2-ethyl-naphthalimide) and the fluorescence switching mechanism following the coordination of Zn^{2+}; (**b**) fluorescence titration spectra for $[Zn^{2+}]$ measured on the "dual" smartphone spectrometer; and (**c**) plot of intensities at λ_{em} = 450 nm measured three times with the smartphone "dual" spectrometer and benchtop spectrofluorimeter [85]

increment of 10 μM (Fig. 4.12b). Both the integrated emission signal and peak intensity approximately at λ_{em} = (445–460) nm rise with increasing $[Zn^{2+}]$. The same samples were measured with a benchtop fluorimeter (VARIAN) for comparison and a plot of the peak intensities from both measurements are shown in Fig. 4.12c. The results are consistent with the spectral changes reported in the literature [143]. The nonlinear fit equation derived from the data (Fig. 4.12c) was used for calibration. The fit equation was uploaded to the smartphone app allowing arbitrary measurements to be performed of samples containing unknown concentrations. To analyze the performance of the device, the instrument was applied to measure water sample of some known $[Zn^{2+}]$ using the fluorescence mode of the smartphone "dual" spectrometer. The data summarized in Fig. 4.13 demonstrate reasonable agreement between the actual concentrations and the smartphone measurements. The observed

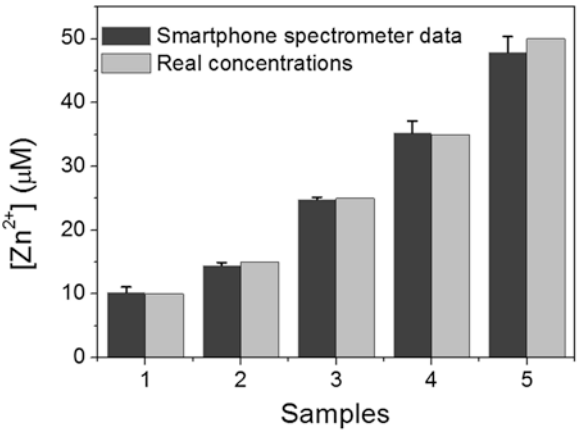

Fig. 4.13 Comparison of the results measured using the mobile fluorimeter with the $[Zn^{2+}]$ in water samples measured by titration [85]

discrepancy is larger than the experimental error of $\Delta I \sim 4.8\%$ from the standard deviation of three measurements. One important factor that can affect the spectral diffraction, resolution and overall measurement is un-collimated light that reaches to the grating surface. These effects have been addressed and will be discussed the modified version of the spectrometer presented in the next Chapter.

4.4 Summary

In this chapter, a smartphone spectrometer with multiple functionality has been demostrated through a step-by-step optical design, 3D fabrication, app development, calibration and finally some proof-of-principle applications. The key challenge in designing smartphone-based spectrometer is to build them in a way that they are completely self-contained where the smartphone battery, which can be recharged anywhere, powers the entire system. After describing the basics of an absorption and fluorescence spectrometer as well as dispersive elements for smartphone spectrometer, in this chapter, we outlined the design and development of smartphone "dual" spectrometers. By integrating multiple optical sources into the smartphone's flash LED circuit, the spectrometer offers multiple functionality, both absorption and fluorescence spectroscopy on a single device. The instrument demonstrates the world's first smartphone battery powered spectroscopic device while providing the additional benefit of multiple functionalities. The proof-of-principle application has been demonstrated by measuring absorption and fluorescence spectra of various chemo-sensor dyes used in public health safety.

Chapter 5
Smartphone Optical Fiber Spectrometers

5.1 Introduction

The advancement of smartphone instrumentation continues to penetrate further in spectroscopy by developing devices that are capable to measure sample in an arbitrary shape and place. In particular, to measure spectra from solids or surfaces, a flexible fiber bundle probe is integrated onto the designed smartphone spectrometer platform demonstrating an optical fiber smartphone spectrometer. The fiber bundle allows light collection in both ways—from source to sample and sample to detector. A customized Android app is written to process spectra on the smartphone platform; the data can be shared or analyzed remotely via the Internet. A step-by-step calibration process was used where specific correction factors are applied to produce an accurate spectral response [98]. The instrument has been demonstrated by measuring the visible absorption spectra of apples during their storage time. The optical fiber smartphone spectrometer was customized further by integrating an array of UV LEDs for fluorescence measurements while powering the entire system using the smartphone's battery, retaining the self-powered credential of the device. Using the instrument, visible fluorescence spectra were measured to characterize vegetable oils. Specifically, it has been shown that fluorescence spectroscopy can identify the visible emission bands of oils. Effects of storage on the overall degradation of olive oil's quality and an analysis of photo- and thermal degradation have been presented. The device demonstrates significant potential in rapid, on-site identification of food quality, the possibility of engaging consumers with quality control and, more broadly, opening up the quality assurance market to the wider public aided by Internet-of-Things (IoT) connectivity.

A. Jamalipour, M. A. Hossain, *Smartphone Instrumentations for Public Health Safety*, Wireless Networks, https://doi.org/10.1007/978-3-030-02095-8_5

5.2 Optical Fiber Smartphone Spectrometer

The majority of smartphone spectroscopy systems, including the "dual" absorption and fluorescence spectrometer, previously presented, are designed to measure samples in liquid phase through a cell, typically a cuvette. However, reflection spectroscopy of solid samples is often important in industrial and agricultural applications, within a human body or other places that are typically hard-to-reach. There are a number of micro-spectrometer suppliers working to meet this goal using small portable spectrometers with separate light, power and computer components [117, 118]. However, the work of the following section presents an alternative approach where the smartphone spectrometer is modified to include an endoscope for the sending and collection of light. This approach offers several benefits over the normal spectrometer, including using the smartphone battery to power the entire system and improve signal collection by avoiding unwanted stray illumination. The ability to access hard-to-reach places such as the inside of shipping cartons, the interior or back of a crop bushel or the inside of a human torso is an added advantage. This section will demonstrate the design, implementation, and application of an optical fiber spectrometer.

5.2.1 Optical Design, Materials and Methods

The optical layout of the optical fiber based endoscopic smartphone spectrometer is shown in Fig. 5.1a. Similar to the previous design, the in-built white flash LED is used as the primary optical source, however, any other external source, such as a UV LED for generating fluorescence, could also be integrated into the system and still be powered solely by the smartphone battery. The flash LED output is fed into the endoscopic fiber bundle using a flexible but highly durable polymer light-guide. The light-guide was made of polyethylene terephthalate (PET) material (L_1 = 16 cm, ϕ_f = 1.75 mm), similar to those used to fabricate 3D-printed optical fiber preforms [169]. An optical fiber bundle endoscope probe (Edmund Optics: Fiberscope, L_2 = 60 cm) is used for light collection from the source to the sample and the sample to detector. This fiber collection of light gives a better signal-to-noise ratio to the camera detection. The flexible fiber bundle also removes the difficulties to reach many difficult to access places as mentioned above. The endoscope probe consists of two types of fibers—illumination fibers and collection fibers. Within the endoscope probe, six fiber bundle rings transmit light from the smartphone source to the sample—these called illumination fiber (see Fig. 5.1b). The reflected or emitted light from the sample is collected through the collection fiber bundle which is positioned at the centre of the ring of the six illumination fiber bundles. At the end of the endoscope probe an objective lens increases light collection. At the other end of the endoscope probe, a second lens is used to collimate the collected light coming out of the fibers. This collimated light subsequently diffracted by a low-cost dispersive element. This diffracted light is finally imaged and calibrated across the CMOS

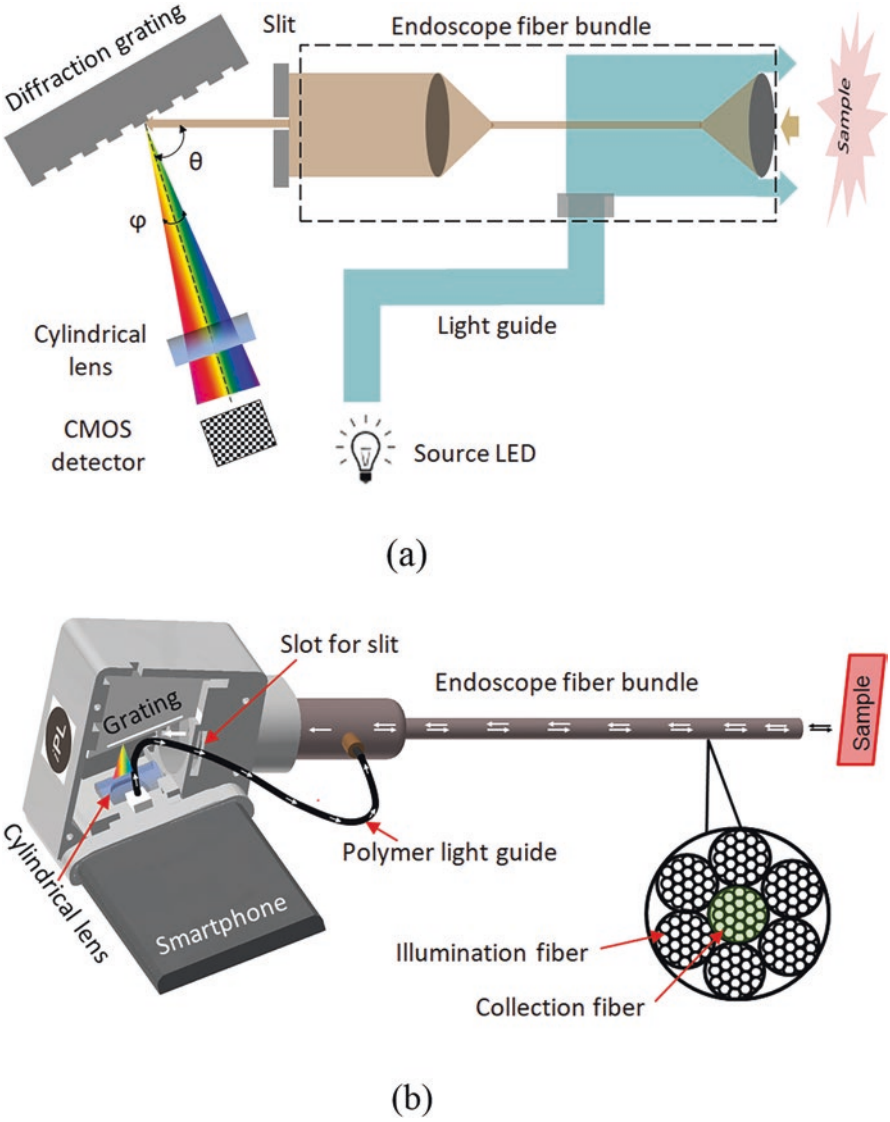

Fig. 5.1 Smartphone optical fibre endoscopic spectrometer: (**a**) the optical layout, and (**b**) the 3D design of the instrument package [98]

chip. A cylindrical lens is also used to improve light collection per pixel on the detector along the diffraction direction. Finally, a customized app is used to analyze and process the spectra.

The collimated beam width has been controlled by using a slit of width, $\omega_{slit} = 0.7$ mm, at the output end of the endoscope probe. As a dispersive element, a cut from a low-cost, standard blank DVD, $a = (3.0 \times 1.5)$ cm^2 was used in this instrument. Whilst not as efficient as a previously used nano-imprinted polymer

grating (Chap. 4), it performed with sufficient efficiency to spectrally disperse enough light onto the detector array. The alternating pits of the DVD had a density, $G \sim 722$ lines/mm [170]. This is also confirmed after measuring the first order diffraction of a red laser pointer ($\lambda_{red} = 660$ nm) at an angle of $\theta \sim 66°$ [$d\sin\theta_{diff} = m\lambda$], where d is the spacing between lines and θ_{diff} varies over a solid angle of $\Delta\varphi \sim 36.5°$. This diffraction angle was maintained when allowing the position of the grating within the spectrometer design.

The optical assembly is positioned within a 3D-printed enclosure designed in AutoCAD Inventor Fusion (Fig. 5.1b) and optimized for a Samsung Galaxy S4 smartphone (Fig. 5.2). The assembly is attached to the rear facing camera such that it is suitable for hand-held operation. The endoscopic fiber bundle is flexible and robust enough to move, probe and reach range of different surfaces.

5.2.2 Spectral Calibration

Calibration of the smartphone spectrometer enables correction of the spectral response corresponding to each pixel point of the diffraction light image on the smartphone screen. In order to achieve accurate response on the smartphone camera within the spectral band, the calibration procedure is divided into two steps: wavelength and intensity calibration.

5.2.2.1 Wavelength Calibration

Calibration of the wavelength (λ-axis) sets individual pixels' positions on the CMOS chip as well as on the AMOLED display to their corresponding wavelength value along the diffraction direction on the produced image. To do this, a broadband light source such as Mercury, Argon or any other fluorescent calibration source that has several emission lines in the visible range can be used [90, 93]. Here, the λ-axis of the spectrum was calibrated by using the emission from two known laser pointers ($\lambda_{green} \sim 530$ nm; $\lambda_{red} \sim 660$ nm). By knowing the spectral separation of the

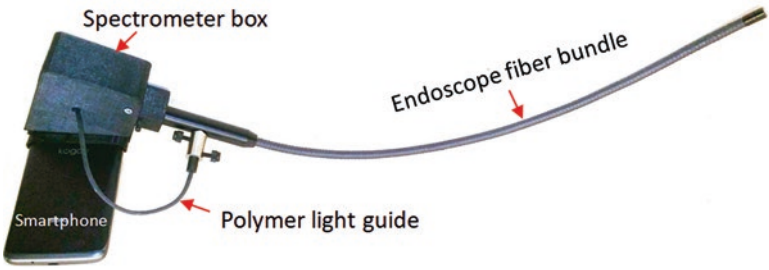

Fig. 5.2 3D printed optical fiber smartphone spectrometer installed on a smartphone

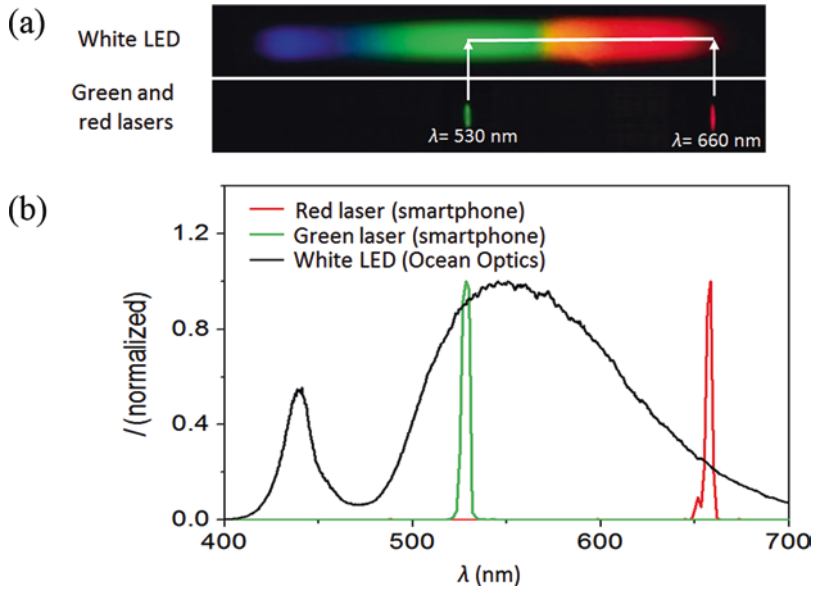

Fig. 5.3 Wavelength calibration of the smartphone spectrometer. (**a**) Diffraction image of a white LED and the location of green and red laser pointers captured on the smartphone camera; (**b**) spectrum of the laser pointers measured on the smartphone and compared to the whole spectrum measured on a standard spectrometer [98]

diffraction images of the laser pointers and their physical separation on the two-dimensional image pixels array, the λ-axis has been calibrated assuming that there is a linear relationship between wavelength and pixel separation. Figure 5.3a shows the smartphone screenshot covering the image of the diffracted light from the white LED as well as the location of the measured green and red laser pointers, also collected on the camera. As an accurate reference, the white light spectrum is measured using a commercially-available and factory-calibrated spectrometer (Ocean Optics HR 4000 model). The green and red laser spectra are measured on the smartphone spectrometer and are shown in Fig. 5.3b. The 489 pixels along the diffraction direction and over a span of $\Delta\lambda \sim 250$ nm determines the maximum possible resolution, $\delta\lambda \sim 0.55$ nm/pixel on the smartphone screen, however, the actual resolution of the devices, $\delta\lambda \sim 2$ nm is determined by the optical slit of width, $\omega_{\text{slit}} \sim 0.7$ mm.

5.2.2.2 Intensity Calibration

By performing an intensity calibration, the response of the CMOS chip is corrected by re-adjusting the RGB filter function for different wavelengths. This is necessary because the CMOS cameras of smartphones are almost always pre-calibrated by manufacturers to produce a real-life image rather showing an actual response, which is defined by the nonlinear sensitivity of the human eye. This means the digital

image produced by today's smartphone camera does not represent the actual response directly from the CMOS detector. Therefore, the V-information in the HSV color model is not sufficient to determine the brightness of the screen image unless the responses at individual RGB channels are recalibrated to reconstruct the actual responses at the detector's output. At present, for many smartphones, it is not practically feasible to access the raw data from the CMOS camera, although this is being addressed in the next generation of smartphones' operating systems [171]. In order to get an accurate V-response, the primary RGB colors also need to be re-calibrated. One option to do this is calibration of the red, green and blue filter response functions $k_R(\lambda)$, $k_G(\lambda)$ and $k_B(\lambda)$ by comparing the measurements on the smartphone spectrometer with those obtained with the Ocean Optics spectrometer (Fig. 5.4b). To do this comparison, the RGB intensity responses from a white LED emission (through a diffuser) are recorded simultaneously on the smartphone and the Ocean Optics spectrometers while varying the emission of the LED using a series resistor (Fig. 5.4a). Let us denote the reference spectrometer's response as $r(\lambda)$, $g(\lambda)$ and $b(\lambda)$, which are measured respectively under the red, green and blue emission bands of the LED. The RGB response function can be defined as

$$\left.\begin{aligned} k_R(\lambda) &= r(\lambda)/R \\ k_G(\lambda) &= g(\lambda)/G \\ k_B(\lambda) &= b(\lambda)/B \end{aligned}\right\} \tag{5.1}$$

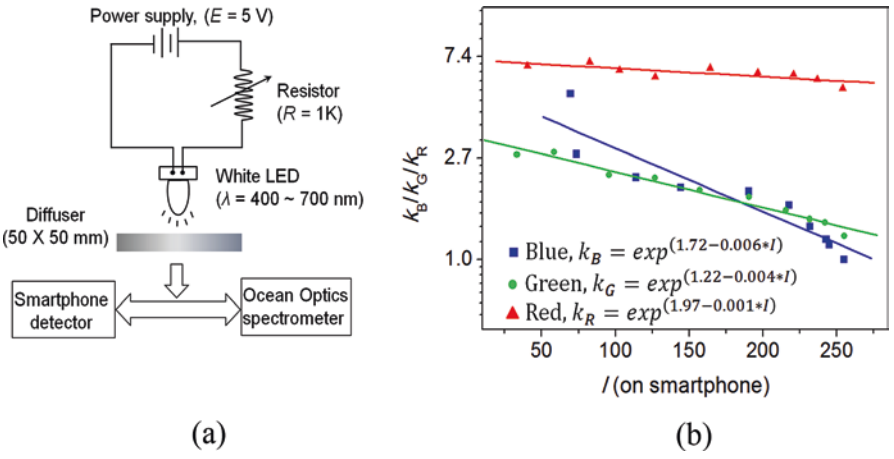

Fig. 5.4 Calibration of smartphone camera with respect to an Ocean Optics spectrometer response: (**a**) schematic to measure the intensity, I response of the red, green and blue channels of the smartphone and commercial spectrometers; and (**b**) plot of calibration factors (k_B, k_G and k_R) on each channel with their fit equations [29]

In the next measurements on the smartphone the actual RGB responses (R', G', and B') are reconstructed by multiplying the coefficients from Eq. (5.1).

$$\left.\begin{aligned} R'(\lambda) &= k_{\mathrm{R}}(\lambda) R \\ G'(\lambda) &= k_{\mathrm{G}}(\lambda) G \\ B'(\lambda) &= k_{\mathrm{B}}(\lambda) B \end{aligned}\right\} \tag{5.2}$$

Additional correction considers the effects of all other optical components that can impact on the excitation as well as emission light during propagation from the source to detector. For example, the polymer light guide and the DVD grating may not be equally efficient across λ and may be less efficient with weak absorption at the shorter wavelengths. The spectrum measured for the whole operating span (λ ~ 400 to 700 nm) of both the smartphone spectrometer, (I, using Eq. (5.2)) and the Ocean Optics spectrometer (I_{r}) are compared, the difference used to apply a correction factor in the app for each wavelength. The final spectra obtained compared well with standard instrument measurements (Fig. 5.5).

$$k(\lambda) = \frac{I(\lambda)[normalized]}{I_r(\lambda)[normalized]} \tag{5.3}$$

$$I'(\lambda) = k(\lambda) I(\lambda) \tag{5.4}$$

The intensity calculated using the HSV model is then corrected for all the additional effects introduced by smartphone and is given by

$$V = I'(\lambda) = \max\left[R'(\lambda) G'(\lambda) B'(\lambda)\right] \tag{5.5}$$

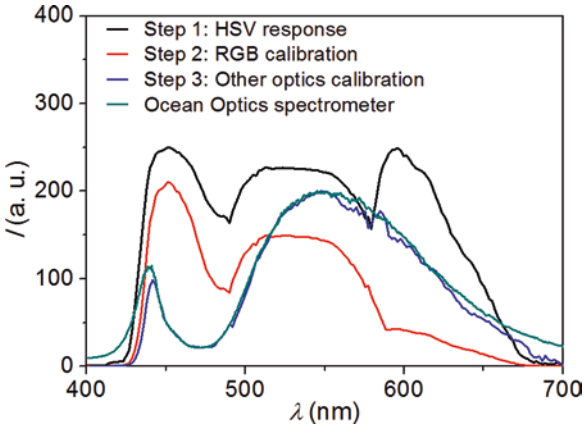

Fig. 5.5 Step-by-step intensity calibration response of the smartphone spectrometer and comparison with an Ocean Optics spectrometer response [98]

5.2.3 Performance Analysis with Slits and a Lens

To improve upon the smartphone "dual" spectrometer, the optical fiber spectrometer addresses the issue of light beam collimation as well as other factors impacting signal collection and spectral resolution. The CMOS pixel density determines the highest possible resolution of the instrument, with today's smartphones offering more than 40MP. However, screen resolution is also an important factor given that the resolution of the spectrometer is dependent on this value as opposed to the CMOS chip pixel density. Whilst not as high density as the CMOS chip, smartphone screen technology is advancing at steady pace, with high-density AMOLEDs currently leading the way. There are of course other factors in the spectrometer set-up that determine the actual resolution, including the width and angular spread of the beam striking the surface. This leads to overlap of wavelengths over finite distances along the chip, leading to low resolution and spectrally broad outputs. To investigate the effects of varying the slit width, the smartphone spectrometer was used to measure the full width half-maximum (FWHM) of a green laser pointer (λ ~ 530 nm) using various slit widths, ω_{slit} ~ 0.0, 2.0, 1.5, 1.0 and 0.7 mm. The results are shown in Fig. 5.6a and for slit widths of ω_{slit} ~ 0.0, 2.0, 1.5, 1.0 and 0.7 mm the corresponding FWHM values were found to be ~12.0, 9.0, 5.0, 3.0 and 2.0 nm respectively. The FWHM value of 2.0 nm is found to be in good agreement with that obtained using the Ocean Optics spectrometer (HR 4000). The corresponding decrease in the detected signal intensity is shown in Fig. 5.6b. As for any spectrometer, there is a trade-off between required optical resolution and sufficient signal intensity that needs to be considered during their design. Further increases in spectral resolution may be obtained using, for example, a customized G-Fresnel lens in a compact design [93]. The signal intensity can be improved significantly by using a cylindrical lens orthogonal to the grating planes after diffraction to collect and focus more light on the detector surface (Fig. 5.6c). A cylindrical lens (f = 2.0 cm) is used in addition to the in-built lens of the smartphone's camera. Other options to improve the resolution of the device in practice include using the diffraction gratings of higher line density and/or increasing the detector's size: $[\delta\lambda \propto 1/GL_D]$ where G is line density and L_{D} is detector size. An example was the previously used nano-imprinted grating of higher line density and groove depth [85]. Increasing the magnification of the focusing lens will increase the image area and also improve resolution.

5.2.4 Spectral Measurements

Performance of the smartphone spectrometer was analyzed by comparing the absorption and fluorescence spectra of Rhodamine B (RhB) dye measured on both the smartphone and a fiber coupled Ocean Optics spectrometer (HR4000). The spectra were overlaid as shown in Fig. 5.7. For measuring absorption with the

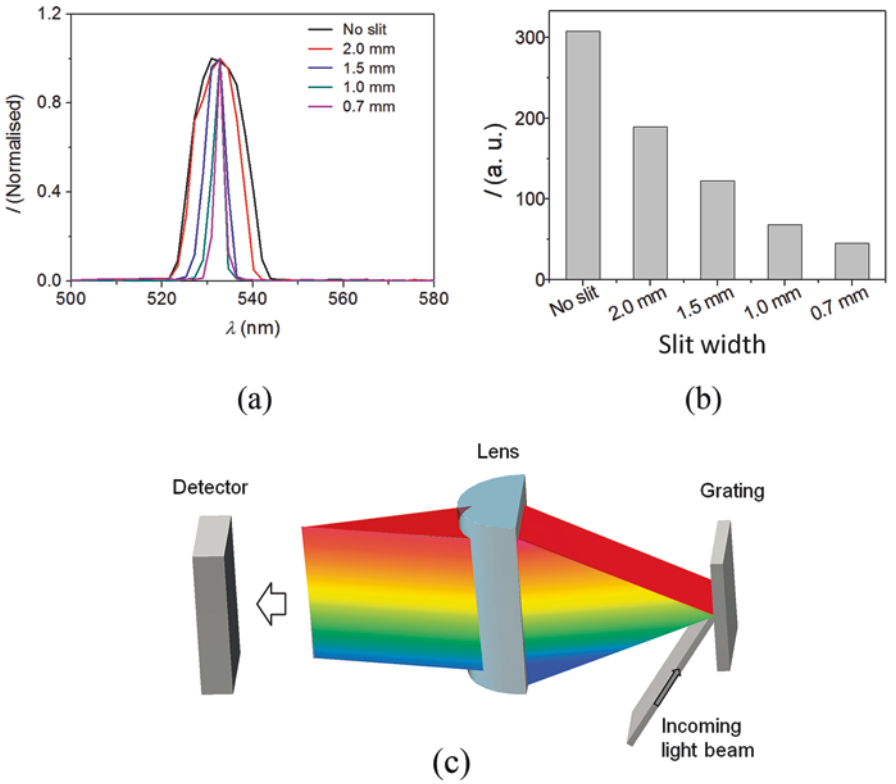

Fig. 5.6 Effect of slit width, ω_{slit} on output spectra: (**a**) green laser ($\lambda_{green} \sim 530$ nm) spectra measured on the smartphone spectrometer with no slit and various ω_{slit}; (**b**) reduction of signal intensity, I with decreasing ω_{slit}; (**c**) schematic showing diffraction of light by the grating and improved light collection using a cylindrical lens orthogonal to the grating plane [98]

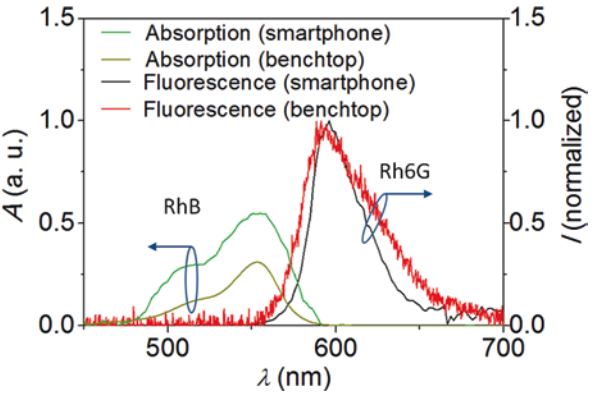

Fig. 5.7 Comparison of the response of smartphone optical fiber spectrometer with the Ocean optics spectrometer. Absorption and fluorescence spectra measured using the smartphone and commercial instrument

smartphone endoscope spectrometer, hydrophilic filter papers were immersed with RhB solutions of different concentration. These papers were then allowed to be dried for 30 min. To obtain absorption spectra, reflection spectra from the dry surface of the filter papers were measured. A reflection spectrum from a blank filter paper containing no dye molecule was used as a reference. In the case of fluorescence measurements, a green LED ($\lambda \sim 530$ nm) was used near to the sample surface to excite the sample.

5.2.4.1 Visible Absorption Spectroscopy of Apple

Finally, to demonstrate the potential of the smartphone spectrometer for food quality control applications, the reflection spectra of an apple (Pink Lady brand, a popular cultivar of Australian apples), under normal supermarket storage conditions were measured. Although near-infrared (NIR) spectroscopies are generally used in qualitative assessment of fruits [172], there are numerous example of visible reflection spectroscopy as an useful and low-cost tool for nondestructive measurements of fruits' pigment contents, such as carotenoids, anthocyanins and chlorophyll—all of which determine the fruit's color and appearance and serving as marker of quality [173]. These parameters are subject to change during ripening, storage and also for various stresses during transportation, including temperature [174]. However, it is an obvious difficult to quantify these parameters from a visual inspection or access the fruits inside a crate during transportation or storage; this is where the endoscope also comes into play.

Before taking spectra from the apple sample, the spectrometer collects a reference spectrum by capturing reflection from a plane mirror and stored within the app memory. The absorption spectrum was determined by comparing the reflection from the apple to the reference reflection (Beer-Lambert's law). Figure 5.8a shows the visible absorption spectra of the Pink Lady apple. The sample apples are collected from a local fruit shop at Sydney (having freshly arrived in the shop within 1 day). The spectra were measured every 24 h for a week under the following condition: temperature, $T \sim 22$ °C, humidity, $H \sim 50\%$ and fluorescent light illumination using common ceiling lights, $I \sim 400$ lux, height, $h \sim 3$ m. After the smart device wirelessly sends the data to a central computer, the spectra are averaged three times and plotted. Each of these spectra was first tested directly on the smartphone. Intensity changes were observed in the RGB bands corresponding to absorption bands centered close to $\lambda \sim 630$, 540 and 440 nm respectively. These bands correlate well respectively with changes in chlorophyll-*b*, anthocyanins and carotenoid levels within the apple [172, 174]. Changes in carotenoids and chlorophyll are associated with the production and accumulation of lipophilic compounds such as chloroplasts and chromoplasts, and may decrease due to a decrease in chlorophyllase activity [174]. The synthesis of anthocyanins determines the red color of an apple and is associated with the formation of red pigment cyanidin-3-galactoside, idaein [175], which can be enhanced by UV radiation from sunlight. Normalized changes in absorption intensity, ΔI, are calculated from the integrated areas under each of the

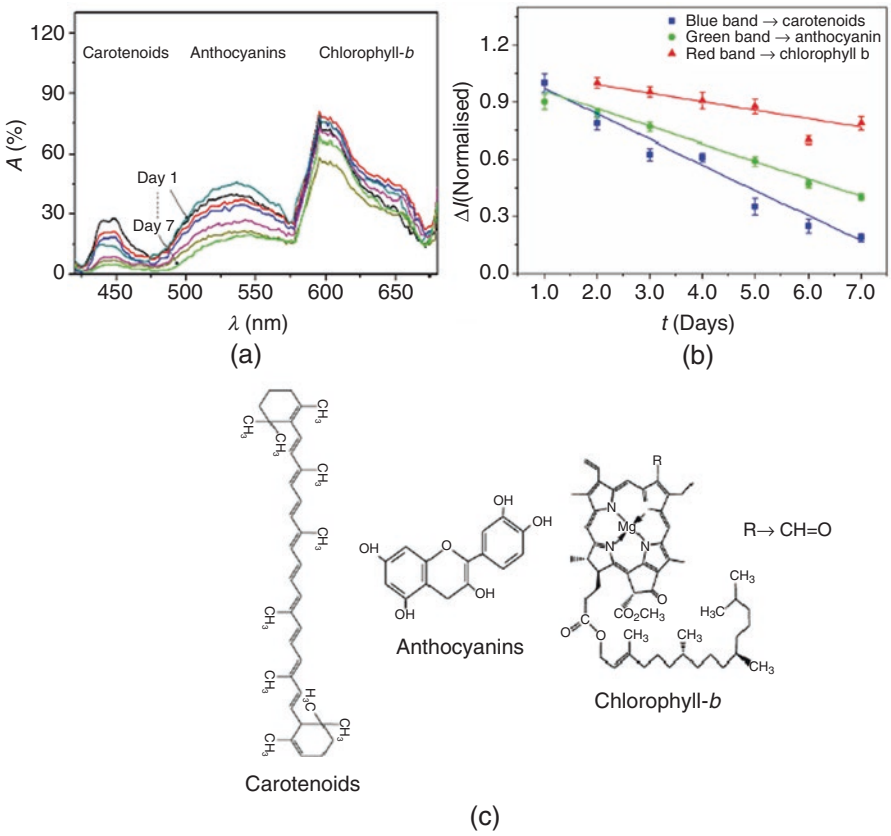

Fig. 5.8 Spectroscopic observation of changes in carotenoids, anthocyanins and chlorophyll-*b* from a Pink Lady apple using the smartphone spectrometer during storage: (**a**) absorbance, *A*, measured over a week at 24 h intervals; (**b**) plot of ΔI vs. *t* [98]

fitted individual bands and plotted in Fig. 5.8b. This figure shows the decrease of these pigments with a corresponding decrease in absorption intensity over time [$dI/dt_{(\text{Carotenoid})} = -0.14 \pm 0.01$, $dI/dt_{(\text{Anthocyanins})} = -0.09 \pm 0.01$; $dI/dt_{(\text{Chlorophyll-}b)} = -0.05 \pm 0.01$]. The analysis found that the rates of carotenoid and anthocyanin decay are larger than the rate of decay of chlorophyll-*b* content.

For an improved standardization and quality assessment of agricultural sectors, this type of data can be used to determine the optimum time for harvesting, transporting and storing agricultural products. In the orchard, an endoscope allows access to fruits away from solar exposure to determine with greater finesse the optimal harvesting conditions for fruits within different parts of a tree or bush. There is also considerable room to extend the device capability by introducing multiple functionalities including fluorescence and reflection.

5.3 Optical Fiber Smartphone Spectrofluorimeter

The optical fiber smartphone absorption spectrometer has been advanced further for fluorescence spectroscopy by integrating an array of UV LEDs while powering the entire system using the smartphone's battery. Using the instrument, visible fluorescence spectra were measured to characterize olive oils. Specifically, we show that fluorescence spectroscopy can identify the visible emission bands of oxidation components within the oils—these fluoresce and are responsible for the degradation of essential chemical compounds within the oil such as unsaturated fatty acid. The device demonstrates significant potential in rapid, on-site identification of food quality allows consumers to engage with quality control and, more broadly, opens up the quality assurance market to the wider public aided by the IoT connectivity. This assurance is crucial for the expansion of Australian food into the region given they are subject to growing criminal imitations and fraud, damaging the internationally recognized Australian brand.

5.3.1 Optical Design and Fabrication

The optical design and operation of the optical fiber smartphone spectrofluorimeter is demonstrated by the layout shown in Fig. 5.9. Although the in-built white flash LED was used as a primary optical source in the previously demonstrated smartphone spectrometer, significant absorption in UV and near-UV has been found to be useful to characterize vegetable oils by fluorescence spectroscopy [176, 177]. The excitation source used in the smartphone spectrometer system is a UV LED (emission peak at λ_{ext} ~ 370 nm with 3dB bandwidth, $\Delta\lambda$ ~ 30 nm), which is powered by a smartphone's battery via its micro-USB port that offers voltage up to ~ 5 V and a maximum current of ~ 500 mA. The fiber bundle probe used to collect fluorescence is the same as that used in the previous design. Considering the possible UV degradation of the fiber, the light propagation through the transmission fiber has been avoided by integrating a custom designed endoscope cap that holds the end of the fiber bundle probe at the centre with the optical sources. In order to produce sufficient illumination over the sample surface, three UV LEDs (5 mm round, 3.8 V, 100 mA) are placed in three suitable slots located around the periphery of the end cap. These parallel connected LEDs are separated equally from each other so that they can produce uniform illumination on the sample surface. A series resistor (R = 22 Ω) is used to limit current and voltage to the LEDs as illustrated in the Fig. 5.10a. The fluorescence emission is collected through the collection fiber bundle, positioned at the centre of the fiber bundle probe where an objective lens at the probe end increases light collection. In order to keep the distance between the surface of the sample's container and the fiber end fixed, the periphery of the endoscope cap is extended a further 1.0 cm from the LEDs and fibers bundle ends. The collected light is then collimated using the second lens on the other end of the probe and subsequently diffracted using a low-cost dispersive element (diffraction

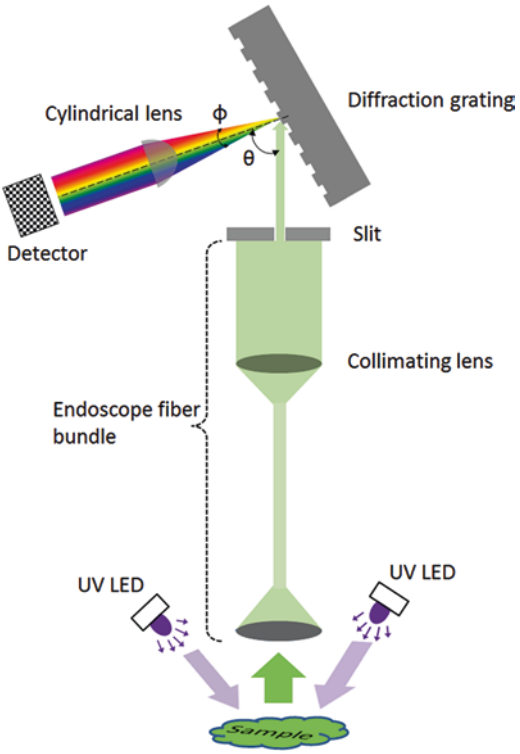

Fig. 5.9 The optical layout of the smartphone endoscope spectrofluorimeter

grating). This diffracted light is finally imaged and calibrated (I vs. λ) across the CMOS chip using the same process outlined in Sect. 5.2.2. A cylindrical lens is also used to improve light collection per pixel onto the detector. As used in our previous device, the diffraction grating is the surface of a DVD. The 3D structure of the smartphone optical fiber spectrofluorimeter with endoscope cap was designed in AutoCAD (Fig. 5.10a) and fabricated similarly using a 3D printer as shown in (Fig. 5.10b).

5.3.2 Smartphone Application Software

A customized Android app is designed to perform the spectral measurements of olive oils and share the results with other devices. The app mainly consists of two functional screens: "TakePic" screen to collect the image of the diffracted light from the fluorescence of oils and "Spectra" screen to process the spectrum. The image information is then processed to generate a spectrum of I vs. λ as well and display the results on the smartphone screen. After opening the app, the user is required to position the end cap of the endoscope fibre bundle onto the surface of the sample of interest (in this case oil in a transparent bottle) so that there is no gap between the

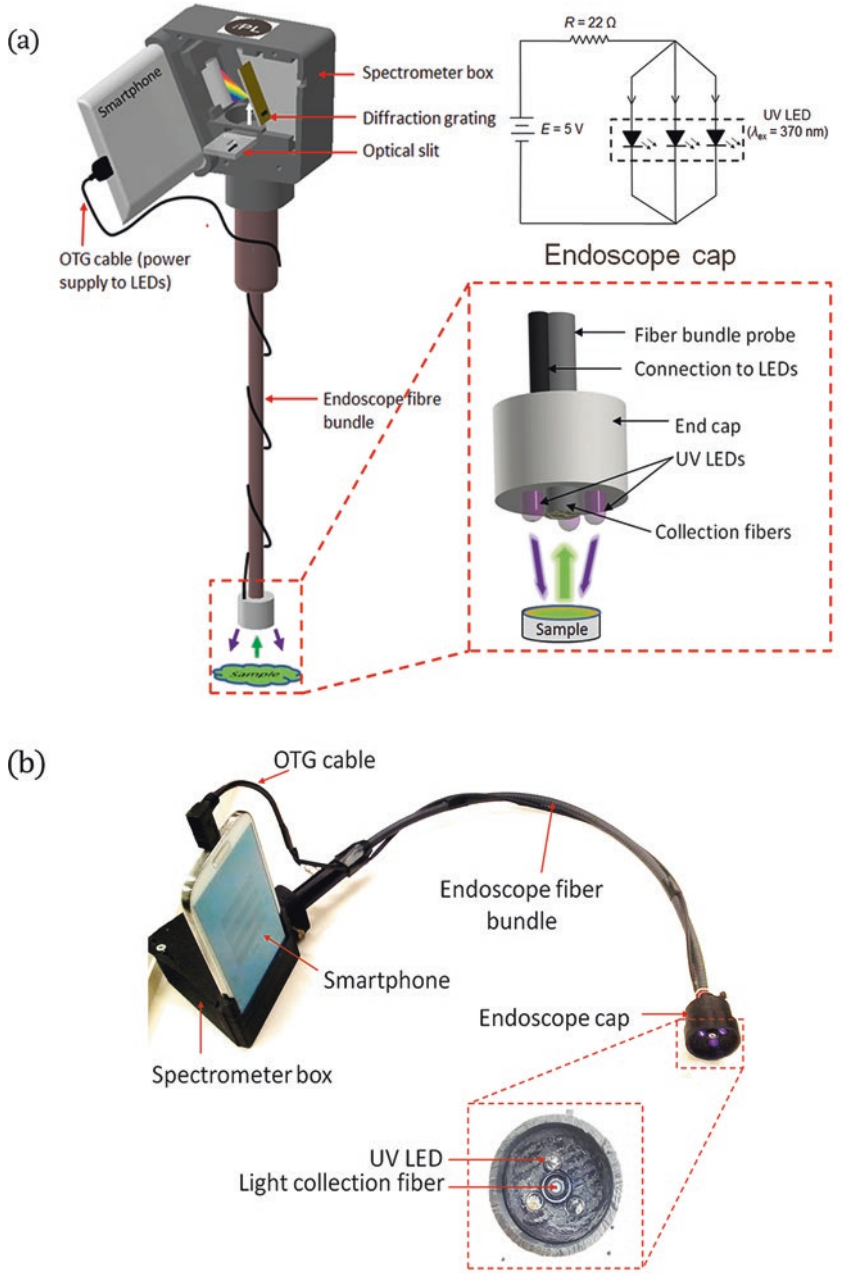

Fig. 5.10 The design of the smartphone optical fiber spectrofluorimeter. (**a**) The 3D configuration of the smartphone optical fibre spectrofluorimeter, inset shows the 3D design of the endoscope cap and the electrical diagram of the fluorescence excitation sources; and (**b**) the actual 3D-printed device installed on an Samsung Galaxy S4 smartphone

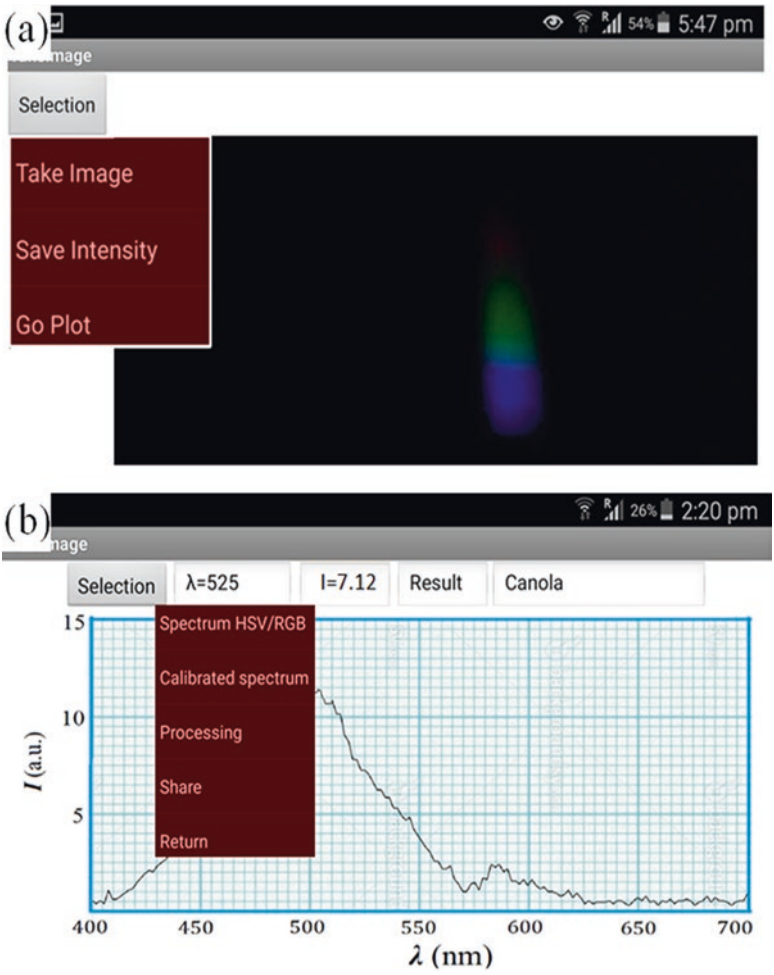

Fig. 5.11 The screenshots of the smartphone Android app measuring fluorescence spectrum of olive oils. (**a**) "TakePic" screen and (**b**) "Spectra" screen

endoscope cap and the surface. The algorithm of the spectral analysis is designed in a similar way as described in Chap. 4.

The screen-shoots of the two main pages of the app are shown in Fig. 5.11. By analyzing the spectrum, the app allows identifying the level of any particular fluorescing compound corresponding to their emission band. For example, the strength of chlorophyll can be observed by monitoring the emission band centred at $\lambda \sim 670$ nm. By selecting the intensity option, the algorithm calculates I at a specific λ and finds the types and quality of the samples after analyzing them from a calibrated correlation. The results can be displayed on the app screen immediately warning the customers/suppliers about any degradation of the oil's quality. This can also be saved to the smartphone memory with date and location using the in-built location sensor (GPS) or sent to a central computer for further analysis and mapping of the oil's quality.

5.3.3 *Fluorescence Spectroscopy of Olive Oils*

Fluorescence spectroscopy of olive oils has traditionally been used to study and characterize chemical composition of oils [176–179]. Fluorescence of native olive oil (to a particular country) can reveal the presence of different fluorophores influenced by various factors including the harvesting method, manufacturing process, degradation, storage condition and/or even the ingredient's chemical composition [177]. The fluorescence signals of different types of oils create complex data with overlapping fluorophore fingerprints that require deconvolution methods and data processing. This processing, analyzing and displaying can often be difficult, time-consuming, and problem-specific. Sometimes procedures are required such as solubilization in solvents, extraction, and treatment with chemicals. The importance for addressing these issues is reflected by the growing number of micro-spectrometer suppliers that aim to serve in the agricultural and food sectors in the fields [117, 118]. They potentially offer standardization and reliable field testing of olive oils, the results of which can be provided on-line to establish real-time feedback between manufacturers, retailers and increasingly consumers. The aim is to strengthen consumer confidence in the authenticity, origin and quality of purchased food. Here, the smartphone spectrofluorimter has been applied to distinguish refined olive oil from extra virgin olive oil, to characterize their degradation under light and heat.

5.3.3.1 Samples

Some commonly used vegetable oils were purchased off-the-shelf from a local supermarket in Sydney, Australia (Table 5.1). A sample of each oil type was transferred to a 21 mL clear glass vial for analysis. A photo of the oils is shown in Fig. 5.12a. The vegetable oil samples include extra virgin olive (EVO, two different brands), refined olive (RO), canola, peanut, rice bran and sunflower oils. Amongst them, olive oil has built a reputation for defending against cardiovascular disease, diabetes, cancer, rheumatoid arthritis, and other diseases [180]. They are pressed from the fruit of the olive tree, and are a source of monounsaturated fatty acid that contains photochemicals. Their flavors range from bland to extremely strong. This particular vegetable oil is graded according to its degree of acidity and the process used to extract the oil. Oil labeled "virgin" is typically cold pressed (a

Table 5.1 Fluorescence intensity at 452 and 670 nm measured for different types of olive oils

Oil type	I_{452} (a. u.)	I_{670} (a. u.)
Extra virgin olive	4.2 ± 1.0	18.4 ± 0.8
Refined olive	24.5 ± 1.5	0.8 ± 0.7
Canola	47.7 ± 2.5	0.7 ± 0.5
Peanut	19.6 ± 1.2	1.1 ± 0.7
Rice bran	38.1 ± 2.6	1.1 ± 0.6
Sunflower	29.7 ± 0.9	1.1 ± 0.7

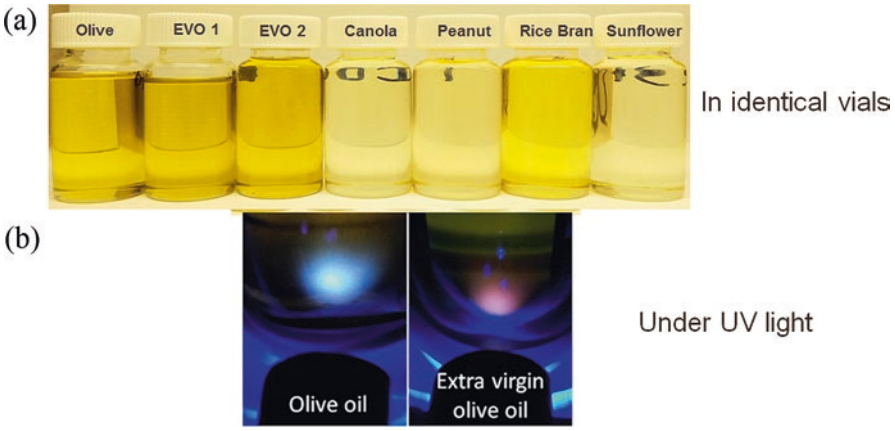

Fig. 5.12 Vegetable oils samples. (**a**) Vegetable oils of different brand collected from a supermarket and put into a 21 mL glass vials; and (**b**) fluorescence image of refined olive and extra virgin olive oils samples placed in front of the fibre probe

process using no heat or chemicals) and contains low levels of acidity. It is a good source of vitamins A, B_2, K, D and E [181]. Oil labeled "pure" uses heat and chemicals to process olive residue from subsequent pressings. Virgin olive oils come from the first pressing of the olives and contain no more than 2% free acidity [182]. They are also considered to have a superior taste compared to refined oils. The EVO oil contains no refined oil at all and retains much higher concentrations of potent compounds, which is considered well worth the higher costs.

5.3.3.2 Classifications of Oils

Each vegetable oil sample has its unique properties, specific uses and customer preferences. The noticeable variants between suppliers make visual inspection and discrimination of the olive oils extremely difficult, made worse when chemicals such as chlorophyll is artificially introduced. To measure the florescence spectrum of oils, the fibre bundle probe is butted against the surface of the glass vials containing the oil samples. By placing the fibre bundle in such a way, the instrument is collecting the front-face fluorescence of the oil, which reduces self-absorption by the oil and represents the true fluorescence compared to the right-angle fluorescence [178].

From the visible fluorescence spectra measured using the smartphone spectrofluorimeter (Fig. 5.13), a significantly weaker blue band at $\lambda_{em} \sim 452$ nm, corresponding to oxidising compounds, is observed in EVO oil compared to the RO and other vegetable oils [176]. These can enable the device distinctively identify the EVO from RO or others assuming that the chlorophyll is not added artificially into the EVO sample. Olive oils are oxidized easily when they come in contact with oxygen or any other parameters such as light, heat etc. The oxidation products have an unpleasant flavor and odor and may adversely affect the

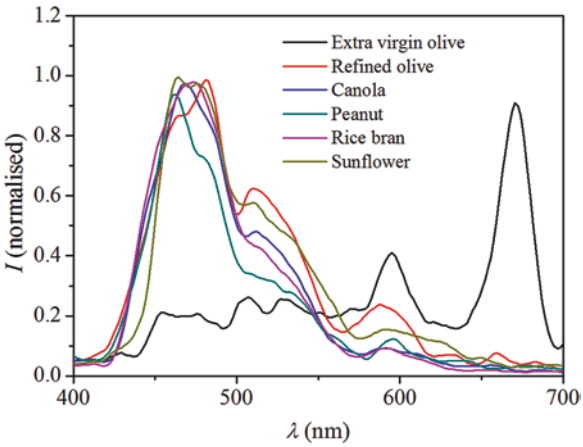

Fig. 5.13 Fluorescence spectra of the different types of vegetable oils measured on the smartphone spectrometer

nutritional constituent of the oil. It also destroys some essential fatty acids including linoleic and linolenic acids.

The unique red band at $\lambda \sim 670$ nm, corresponding with chlorophyll-*a*, is observed in EVO oil. A weaker emission band in the EVO near to $\lambda \sim 600$ nm is due to the chlorophyll-*b*. The strong chlorophyll-*a* emission band is absent in RO and other vegetable oil samples and the results are consistent with the spectra reported in [176, 178]. One of the important properties of olive oils is their anti-oxidants that provide resistance against oxidization of the oils. Chlorophyll has no physiological effect on human health but in olive oil, it acts as an anti-oxidant in the dark environment. Therefore, the presence of chlorophyll is a good indicator of olive oils oxidation status and therefore freshness of the oil [180].

By analyzing the individual bands at 452 and 670 nm, two distinctive intensity values (I_{452} and I_{670}) are obtained as summarized in Table 5.1. In the smartphone app, the algorithm compares these intensity values to find out the type and condition of the oil. A ~ 4-fold increase of the I_{670} value compared with the I_{452} is recorded in EVO oils giving a means to distinguish EVO from RO and other vegetable oils.

5.3.3.3 Storage Effects

The typical characteristics and chemical composition of olive oils are thought to be altered by several factors, including olive variety, horticulture, olive maturation, milling processing method, extraction method, storage condition, and oil container materials [177]. In order to observe the effects of storage effects, we have stored all olive oils for $t = 1$ month under normal supermarket conditions: temperature, $T = 22$ °C, humidity, $H = 50\%$ and normal fluorescent light illumination (common ceiling light with $I \sim 400$ lux, distance from the oils sample, $h \sim 3$ m). Spectroscopic changes in RO and EVO oils are shown in Fig. 5.14a, b respectively. The results

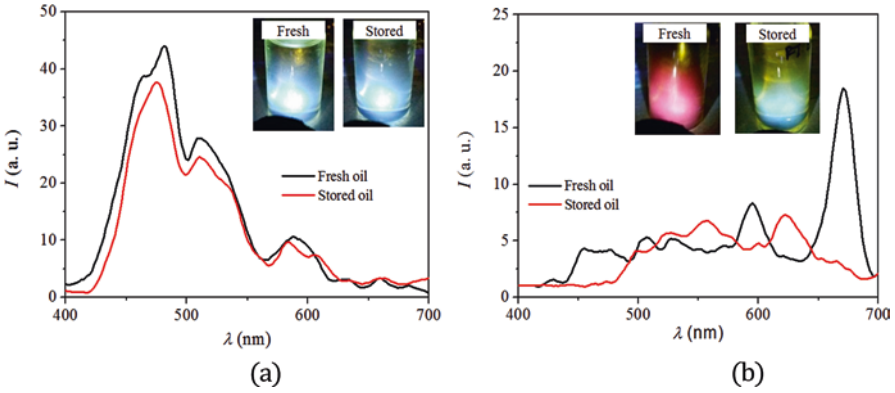

Fig. 5.14 Storage effects on fluorescence spectrum of different vegetable oils: (**a**) refined olive oil; and (**b**) extra virgin olive oil. Insets showing the fluorescent image of the oils sample in glass vial when excited by 370 nm UV LED

indicate significant degradation of overall fluorescence in EVO oil (~4.5-fold) during the storage time as compared to the RO oil (~1.2-fold). The red fluorescence in the EVO disappears and turned to a weak greenish-blue. However, the intensity value corresponding to the oxidation products (I_{452}) in the stored EVO is still much weaker than that of the RO and others. Among the different storage parameters, light (photo-degradation) and heat (thermal-degradation) play a significant role on the stability and quality of the olive oils by oxidisation [180].

5.3.3.4 Photo-degradation

The oxidization of EVO oils that eventually causes the strong degradation of the oil's quality is attributed primarily due to the exposure of light [178]. The photo-oxidization happens more likely in EVO oil than RO oil due to the presence of the chlorophyll pigments. Although the chlorophyll pigment serves as an anti-oxidant in the dark, it promotes formation of oxygen radicals and accelerates oxidation in light. Chlorophyll pigments in olive oils are likely to be degraded by demetalation—a light-favoured process that generates colorless molecules in oils. Therefore, it is reasonable to store and sell EVO oils to its consumers within an opaque bottle or container that is resistive to light penetration. But some of them can also be found in transparent bottle. To study this effect, we compared degradation of oils in transparent and opaque glass bottles after 1 month. A significant difference in overall fluorescence particularly in the chlorophyll band is observed. The oil stored in a completely dark bottle is found to exhibit the strongest red fluorescence. On the other hand, very weak fluorescence is observed in the oil stored in transparent bottle where the red fluorescence band diminished to almost zero and the sample turned into greenish-blue (Fig. 5.15).

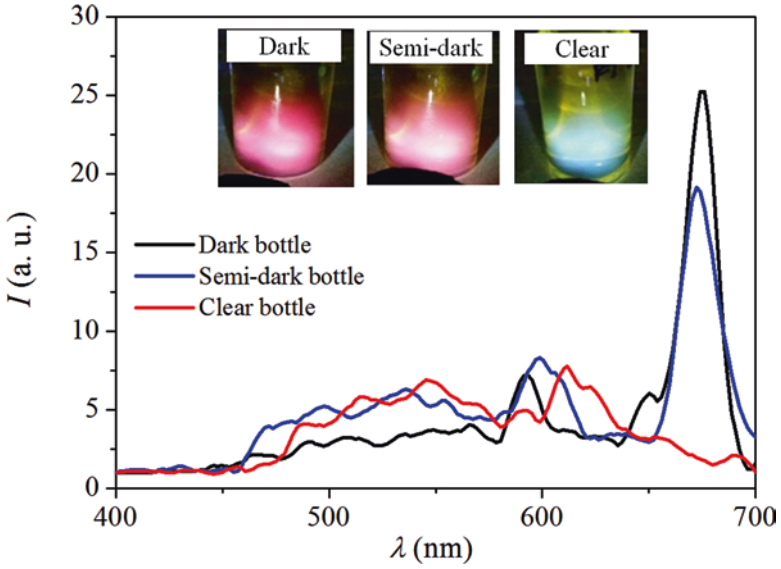

Fig. 5.15 Fluorescence of extra virgin olive oil's stored in bottles of different opacity. Insets showing the fluorescent image of the oils sample in glass vial when excited by 370 nm UV LED

5.3.3.5 Thermal Degradation

Besides photo-oxidation, heat exposure can also cause olive oil to turn rancid and possibly degrade the fluorescence [178, 182]. This degradation is ascribed to a decrease of the hydroxytyrosol with heat exposure. Plant oils rich in poly-unsaturated fatty acids have a limited shelf-life and regular consumption of rancid oils (from prolonged storage or overheating) may have negative health consequences. In order to verify thermal degradation, we have heated the oil samples from room $T \sim 22$ to 200 °C and measured the fluorescence spectrum using the smartphone spectro-fluorimeter. To ensure the homogeneity of T among different samples, the samples were heated simultaneously. Spectra were measured after heating the samples up to a specific T and then allowed to cool down to room temperature. After heating, the samples are kept in a dark chamber ensuring no photo-degradation affecting the results. Spectra measured at 22 °C and after heating to 200 °C are shown in Fig. 5.16a, b for RO and EVO respectively. Fluorescence intensities at $\lambda \sim 452$ and 670 nm for RO and EVO oils are plotted respectively in Fig. 5.16c, d. Refined olive oils are found to be relatively more stable than the EVO oil within the experimental error ranges. The oxidation compounds band in EVO oil increases ~50% with heating up to 200 °C whereas the chlorophyll bands are found to be decreased by ~40%. The decrease in fluorescence is attributed to the formation of oxidation products such as inflammatory peroxides and hydroperoxides and the results are consistent with those obtained using standard instruments [176].

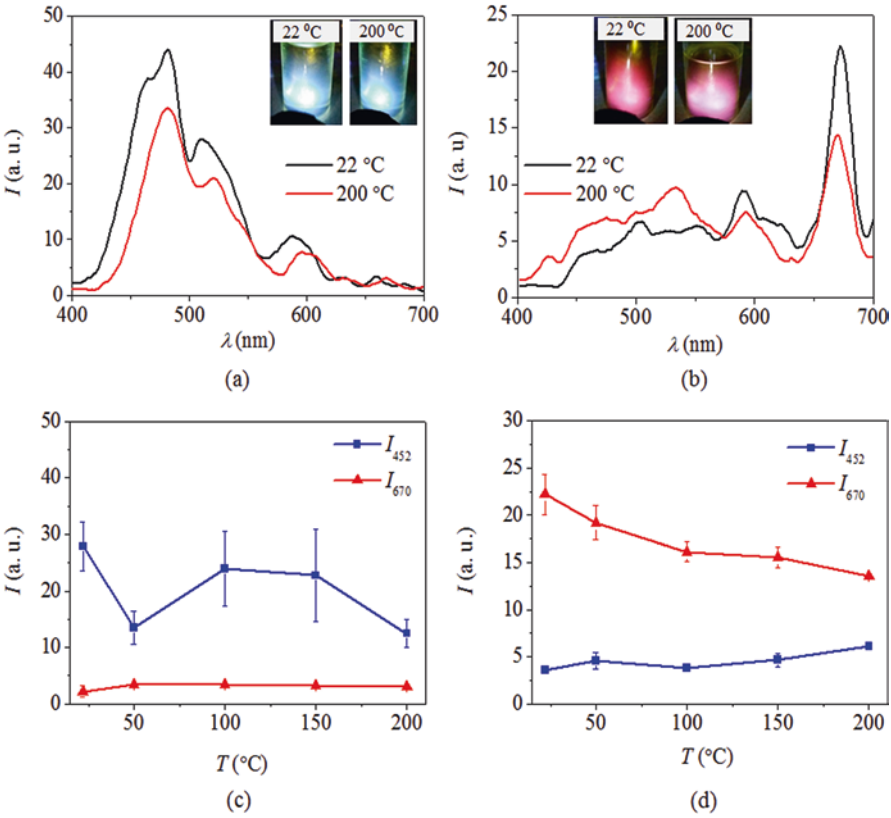

Fig. 5.16 Thermal degradation measurements of—(**a**) RO and (**b**) EVO oils using the smartphone spectrofluorimeter. Fluorescence spectrum measured at 22 and 200 °C. Relative intensity changes at oxidising phenolic and chlorophyll bands from room temperature (22 °C) to 200 °C of (**c**) RO and (**d**) EVO oils

5.4 Summary

This chapter demonstrated the development of smartphone optical fiber spectrometers for absorption and fluorescence spectroscopy. Addition of fiber bundle probe allows light collection from difficult-to-access areas and eliminates the effect of variability in ambient illumination making it ideal for field diagnostics. The optical fibre spectrometer has been demonstrated for food quality assessment such as pigment analysis during storage of fruits or quality and degradation of olive oils. Data can be shared or processed remotely via the Internet, perhaps through a digitized cloud collecting data from many of such instruments or combined to allow real-time mapping within a potential IoT application.

Bibliography

1. T. Nick, "*A modern smartphone or a vintage supercomputer: which is more powerful*," PhoneArena.com, 14 Jun 2014. [Online]. Available: http://www.phonearena.com/news/A-modernsmartphone-or-a-vintage-supercomputer-which-is-more-powerful_id57149.
2. N. D. Lane, E. Miluzzo, H. Lu, D. Peebles, T. Choudhury, and A. T. Campbell, "A survey of mobile phone sensing," *IEEE Comm. Magazine*, pp. 140-150, Sep. 2010.
3. P. M. Barrett and E. J. Topol, "Smartphone medicine," *IEEE Spotlight*, pp. 52-54, IT Pro, May/Jun. 2016.
4. C.-Y. Chen, Y.-H. Chen, C.-F. Lin, C.-J. Weng, and H.-C. Chien, "A review of ubiquitous mobile sensing based on smartphone," *AUSMT*, 4(1), pp. 13-18, Mar. 2014.
5. S. K. Vashist, E. M. Schneider, and J. H. T. Luong, "Commercial smartphone-based devices and smart applications for personalized healthcare monitoring and management," *Diagnostics*, 4, pp. 104-128, Apr. 2014.
6. X. Xu, A. Akay, H. Wei, S. Wang, B. Pingguan-Murphy, B.-E. Erlandsson, X. Li, W. Lee, J. Hu, L. Wang, and F. Xu, "Advances in smartphone-based point-of-care diagnostics," *Proceedings of the IEEE*, 103(2), pp. 236-247, Mar. 2015.
7. A. Grünerbl, A. Muaremi, V. Osmani, G. Bahle, S. Öhler, G. Tröster, O. Mayora, C. Haring, and P. Lukowicz, "Smartphone-based recognition of states and state changes in bipolar disorder patients," *IEEE J. Biomed. Health Inform*., 19(1), pp. 140-148, Jan. 2015.
8. D. Lakens, "Using a smartphone to measure heart rate changes during relived happiness and anger," *IEEE Trans. Affective Computing*, 4(2), pp. 238-241, Apr.-Jun. 2013.
9. M.-Z. Poh, K. Kim, A. Goessling, N. Swenson, and R. Picard, "Cardiovascular monitoring using earphones and a mobile device," *IEEE Pervasive Computing*, 11(4), pp. 18-26, Dec. 2012.
10. W. Z. Khan, Y. Xiang, M. Y Aalsalem, and Q. Arshad, "Mobile phone sensing systems: a survey," *IEEE Comm. Surveys & Tutorials*, 15(1), pp. 402-427, Jan. 2013.
11. S. Yu, W. Xiao, Q. Fu, Z. Wu, C. Yao, H. Shen, and Y. Tang, "A portable chromium ion detection system based on a smartphone readout device," *Anal. Methods*, 8(38), pp. 6877-6882, Oct. 2016.
12. K. E. McCracken and J.-Y. Yoon, "Recent approaches for optical smartphone sensing in resource limited settings: a brief review," *Anal. Methods*, 8(36), pp. 6591-6601, Sep. 2016.
13. K. E. McCracken and J.-Y. Yoon, "Recent approaches for optical smartphone sensing in resource-limited settings: a brief review," *Anal. Methods*, 8(36), pp. 6591-6601, Sep. 2016.
14. Y. Intaravannea, S. Sumriddetchkajorn, and J. Nukeawa, "Cell phone-based two-dimensional spectral analysis for banana ripeness estimation" *Sens. Actuat. B Chem.*, 168, pp. 390–394, Jun. 2012.

A. Jamalipour, M. A. Hossain, *Smartphone Instrumentations for Public Health Safety*, Wireless Networks, https://doi.org/10.1007/978-3-030-02095-8

15. S. Sumriddetchkajorn, K. Chaitavon, and Y. Intaravanne, "Mobile-platform based colorimeter for monitoring chlorine concentration in water" *Sens. Actuat. B Chem.*, 191, pp. 561–566, Feb. 2014.
16. B. Cortazar, H. C. Koydemir, D. Tseng, S. Feng, and A. Ozcan, "Quantification of plant chlorophyll content using Google Glass," *Lab Chip*, 15(7), pp. 1708-16,Apr. 2015.
17. Ocean Control, VIC, Australia, *Smartphone electromagnetic sensor*, [Online]. Available: https://oceancontrols.com.au/ESS-002.html.
18. Ocean Control, VIC, Australia, *Smartphone UV sensor*, [Online]. Available: https://oceancontrols.com.au/ESS-001.html.
19. K. Yang, H. Peretz-Soroka, Y. Liu, and F. Lin, "Novel developments in mobile sensing based on the integration of microfluidic devices and smartphones," *Lab Chip*, 16(6), pp. 943-958, Mar. 2016
20. W. Martinez, S. T. Phillips, E. Carrilho, S. W. Thomas, H. Sindi, and G. M. Whitesides, "Simple telemedicine for developing regions: Camera phone and paper based microfluidic devices for real-time, off-site diagnosis," *Anal. Chem*., 80(10), pp. 3699-3707, Apr. 2008.
21. H. Parastar and H. Shaye, "MVC app: A smartphone application for performing chemometric methods," *Chemometr. Intell. Lab. Syst.*, 147, pp. 105-110, Oct. 2015.
22. Google Play, *AssayColor*, [Online]. Available: https://play.google.com/store/apps/details?id=com.alidans.assaycolor&hl=en
23. Google Play, *Technical Analysis Tool*, [Online]. Available: https://play.google.com/store/apps/details?id=ua.antonSydorenko.easyTechAnalysis&hl=en
24. S. Wang, R. Akbas, and U. Demirci "Microchip ELISA coupled with cell phone to detect ovarian cancer HE4 biomarker in urine" *Methods Mol Biol*., 1256, pp. 111–21. (2015).
25. T. Guo, R. Patnaik, K. Kuhlmann, A. J. Rai, and S. K. Sia, "Smartphone dongle for simultaneous measurement of hemoglobin concentration and detection of HIV antibodies," *Lab Chip*, 15(17), pp. 3514-20,Sep. 2015.
26. S. Wang, X. Zhao, I. Khimji, R. Akbas, W. Qiu, D. Edwards, D. W. Cramer, B. Ye, and U. Demirci, "Integration of cell phone imaging with microchip ELISA to detect ovarian cancer HE4 biomarker in urine at the point-of-care," ***Lab Chip*, 11(20)**, pp. 3411-3418, Oct. 2011.
27. V. Oncescu, D. O'Dell, and D. Erickson, "Smartphone based health accessory for colorimetric detection of biomarkers in sweet and saliva," *Lab Chip*, 13(16), pp. 3232-8, Aug. 2013.
28. L. Shen, J. A. Hagen, and I. Papautsky,"Point-of-care colorimetric detection with a smartphone," *Lab Chip*, 12(21), pp. 4240-4243,Oct. 2012.
29. M. Y. Jia, Q. S. Wu, H. Li, Y. Zhang, Y. F. Guan, and L. Feng, "The calibration of cellphone camera-based colorimetric sensor array and its application in the determination of glucose in urine," *Biosens. Bioelectron.*, 74, pp. 1029-1037, Dec. 2015.
30. J. I. Hong and B. Y. Chang, "Development of smartphone-based colorimetry for multi-analyte sensing arrays" *Lab Chip*, 14(10), pp. 1725-32, May 2014.
31. V. Oncescu, M. Mancuso, and D. Erickson, "Cholesterol testing on a smartphone" *Lab Chip*, 14(4), pp. 759–763, Feb. 2014.
32. M. Mancuso, E. Cesarman, and D. Erickson, "Detection of Kaposi's sarcoma associated herpesvirus nucleic acids using a smartphone accessory," *Lab Chip*, 14(19), pp. 3809-16,Oct. 2014.
33. M. Pohanka "Photography by cameras integrated in smartphones as a tool for analytical chemistry represented by anbutyrylcholinesterase activity assay," *Sensors*, 15(6), pp. 13752-62, Jun. 2015.
34. S. Lee, V. Oncescu, M. Mancuso, S. Mehta, and D. Erickson "A smartphone platform for quantification of vitamin D levels," *Lab Chip*, 14(8), pp. 1437-42, Apr. 2014.
35. N. S. K. Gunda, S Naicker, S Shinde, S Kimbahune, S Shrivastavac, and S Mitra, "Mobile water kit (MWK): a smartphone compatible low-cost water monitoring system for rapid detection of total coliform and E. coli," *Anal. Methods,* 6(16), pp. 6236–6246, Aug. 2014.
36. T. S. Park and J. Y. Yoon, "Smartphone detection of Escherichia coli from field water samples on paper microfluidics," *IEEE Sensors J.*15(3), pp. 1902-1907, Mar. 2015.

37. B. Y. Chang "Smartphone-based chemistry instrumentation: digitization of colorimetric measurements" *Bull. Korean Chem. Soc*., 33(2), pp. 549-552, 2012.
38. L. J. Loh, G. C. Bandara, G. L. Weber, and V. T. Remcho "Detection of water contamination from hydraulic fracturing wastewater: a μPAD for bromide analysis in natural waters," *Analyst,* 140(16), pp. 5501-7, Aug. 2015.
39. S. Sumriddetchkajorn, K. Chaitavon, and Y. Intaravanne "Mobile device-based self-referencing colorimeter for monitoring chlorine concentration in water" *Sens. Actuat. B Chemical*, 182, pp. 592-597, Jun. 2013.
40. Q. Wei, R. Nagi, K. Sadeghi, S. Feng, E. Yan, S. J. Ki, R. Caire, D. Tseng, and A. Ozcan, "Detection and spatial mapping of mercury contamination in water sample using a smartphone," *ACS Nano*, 8(2), pp. 1121-9, Feb. 2014.
41. T. S. Park, C. Baynes, S.-I. Cho and J.-Y. Yoon, "Paper microfluidics for red wine tasting," *RSC Adv.*, 4(46), pp. 24356-62, May 2014.
42. M. Zangheri, L. Cevenini, L. Anfossi, C. Baggiani, P. Simoni, F. D. Nardo, and A. Roda, "A simple and compact smartphone accessory for quantitative chemiluminescence base lateral flow immunoassay for salivary cortisol detection," *Biosens. Bioelectron.*, 64, pp. 63-68, Feb. 2015.
43. E. Lebiga, R. E. Fernandez, and A. Beskok, "Confined chemiluminescence detection of nanomolar levels of H_2O_2 in a paper-plastic disposable microfluidic device using a smartphone," *Analyst*, 140(15), pp. 5006-11, Aug. 2015.
44. Q. Mei, H. Jing, Y. Li, W. Yisibashaer, J. Chen, B. N. Li, and Y. Zhang, "Smartphone based visual and quantitative assays on upconversional paper sensor," *Biosens. Bioelectron.*, 75, pp. 427-432, Jan. 2016.
45. A. Roda, E. Michelini,L. Cevenini,D. Calabria,M. M. Calabretta, and P. Simoni, "Integrating biochemiluminescence detection on smartphones: mobile chemistry platform for point-of-need analysis," *Anal. Chem.*, 86(15), pp. 7299-304, Aug. 2014.
46. O. Mudanyali, S. Dimitrov, U. Sikora, S. Padmanabhan, I. Navruz, and A. Ozcan, "Integrated rapid-diagnostic-test reader platform on a cellphone," *Lab Chip*, 12(15), pp. 2678-86, Aug. 2012.
47. S. Sumriddetchkajorn, K. Chaitavon, and Y. Intaravanne "Mobile device-based self-referencing colorimeter for monitoring chlorine concentration in water" *Sens. Actuat. B Chemical*, 182, pp. 592-597, Jun. 2013.
48. A. F. Coskun, J. Wong, D. Khodadadi, R. Nagi, A. Tey, and A. Ozcan, "A personalize food allergen testing platform on a cellphone," *Lab Chip*, 13(4), pp. 636-40, Feb. 2013.
49. H. Zhu, U. Sikora, and A. Ozcan, "Quantum dot enabled detection of Escherichia coli using a cell phone," *Analyst*, 137(11), pp. 2541-44, Jun. 2012.
50. C. A. D. Villiers, M. C. Lapsley, and E. A. H. Hall, "A step towards mobile arsenic measurement for surface waters," *Analyst*, 140(8), pp. 2644-55,Apr. 2015.
51. Q. Wei, R. Nagi, K. Sadeghi, S. Feng, E. Yan, S. J. Ki, R. Caire, D. Tseng, and A. Ozcan, "Detection and spatial mapping of mercury contamination in water sample using a smartphone," *ACS Nano*, 8(2),pp. 1121-9, Feb. 2014.
52. S. K. Vashist, E. M. Schneider, R. Zengerle, F. Stetten, and J. H. T. Luong, "Graphene-based rapid and highly-sensitive immunoassay for C-reactive protein using a smartphone-based colorimetric reader," *Biosens. Bioelectron.*, 66, pp. 169–176, Apr. 2015.
53. L. Yu, Z. Z. Shi, C. Fang, Y. Y. Zhang, Y. S. Liu, and C. M. Li, "Disposable lateral flow-through strip for smartphone-camera to quantitatively detect alkaline phosphatase activity in milk," *Biosens. Bioelectron.*, 69, pp. 307–315,Jul. 2015
54. G. Rateni, P. Dario and F. Cavallo "Smartphone-based food diagnostic technologies: A Review" Sensors, 17, p. 1453 (2017).
55. H. Zhu, S. O. Isikman, O. Mudanyali, A. Greenbauma, and A. Ozcan, "Optical imaging techniques for point-of-care diagnostics," *Lab Chip*, 13(1), pp. 51-67, Jan. 2013.
56. A. Skandarajah, C. D. Reber, N. A. Switz, and D. A. Fletcher, "Quantitative imaging with a mobile phone microscope," *PLoS ONE*, 9(5), p. e96906, May 2014.

57. N. A. Switz, M. V. D'Ambrosio, and D. A. Fletcher, "Low-cost mobile phone microscopy with a reversed mobile phone camera lens," *PLoS ONE*, 9(5), p. e95330, May 2014.
58. H. Zhu, S. Mavandadi, A. F. Coskun, A. Yaglidere, and A. Ozcan, "Optofluidic fluorescent imaging cytometry on a cell phone," *Analyt. Chem.*, 83(17), pp. 6641-6647, Sep. 2011.
59. D. Tseng, O. Mudanyali, C. Oztoprak, S. O. Isikman, I. Sencan, O. Yaglideresa, and A. Ozcan, "Lens free microscopy on a cellphone," *Lab Chip*, 10(14), pp. 1787–1792,Jul. 2010.
60. C. J. Tuijn, B. J. Hoefman, H. Beijma, L. Oskam, and N. Chevrollier, "Data and image transfer using mobile phones to strengthen microscopy-based diagnostic services in low and middle income country laboratories," *PLoS ONE*, 6(12), p. e28348, Dec. 2011.
61. S. A. Lee and C. Yang, "A smartphone-based chip-scale microscope using ambient illumination" *Lab Chip*, 14(16), pp. 3056–3063,Aug. 2014.
62. D. N. Breslauer, R. N. Maamari, N. A. Switz, W. A. Lam, and D. A. Fletcher, "Mobile phone based clinical microscopy for global health applications," *PLoS ONE*, 4(7), p. e6320, Jul. 2009.
63. Q. Wei, W. Luo, S. Chiang, T. Kappel, C. Mejia, D. Tseng, R. Y. L. Chan, E. Yan, H. Qi, F. Shabbir, H. Ozcan, S. Feng, and A. Ozcan, "Imaging and sizing of single DNA molecules on a mobile phone," *ACS Nano,* 8(12), pp. 12725-33, Dec. 2014.
64. T. S. Park, W. Li, K. E. McCracken, and J.-Y. Yoon, "Smartphone quantifies Salmonella from paper microfluidics," *Lab Chip*, 13(24), pp. 4832-4840,Dec. 2013.
65. H. Zhu, I. Sencan, J. Wong, S. Dimitrov, D. Tseng, K. Nagashima, and A. Ozcan, "Cost-effective and rapid blood analysis on a cell-phone," *Lab Chip*, 13(7), pp. 1282-88, Apr. 2013.
66. I. I. Bogoch, J. R. Andrews, B. Speich, J. Utzinger, S. M. Ame, S. M. Ali, and J. Keiser, "Mobile phone microscopy for the diagnosis of soil-transmitted helminth infections: a proof-of-concept study," *Am. J. Trop. Med. Hyg*., 88(4), pp. 626-629, Apr. 2013.
67. F. Li, Y. Bao, D. Wang, W. Wang, and L. Niu, "Smartphones for sensing," *Sci. Bull.*, 61(3), 190–201, Feb. 2016.
68. J. Canning, A. Lau, M. Naqshbandi, I. Petermann, and M. J. Crossley, "Measurement of fluorescence in a Rhodamine-123 doped self-assembled 'giant' mesostructured silica sphere using asmartphone as optical hardware," *Sensors*, 11(7), pp. 7055–7062, Jul. 2011.
69. J. Canning, M. Naqshbandi, and M. J. Crossley, "Measurement of Rhodamine B absorption in self-assembled silica microwires using a Tablet as the optical source," *Proc. SPIE*, 8351, pp. 83512E-1–83512E-5, Jan. 2012.
70. P. Wargocki, W. Deng, A. G. Anwer, and E. M. Goldys, "Medically relevant assays with a simple smartphone and tablet based fluorescence detection system," *Sensors*, 15(5), pp. 11653-11664, May 2015.
71. P. Preechaburana, M. C. Gonzalez, A. Suska, and D. Filippini, "Surface plasmon resonance chemical sensing on cell phones" *Angew. Chem. Int. Ed*. 51, pp. 11585–11588, Oct. 2012.
72. H. Zhu, O. Yaglidere, T. Su, D. Tseng, and A. Ozcan, "Cost-effective and compact wide-field fluorescent imaging on a cell phone," *Lab Chip*, 11(2), pp. 315-322, Jan. 2011.
73. S. K. J. Ludwig, H. Zhu, S. Phillips, A. Shiledar, S. Feng, D. Tseng, L. A. Ginkel, M. W. F. Nielen, and A. Ozcan, "Cellphone-based detection platform for rbST biomarker analysis in milk extracts using a microsphere fluorescence immunoassay," *Anal. Bioanal. Chem.*, 406(27), pp. 6857–6866, Nov. 2014.
74. H. C. Koydemir, Z. Gorocs, D. Tseng, B. Cortazar, S. Feng, R. Y. L. Chan, J. Burbano, E. McLeod, and A. Ozcan "Rapid imaging, detection and quantification of Giardia lamblia cysts using mobile-phone based fluorescent microscopy and machine learning," *Lab Chip*, 15(5), pp. 1284-1293, Mar. 2015.
75. Z. J. Smith, K. Chu, A. R. Espenson, A. Gryshuk, M. Molinaro, D. M. Dwyre, S. Lane, D. Matthews, and S. Wachsmann-Hogiu, "Cell phone-based platform for biomedical device development and education applications," *PLoS ONE*, 6(3), p. e17150, Mar. 2011.
76. R.D. Stedtfeld, D. M. Tourlousse, G. Seyrig, T. M. Stedtfeld, M. Kronlein, S. Price, F. Ahmad, E. Gulari, J. M. Tiedje, and S. A. Hashsham, "Gene-Z: a device for point of care genetic testing using a smartphone," *Lab Chip*, 12(8) pp. 1454–1462, Apr. 2012.

77. A. I. Barbosa, P. Gehlot, K. Sidapra, A. D. Edwards, and N. M. Reis, "Portable smartphone quantitation of prostate specific antigen (PSA) in a fluoropolymer microfluidic device," *Biosens. Bioelectron.*, 70, pp. 5-14, Aug. 2015.
78. B. Awqatty, S. Samaddar K. J. Cash, H. A. Clark, and J. M. Dubach, "Fluorescent sensors for the basic metabolic panel enable measurement with a smart phone device over the physiological range," *Analyst*, 139(20), pp. 5230-8, Oct. 2014.
79. E. Petryayeva and W. R. Algar, "Single-step bioassays in serum and whole blood with a smartphone, quantum dots and paper in- PDMS chips," *Analyst*, 140(20), pp. 4037-4045, Jun. 2015.
80. C. F. Fronczek, T. S. Park, D. K. Harshman, A. M. Nicolini, and J.-Y. Yoon, "Paper microfluidic extraction and direct smartphone-based identification of pathogenic nucleic acids from field and clinical samples," *RSC Adv.*, 4(22), pp. 11103-10, Feb. 2014.
81. S. Wang and X. Zhou, "Spectroscopic sensor on mobile phone," US Patent 20060279732 A1, Dec 14, 2006.
82. Z. J. Smith, K. Chu, A. R. Espenson, M. Rahimzadeh, A. Gryshuk, M. Molinaro, D. M. Dwyre, S. Lane, D. Matthews, and S. W. Hogiu, "Cell-phone-based platform for biomedical device development and education applications" *PLoS ONE*, 6(3), p. e17150, Mar. 2011.
83. H. Yu, Y. Tan, and B. T. Cunningham, "Smartphone fluorescence spectroscopy," *Anal. Chem.*, 86(17), pp. 8805-13, Sep. 2014.
84. K. D. Long, H. Yu, and B. T. Cunningham, "Smartphone instruments for portable enzyme-linked immunosorbent assay," *Biomed. Opt. Express*, 5(11), pp. 3792-806, Nov. 2014.
85. M. A. Hossain, J. Canning, S. Ast, K. Cook, P. J. Rutledge, and A. Jamalipour, "Combined 'dual' absorption and fluorescence smartphone spectrometers," *Opt. Lett*. 40(8), pp. 1737–1740, Apr. 2015.
86. S. Dutta, A. Choudhury, and P. Nath, "Evanescent wave coupled spectroscopic sensing using smartphone," *IEEE Phot. Tech. Lett.,* 26(6), 568-570, Mar. 2014.
87. S. Dutta, D. Sarma, A. Patel, and P. Nath, "Dye-assisted pH sensing using a smartphone" *IEEE Phot. Tech. Lett*., 27(22), pp. 2363–2366, Nov. 2015.
88. S. Dutta, G. P. Saikia, D. J. Sarma, K. Gupta, P. Das, and P. Nath, "Protein, enzyme and carbohydrate quantification using smartphone through colorimetric digitization technique," *J. Biophotonics*, 2016, pp. 1–11, May 2016.
89. E. K. Grasse, M. H. Torcasio, and A. W. Smith, "Teaching UV–Vis spectroscopy with a 3D-printable smartphone spectrophotometer," *J. Chem. Educ*., 93(1), pp. 146–151, Nov. 2016.
90. Y. Wang, X. Liu, P. Chen, N. T. Tran, J. Zhang, W. S. Chia, S. Boujday, and B. Liedberg "Smartphone spectrometer for colorimetric bio-sensing," *Analyst*, 141(11), pp. 3233-38, Jun. 2016.
91. E. Petryayevaand W. R. Algar, "A job for quantum dots: use of a smartphone and 3D-printed accessory for all-in-one excitation and imaging of photoluminescence," *Anal. Bioanal. Chem*., 408(11), pp. 2913–2925 Apr. 2016.
92. C. Zhang, G. Cheng, P. Edwards, M.-D. Zhou, S. Zheng, and Z. Liu, "G-Fresnel smartphone spectrometer," *Lab Chip*, 16(2), pp. 246-250, Jan. 2016.
93. M. A. Hossain, "Eat-by-Phone: Smartphone-based instruments for food quality assurance" Leveraging Technology for a Better Tomorrow, IEEE Day 2018, Khulna University of Engineering and Technology, Oct. 2018.
94. L.-J. Wang, Y.-C. Chang, R. Sun, and L. Li, "A multichannel smartphone optical biosensor for high-throughput point-of-care diagnostics," *Biosens. Bioelectron.*, 87, pp. 686–692, Jan. 2017.
95. G. K. Özdemir, A. Bayram, V. Kılıçc, N. Horzumd, and M. E. Solmaz, "Smartphone-based detection of dyes in water for environmental sustainability," *Anal. Methods*, 9(4), pp. 579–585 (2017).
96. L.-J. Wang, Y.-C. Chang, X. Ge, A. T. Osmanson, D. Du, Y. Lin, and L. Li, "Smartphone optosensing platform using a DVD grating to detect neurotoxins," *ACS Sens*., 1(4), pp. 366–373, Jan. 2016.

97. M. N. KamelBoulos, A. C. Brewer, C. Karimkhani, D. B. Buller, and R. P. Dellavalle, "Mobile medical and health apps: state of the art, concerns, regulatory control and certification," *Online J. Public Health Inform*., 5(3), p. 229, Feb. 2014.
98. ALPhANOV, Centre TechnologiqueOptiqueet Lasers, "GOSPECTRO – THE POWER OF SPECTROSCOPY AT YOUR FINGERTIPS," [Online available] http://www.alphanov.com/223-news-gospectro-the-power-of-spectroscopy-at-your-fingertips.html (accessed on 20 June 2017).
99. D. Gallegos, K. D. Long, H. Yu, P. P. Clark, Y. Lin, S. George, P. Natha, and B. T. Cunningham, "Label-free biodetection using a smartphone," *Lab Chip*, 13(11),pp. 2124-2132, Jun. 2013.
100. S. Dutta, K. Saikia, and P. Nath, "Smartphone based LSPR sensing platform for bioconjugation detection and quantification," *RSC Adv.*, 6(26), pp. 21871-80, Feb. 2016.
101. K. Bremer and B. Roth, "Fibre optic surface plasmon resonance sensor system designed for smartphones," *Opt. Express*, 23(13), pp. 17179-17184, Jun. 2015.
102. Y. Liu, Q. Liu, S. Chen, F. Cheng, H. Wangn, and W. Peng, "Surface plasmon resonance biosensor based on smart phone platforms," *Sci. Rep.*, 5, p. 12864, Aug. 2015.
103. J. L. Delaney, E. H. Doeven, A. J. Harsant, and C. F. Hogan "Use of a mobile phone for potentiostatic control with low cost paper-based microfluidic sensors," *Anal. Chim. Acta*, 790, pp. 56–60, Aug. 2013.
104. J. L. Delaney, C. F. Hogan, J. Tian, and W. Shen "Electrogenerated chemiluminescence detection in paper-based microfluidic sensors," *Anal. Chem*., 83(4), pp. 1300–1306, Feb. 2011.
105. E. H. Doeven, G. J. Barbante, A. J. Harsant, P. S. Donnelly, T. U. Connell, C. F. Hogan, and P. S. Francis, "Mobile phone-based electrochemiluminescence sensing exploiting the 'USB On-The-Go' protocol," *Sen. Actuat. B Chem.*, 216, pp. 608–613, Sep. 2015.
106. X. Wang, M. R. Gartia, J. Jiang, T.-W. Chang, J. Qian, Y. Liu, X. Liu, and G. L. Liu, "Audio jack based miniaturized mobile phone electrochemical sensing platform,"*Sen. Actuat. B Chem.*, 209, pp. 677–685, Mar. 2015.
107. M. Velikov, R. L. Smeets, J. T. V. Scheltinga, P. J.F. Lucas, and M. Spaanderman, "Smartphone-based analysis of biochemical tests for health monitoring support at home," *Healthc. Technol. Lett*., 1(3), pp. 92–97, Sep. 2014.
108. H. Zhu, I. Sencan, J. Wong, S. Dimitrov, D. Tseng, K. Nagashima, and A. Ozcan, "Cost-effective and rapid blood analysis on a cell-phone," *Lab Chip*, 13(7), pp. 1282-88, Apr. 2013.
109. I. I. Bogoch, J. R. Andrews, B. Speich, J. Utzinger, S. M. Ame, S. M. Ali, and J. Keiser, "Mobile phone microscopy for the diagnosis of soil-transmitted helminth infections: a proof-of-concept study," *Am. J. Trop. Med. Hyg*., 88(4), pp. 626-629, Apr. 2013.
110. F. Li, Y. Bao, D. Wang, W. Wang, and L. Niu, "Smartphones for sensing," *Sci. Bull.*, 61(3), 190–201. Feb. 2016.
111. M. A. Hossain, J. Canning, S. Ast, P. Rutledge, T. L. Yen, R. Webster, and A. Jamalipour, "Centralised and portable "network forensics" using smartphone-based diagnostics: Case Study – the mapping of tap water pH across Sydney, Australia" *Proc. IEEE Photonic Conference,* 2014, pp. 564–565.
112. A. Hossain, J. Canning, S. Ast, P. Rutledge, and A. Jamalipour, "Early warning smartphone diagnostics for water security and analysis using real-time pH mapping," *Phot. Sensors*, 5(4), pp. 289-297, Dec. 2015.
113. X. Hong, V. K. Nagarajan, D. H. Mugler, and B. Yu, "Smartphone microendoscopy for high resolution fluorescence imaging," *J. Innovative Optical Health Sciences*, 9(5), pp. 1650046-52, Mar. 2016.
114. J. Canning "Smartphone spectrometers and other instrumentation," Sensing & Measurement, *SPIE Newsroom*, 8 Jan. 2016.
115. M. A. Hossain, J. Canning, S. Ast, P. Rutledge, T. L. Yen, and A. Jamalipour, "Lab-in-a-phone: Smartphone-based portable fluorometer for pH measurements of environmental water," *IEEE Sensors J.*, 15(9), pp. 5095-5102, Sep. 2015.
116. M. A. Hossain, J. Canning, T. L. Yen, S. Ast, P. Rutledge, and A. Jamalipour "A smartphone fluorometer - the lab-in-a-phone"*Proc. OSA,* Advanced Photonics - Optical Sensors, 2014, p. SeTh2C.1

117. M. A. Hossain, J. Canning, S. Ast, P. Rutledge, T. L. Yen, R. Webster, and A. Jamalipour, "Centralised and portable "network forensics" using smartphone-based diagnostics: Case Study – the mapping of tap water pH across Sydney, Australia" *Proc. IEEE Photonic Conference,* 2014, pp. 564–565.
118. M. A. Hossain, J. Canning, S. Ast, P. Rutledge, and A. Jamalipour, "Early warning smartphone diagnostics for water security and analysis using real-time pH mapping," *Phot. Sensors*, 5(4), pp. 289-297, Dec. 2015.
119. J. Canning, M. A. Hossain, and A. Jamalipour, "Smartphone spectrometers," *Proc. Australian and New Zealand Conference on Optics and Photonics (ANZCOP)*, Nov.- Dec. 2015.
120. M. A. Hossain, S. Ast, J. Canning, K. Cook, P. J. Rutledge, and A. Jamalipour, "Fluorescent measurements of Zn^{2+} on a smartphone," *Proc. SPIE 9655*, *5th Asia Pacific Optical Sensors Conference,* Jul. 2015.
121. M. A. Hossain, J. Canning, K. Cook, S. Ast, P. J. Rutledge, and A. Jamalipour, "Absorption and fluorescence spectroscopy on a smartphone," *Proc. SPIE 9655*, *5th Asia Pacific Optical Sensors Conference,* Jul. 2015.
122. M. A. Hossain, J. Canning, K. Cook, and A. Jamalipour, "Smartphone spectrometer with fiber endoscope probe" *Proc. Australian and New Zealand Conference on Optics and Photonics (ANZCOP)*, Nov.- Dec. 2015.
123. M. A. Hossain, J. Canning, K. Cook, and A. Jamalipour, "Portable smartphone optical fibre spectrometer" *Proc. SPIE 9634, 24th Optical Fiber Sensors Conferences,* Sep. 2015.
124. M. A. Hossain, J. Canning, Z. Yu, S. Ast, P. J. Rutledge, J. K.-H. Wong, A. Jamalipour, and M. J. Crossley "Time-resolved and temperature tuneable measurements of fluorescent intensity using a smartphone fluorimeter" *Analyst*, 142, 1953-1961, May 2017.
125. M. A. Hossain, Z. Yu, J. Canning, S. Ast, P. J. Rutledge, J. K.-H. Wong, M. J. Crossley, and A. Jamalipour, "Temperature controlled portable smartphone fluorimeter,"*Proc. OSA, 6th Asia Pacific Optical Sensors Conference*, Oct. 2016, p. W2A.2.
126. J. Canning, S. Ast, M. A. Hossain, H. Chan, P. J. Rutledge, and A. Jamalipour, "Bend and twist intramolecular charge transfer and emission for selective metal ion sensing," *Opt. Mat. Express*, 5(11), pp. 2675-2681, Oct. 2015.
127. J. Canning, M. A. Hossain, and S. Ast, "Smart Sensing: Combining Photonics, Smart Devices and Chemosensor Dyes for Characterising and Separating Metal Ions," *Proc. OSA, 6th Asia Pacific Optical Sensors Conference*, Oct. 2016, p. Th2A.1.
128. J. Canning, S. Ast, M. A. Hossain, H. Chan, P. J. Rutledge, and A. Jamalipour, "Metal ion detection by twist-induced charge transfer within a fluoro-ionophore: molecular photovoltaics and mechanics for IoT lab-in-a-phone" *Proc. Int. Conf. on Small Science*, Nov. 2015.
129. J. Canning, "Optically induced charge transfer as the foundation for nanobot technology," *Proc. OSA, Photonics and Fiber Technology, Bragg Gratings, Photosensitivity, and Poling in Glass Waveguides*, Sep. 2016, p. JT4A.2.
130. The Royal Swedish Academy of Sciences, Stockholm, Sweden, *Molecular Machines, Scientific Background on the Nobel Prize in Chemistry 2016*, [Online]. Available: https://www.nobelprize.org/nobel_prizes/chemistry/laureates/2016/advanced-chemistryprize2016.pdf
131. M. A. Hossain, J. Canning, K. Cook, and A. Jamalipour, "Smartphone laser beam spatial profiler," *Optics Letters*, 40(22), pp. 5156-5159, Nov. 2015.
132. M. A. Hossain, J. Canning, K. Cook, and A. Jamalipour, "Smartphone laser beam profiler," *Proc. Australian and New Zealand Conference on Optics and Photonics (ANZCOP)*, Nov.- Dec. 2015.
133. M. A. Hossain, J. Canning, K. Cook, S. Ast, and A. Jamalipour, "Photo- and thermal degradation of olive oil measured using an optical fibre smartphone spectrofluorimeter," Accepted paper in the *25th Optical Fiber Sensor (OFS25) Conference*.
134. David Pile "Imaging and sensing: Portable profiler," *Nat. Photon. News*, 10, 8, Jan. 2016.
135. J. R. Lakowicz, "Instrumentation for fluorescence spectroscopy," in *Principles of fluorescence spectroscopy* 3rd ed., Springer, NY 10013, USA. 2006, pp. 27-60.

136. 3D Spectra Tech, *What is 3D printing*, 3D Spectra Technologies LLP, [Online available] http://www.3dspectratech.com/what-is-3d-printing.
137. M. S. Alexiou, V. Tychopoulos, S. Ghorbanian, J. H. P. Tyman, R. G. Brown, and P. I. Brittain, "The UV–visible absorption and fluorescence of some substituted 1,8-naphthalimides and naphthalic anhydrides," *J. Chem. Soc. Perkin. Trans. 2*, 1990(5), pp. 837–842, Jan. 1990.
138. A. P. de Silva, H. Q. N. Gunaratne, T. Gunnlaugsson, A. J. M. Huxley, C. P. McCoy, J. T. Rademacher, and T. E. Rice, "Signaling recognition events with fluorescent sensors and switches," *Chem. Rev.*, 97(5), pp. 1515–1566, Aug. 1997.
139. J. K. Tusa, and H. R. He, "Critical care analyzer with fluorescent optical chemosensors for blood analytes," *J. Mat. Chem*., 15(27–28), pp. 2640-2647, Jul. 2005.
140. R. Parkesh, T. C. Lee, and T. Gunnlaugsson, "Highly selective 4-amino-1,8-naphthalimide based fluorescent photoinduced electron transfer (PET) chemosensors for Zn(II) under physiological pH conditions," *Org. Biomol. Chem*., 5(2), pp. 310–317, Jan. 2007.
141. S. Ast, P. J. Rutledge, and M. H. Todd, "Reversing the triazole topology in a cyclam-triazole-dye ligand gives a 10 fold brighter signal response to Zn^{2+} in aqueous solution," *Eur. J. Inorg. Chem.*, 2012(34), pp. 5611–5615, Dec. 2012.
142. M. Yu, Q. Yu, P. J. Rutledge, and M. H. Todd, "A fluorescent allosteric scorpion and complex visualizes a biological recognition event," *ChemBioChem*, 14(2), pp. 224–229, Jan. 2013.
143. A. P. de Silva, H. Q. N. Gunaratne, J.-L. Habib-Jiwan, C. P. McCoy, T. E. Rice, and J.-P. Soumillion, "New fluorescent model compounds for the study of photoinduced electron transfer: The influence of a molecular electric field in the excited state," *Angew. Chem. Int. Ed. Eng*., 34(16), pp. 1728–1731, Sep. 1995.
144. Google Play, *Color Grab*, Loomatix Group. [Online]. Available: https://play.google.com/store/apps/details?id=com.loomatix.colorgrab&hl=en
145. Australian government's National Health and Medical Research Council, "Australian drinking water guidelines 6," *National Water Quality Management Strategy*, 2013, 2: 174.
146. Sydney Water, Quarterly Drinking Water Quality Report, 1 Jul. 2013 to 30 Sep. 2013, Sydney, Australian: Sydney Water. www.sydneywater.com.au, 2014.
147. A.G. Dickson, C.L. Sabine, and J.R. Christian, "Guide to best practices for ocean CO_2 measurements," PICES Special Publication 3, 2007, Ch. 5, p. 191.
148. HI 98106, Champ® pH Tester, Hanna Instruments [Online]. Available: http://www.hannainst.com/usa/prods2.cfm?id=040003&ProdCode=HI%2098106
149. J. S. Hall, J. G. Szabo, S. Panguluri, and G. Meiners, *Distribution System Water Quality Monitoring: Sensor Technology Evaluation Methodology and Results*, Cincinnati, U. S. A.: U. S. Environmental Protection Agency, 2009.
150. P. H. Gleick, "Water and terrorism," *Water Policy*, 8(6), pp. 481–503, 2006.
151. J. V. Capella, A. Bonastre, R. Ors, and M. Peris, "A wireless sensor network approach for distributed in-line chemical analysis of water," *Talanta*, 80(5), pp. 1789–1798,Mar. 2010.
152. R. Cheikhousman, M. Zude, D. J. R. Bouveresse, C. L. Leger, D. N. Rutledge, and I. B. Aragon, "Fluorescence spectroscopy for monitoring deterioration of extra virgin olive oil during heating," *Anal. Bioanal. Chem*., 382(6), pp. 1438–1443, Jul. 2005.
153. J. Ayton, R. J. Mailer and K. Graham, "The Effect of Storage Conditions on Extra Virgin Olive Oil Quality," in *RIRDC Publication No. 12/024, Rural Industries Research and Development Corporation*, Apr. 2012.
154. B. B. Das, F. Liu, and R. R. Alfano, "Time-resolved fluorescence and photon migration studies in biomedical and model random media,"*Rep. Prog. Phys*., 60(2), pp. 227-292, Feb. 1997.
155. D. Erickson, D. Sinton, and D. Li, "Joule heating and heat transfer in poly(dimethylsiloxane) microfluidic systems," *Lab Chip*, 3(3), pp. 141-9, Aug. 2003.
156. D. Ross, M. Gaitan, and L. E. Locascio, "Temperature measurement in microfluidic systems using a temperature-dependent fluorescent dye," *Anal. Chem*., 73(17), pp. 4117-23, Sep. 2001.
157. S. Ast, S. Kuke, P. J. Rutledge, and M. H. Todd, "Using click chemistry to tune the properties and the fluorescence response mechanism of structurally similar probes for metal ions," *Eur. J. Inorg. Chem*., 2015(1), pp. 58-66, Jan. 2015.

158. E. Tamanini, A. Katewa, L. M. Sedger, M. H. Todd, and M. Watkinson, "A synthetically simple, click-generated cyclam-based zinc(II) sensor," *Inorg Chem*., 48(1), pp. 319-24, Jan. 2009.
159. *Arduino Uno and Genuino Uno*, ARDUINO. [Online]. Available: https://www.arduino.cc/en/Main/ArduinoBoardUno.
160. Y. Y. Chen and A. W. Wood, "Application of a temperature-dependent fluorescent dye (Rhodamine B) to the measurement of radiofrequency radiation-induced temperature changes in biological samples," *Bioelectromagnetics*, 30(7), pp. 583-90, Oct. 2009.
161. N. Kuzkova, O. Popenko, and A. Yakunov, "Application of temperature-dependent fluorescent dyes to the measurement of millimeter wave absorption in water applied to biomedical experiments," *Int. J. Biomed. Imaging*, 2014, p. 243564, Nov. 2014.
162. J. Canning, "Optically induced charge transfer as the foundation for nanobot technology," *Australian Conference on Optical Fibre Technology*, Sydney Australia, 5–8 September 2016.
163. T. S. Park, W. Li, K. E. McCracken, and J.-Y. Yoon, "Smartphone quantifies Salmonella from paper microfluidics," *Lab Chip*, 13(24), pp. 4832-4840, Dec. 2013.
164. G. Gauglitz and T. Vo-Dinh, Handbook of spectroscopy, Weinheim. WILEY-VCH, 2003.
165. J. M. Lerner, and A. Thevenon, *The Optics of Spectroscopy*, Horiba Scientific. [Online]. Available: http://www.horiba.com/us/en/scientific/products/optics-tutorial/.
166. J. Poulin and R. Kashyap, "Novel tuneable on-fiber polymeric phase-mask for fiber and planar waveguide Gragg grating fabrication," *Opt. Express*, 13(12), pp. 4414-19, Jun. 2005.
167. Ibsen Photonics "Spectrometer design guide," [Online available]: https://ibsen.com/technology/spectrometerdesign-guide/ (accessed on 17 Oct. 2018)
168. Bumper, [Online]. Available: https://publiclab.org/notes/MrBumper/01-11-2015/preparing-a-dvd-r-to-act-as-a-diffractiongrating.
169. T. C. Stubbings and H. Hutter, "Combining multispectral image information using color," *Anal. Chem*. 72(7), pp. 282A-288A, Apr. 2000.
170. K. Cook, J. Canning, S. Leon-Saval, Z. Reid, M. A. Hossain, J. Comatti, Y. Luo, and G. D. Peng "Air-structured optical fiber drawn from a 3D-printed preform," *Opt. Lett.*, 40(17), pp. 3966-3969, Sep. 2015.
171. S. Shankland, *How Android 5.0 lets you get raw for better photos*, CNET. [Online]. Available: https://www.cnet.com/news/android-lollipop-opens-high-end-photography-options/.
172. B. Woods, "Smartphone screens explained: Display types, resolution and more," Androidpit. [Online]. Available: https://www.androidpit.com/smartphone-displays-explained?nocol=1.
173. R. Beghi, A. Spinardi, L. Bodria, I. Mignani, and R. Guidetti, "Apples nutraceutic properties evaluation through a visible and near-infrared portable system," *Food Bioprocess Technol*. 6(9), pp. 2547–2554, Sep. 2013.
174. M. N. Mertzlyak, A. E. Solovchenko, and A. A. Gitelson, "Reflectance spectral features and non-destructive estimation of chlorophyll, carotenoid and anthocyanin content in apple fruit," *Postharvest Biol. Technol*. 27(2), pp. 197-211, Feb. 2003.
175. R. D. Pelayo, L. G. Guerrero, and D. H. Méndez, "Chlorophyll and carotenoid pigments in the peel and flesh of commercial apple fruit varieties," *Food Res. Int*., 65(B), pp. 272–281, Nov. 2014.
176. C. E. Sando "Coloring matters of Grimes Golden, Jonathan, Stayman and Winesap apples," *J. Biol. Chem*., 117, pp. 45–56, Jan. 1937.
177. Y. Gilbert, M. Kongbonga, H. Ghalila, M. B. Onana, Y. Majdi, Z. B. Lakhdar, H. Mezlini, and S. S. Ghalila, "Characterization of vegetable oils by fluorescence spectroscopy," *Food Nutr. Sci*., 2(7), pp. 692-699, Sep. 2011.
178. C. E. T. D. Silva, V. L. Filardi, I. M. Pepe, M. A. Chaves, and C. M. S. Santos, "Classification of food vegetable oils by fluorimetry and artificial neural networks," *Food Control*, 47, pp. 86-91, Jan. 2015.
179. M. Zandomeneghi, L. Carbonaro, and C. Caffarata "Fluorescence of vegetable oils: olive oils," *J. Agric. Food Chem*., 53(3), pp. 759-766, Feb. 2005.

180. G. Tomazzoni, M. Meira, C. M. Quintella, G. F. Zagonel, B. J. Costa, P. R. D. Oliveira, I. M. Pepe, and P. R. D. C. Neto, "Identification of vegetable oil or biodiesel added to diesel using fluorescence spectroscopy and principal component analysis," *J. Am. Oil Chemists' Society*, 91(2), pp. 215–227, Feb. 2014.
181. "Health and Olive Oil," The Olive Oil Source, CA, USA. [Online]. Available: http://www.oliveoilsource.com/page/health-and-olive-oil.
182. N. Ramanujam, "Fluorescence spectroscopy in vivo," in *Encyclopedia of Analytical Chemistry*, John Wiley and Sons Ltd. Chichester, 2000; pp. 20–56.